Metal–Organic Framework-Based Electrocatalysts for CO$_2$ Reduction

Syed Shoaib Ahmad Shah, Tayyaba Najam, Ming Wen, Shuang-Quan Zang, Amir Waseem, and Hai-Long Jiang*

The increasing concentration of CO$_2$ is alarming for modern society and the reduction of CO$_2$ into valuable products is the unique solution. Metal–organic frameworks (MOFs), constructed by organic linkers interconnected with metal (oxide) nodes, with high porosity and large surface area, have become an emerging class of electrocatalysts for reduction of CO$_2$. Herein, the recent advancements in MOF-based electrocatalysts for the reduction of CO$_2$, abridged the recent strategies to enhance the performance are summarized and the structure–activity relationship is discussed to provide a comprehensive route for the rational design of novel catalysts. Moreover, the specially focused aspect is to summarize recent strategies of structure tuning, manipulating the electronic structure and enhancing the active site density to well exposed single-atom active sites. In addition, some demerits and proposed future perspectives are also discussed.

1. Introduction

Rapid industrial, economic developments, and the extreme depletion of fossil fuels have created a number of problems for modern society. Among others, the alarming problem is the high concentration of as-emitted CO$_2$ in the environment,

S. S. A. Shah, M. Wen, H.-L. Jiang
Hefei National Laboratory for Physical Sciences at the Microscale
CAS Key Laboratory of Soft Matter Chemistry
Department of Chemistry
University of Science and Technology of China
Hefei, Anhui 230026, P. R. China
E-mail: jianglab@ustc.edu.cn

T. Najam
Institute for Advanced Study and Institute of Microscale Optoelectronics
Shenzhen University
Shenzhen 518060, P. R. China

M. Wen, S.-Q. Zang
Green Catalysis Center and College of Chemistry
Zhengzhou University
Zhengzhou 450001, China

A. Waseem
Analytical Lab
Department of Chemistry
Quaid-i-Azam University
Islamabad 45320, I. R. Pakistan

The ORCID identification number(s) for the author(s) of this article can be found under https://doi.org/10.1002/sstr.202100090.

which is now impossible to reduce by natural CO$_2$ cycle, i.e., photosynthesis in plants.[1] The predicted future is worse concerning global warming and even leading to hypercapnia, which would have an impact on every living species on the planet. Furthermore, it is anticipated that at the end of this century, the concentration of atmospheric CO$_2$ would reach its peak of 850 ppm, resulting in a drastic change in global atmospheric chemistry.[2,3]

To reduce CO$_2$ levels in the atmosphere and the harmful effects associated with it, it is necessary to isolate and capture carbon dioxide from its sources such as industries and power plants. Recently, some strategies are being applied for the capture and storage of extra CO$_2$, including chemical/physical adsorption of CO$_2$ onto the porous materials.[4,5] Nevertheless, most technologies contribute extraordinary costs and/or consumptions of energy and usually applied methods for the storage of CO$_2$ are based on marine or geological, meanwhile, this approach is unlikely to affect soil and marine biology. So, converting CO$_2$ into value-added goods is an emerging strategy to lower the CO$_2$ concentration in environment as well as cost of methodology. Consequently, the research for facile and convenient methods for CO$_2$ conversion is emerging in this decade. In a review, Perathoner and coworkers explained leading routes for converting CO$_2$ (as a carbon source) into valuable chemicals using renewable energy.[6] Accordingly, carbon dioxide is being used for the synthesis of useable products such as fuels and fine chemicals including CO, alcohols, formaldehyde and formates, etc. Currently, renewable energy, for example solar, is being used as a source of energy directly (photocatalysis) or indirectly (electrocatalysis) for conversion of CO$_2$.[3,7–10] Subsequently, the demand of specific catalysts is ever-increasing which can play according to the requirement of application. Therefore, search of new materials for CO$_2$ conversion as well as alternative clean energy for the proposed clean economy has aroused wide interest.[11]

The electroreduction of CO$_2$ offers a compelling route to energy conversion and/or high value chemical manufacturing.[12–14] This electrochemical method for converting CO$_2$ into fuels by using abundant renewable energy resources is an attractive platform to reduce the harmful effects of carbon dioxide as well as a source of fine chemicals.[12,15,16] But the sluggish reaction kinetics, which comprises several steps of electron and proton transfers, accompanied by competing hydrogen evolution

reaction (HER) leads to poor productivity and efficacy. These are the chief obstacles to the practical use of an electrocatalyst to reduce CO_2 emissions.[17–19] Consequently, it is urgent to fabricate efficient and selective electrocatalysts for CO_2 reduction reaction (CO_2RR), which can perform at low potential with a good yield of selective product, but this remains a major challenge.

Metal–organic frameworks (MOFs) are emerging porous structures, containing a strong coordination of metals with ligands.[20] The MOFs are fascinating considerations because of having diverse, tunable structural properties including but not limited to highly porous surface area, strong organic and inorganic catalytic sites and tunable postsynthetic structure.[21–23] This unique stuff marks these emerging materials for widespread applications, such as catalysis (photo-, electrocatalysis) energy storage, gas storage, adsorption of toxics, and so on.[3,7,24–41] In 2012, MOFs were first time used as electrocatalyst for CO_2RR,[42,43] and the copper rubeanate MOF (CR-MOF) showed improved CO_2RR performance.[42] Because the CO_2RR takes place at a complex three-phase interface of liquid electrolyte–gaseous CO_2–solid catalyst. The electrocatalytic processes mainly involve the following critical steps: CO_2 activation, surface reaction, and product desorption processes including 1) electron transfer, 2) mass diffusion, and 3) electrochemical reaction on the surface via three-phase interface. The resultant catalytic activity is totally based on these three factors which are summarized in the term "proficiency of active sites." MOFs provide a broad opportunity in manufacturing diversified catalytic materials with several advantages: 1) ensuring high mass transfer and availability of active sites, 2) controlling the electronic structure by facile heteroatom doping, 3) inheriting the pristine-MOFs' characteristics after electrochemical/thermal decomposition/pyrolysis. Therefore, MOF-based porous materials, with the aforementioned characteristics features are very promising candidates for CO_2 electrocatalysis. MOF-derived materials, even after rational pyrolysis, retained their inherited characteristics features, e.g., greater surface area, porosity and uniform distribution of active sites with addition of electronic conductivity due to in situ produced heteroatom-doped graphitic carbon. There are several reviews published on the characteristics features of MOF-based materials for several applications.[3,7,21,24,44–47] Recently, our group has published a prestigious review on applications of MOFs for carbon capture and conversion, which summarizes the comprehensive and significant developments in preparing MOFs and their composites/derived materials for carbon capture and conversion including CO_2 storage, photocatalytic and electrocatalytic CO_2 conversion into value-added products.[48] Further, Wang and coauthors have summarized recent developments on electrocatalytic CO_2RR with the main focus of heterogeneous immobilization of homogeneous molecular catalysts.[49] However, the MOF-based/derived catalysts for solely electrocatalytic CO_2RR are rarely reviewed, being an emerging concern, it is necessary to summarize the recent developments and merits/demerits of MOFs for electrocatalytic CO_2RR, it will be helpful for the rational design of new catalysts as well as commercialization of this technology.

Herein, we have combined two research hotlines (MOFs and CO_2RR) and summarized the developments of MOF-based/derived electrocatalysts for CO_2RR. We have abridged the recent strategies to enhance the performance and discussed the structure–activity relationship to provide a comprehensive route for the rational design of novel catalysts. Moreover, MOF-based/derived electrocatalysts are especially focused on the aspects of structure tuning, manipulating the electronic structure by heteroatom doping and enhancing the active site density to well exposed single-atom active sites. In addition to these fundamental strategies applied for enhancing the performance of MOF-based electrocatalysts, some demerits, and proposed future perspectives are also discussed.

2. Thermodynamics, Kinetics, and Mechanism of Electrocatalytic CO_2RR

2.1. Thermodynamics of Electrocatalytic CO_2RR

The C—O bond length in CO_2 shows a certain degree of triple bond characteristic because of the small distance among oxygen–carbon atoms. In this way, carbon dioxide behaves as a relatively static and stable chemical; the energy is required in huge quantities (bond energy $= 750 \, \text{kJ mol}^{-1}$) and effective catalysts to efficiently convert CO_2 into other products.[50]

A demonstration of the molecular orbital map of CO_2 shows a fully formed and interconnected orbit representing a very stable molecule (**Figure 1**a).[51] The first step in activating and converting a molecule is the transfer of electron (i.e., a reduction process) that has the σ^* lowest unoccupied molecular orbital (LUMO) to combat binding. The highest occupied molecular orbital (HOMO) with its strongly localized electron density as oxygen in-plane lone pairs is conducive to interactions with electrophiles. This leads to an intensification between C—O distance/bond length and manifests itself in the first inclination of the linear molecule. The electrophiles and nucleophiles can be attached easily with this bent molecule via its charged localized orbital boundaries. However, this electronic CO_2 reduction to CO_2^- is a very endogenous pathway that occurs at high potential (Figure 1b).[52] As there is a huge obstacle among curved anion and linear molecules, the next steps, i.e., the proton-coupled electron transfers are thermodynamically more favorable than the initial reaction step.[53]

The electrochemical CO_2RR can be allocated into various main points: 1) CO_2 absorption on catalyst's surface; 2) electrons and/or proton transfer, cleavage of C—O bonds with the intermediates formation; 3) removal of products from the surface of catalysts. By considering these steps, CO_2RR is a more complex multilevel interface process that typically involves different interaction pathways with the transmission of 2, 4, 6, 8, or 12 electrons,[11] leading to the production of various molecules in the electrochemical system (Section 2.2). The production of various products, i.e., C1 and C2 or C2+, depends upon numerous factors, such as nature and density of active sites, strength of applied potential and electrolyte, etc. As the theoretical potential for CO_2RR is a continuous value, many products are one of the possibilities in thermodynamic competition. Therefore, selective production of target molecules is an important criterion for the usefulness of the comeback to CO_2 reduction.
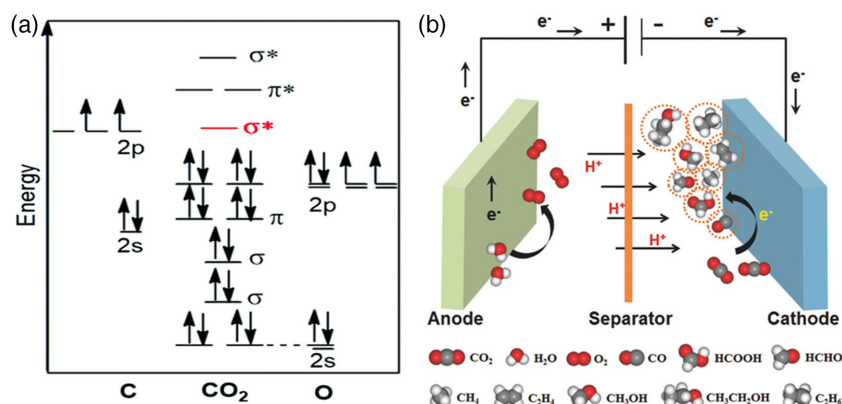
Figure 1. a) Electron distributions in CO_2 molecule based on molecular orbital theory (MOT). Reproduced with permission.[51] Copyright 2020, The Royal Society of Chemistry. b) The activation and consequent reduction reaction including possible products in an electrochemical system. Reproduced under the terms of the Creative Commons CC-BY license.[52] Copyright 2017, The Authors. Published by Wiley-VCH.

2.2. Kinetics and Mechanism of Electrocatalytic CO_2RR

Although electrochemical pathways are thermodynamically favorite, the total barrier of energy (called overpotential) determines virtual selectivity between products. Increased selectivity and intensity of current, as well as strong and stable long working hours, are essential for the further alteration to commercial viability.[54] The mechanistic studies of CO_2RR are divided into two step process: formation of intermediates and formation of final products, it is varied from product to product. The C1 products (CO, HCOOH) usually follow the decisive first step, CO_2 is activated ($*CO_2^{.-}$) by absorbing one electron on the surface of catalyst.[55–58] The proton-coupled electron transfer process is occurred by combining the C atom with ($*CO_2^{.-}$) forming a key intermediate ($*COOH$). The $*COOH$ intermediate can be converted into final products CO by second-step proton-coupled electron transfer process. By the combination of O atom with $*CO_2^{.-}$ and protonation of O atom produced $*OCHO$ intermediate, which is converted to HCOOH or formate by proton-coupled electron transfer reaction.[59] For the mechanism of CO_2RR to methane, methanol, and formaldehyde, theoretical and experimental studies investigated that the first-step intermediate is $*CO$.[55,60] The hydrogenation of $*CO$ produced intermediates $*HCO$, $*H_2CO$, and $*H_3CO$, which are converted into CH_4, HCHO, and CH_3OH, respectively. However, two different arguments are standing for the conversion of $*CO$ to CH_4. One proposed route is the reduction of $*CO$ into $*C$ via $*COH$ intermediate, which can be further expanded that $*CH$, $*CH_2$, and $*CH_3$ can also be reduced to $*C$ and finally produce CH_4.[61,62] The most accepted route via experimental and theoretical calculations is proposed: $*CO \rightarrow *CHO \rightarrow *CH \rightarrow *CH_2 \rightarrow *CH_3 \rightarrow *+CH_4$.[63]

Further, for the production of C2+ products, $*CO$ intermediates pathway is usually followed and reduction of $*CO$ determine the final production accompanied with experimental conditions.[64,65] For example, ethane is produced through $*CH$ intermediate by proton-coupled electron transfer reaction, following the protonation of $*CH$ to $*CH_3$. The dimerization of $*CH_3$ produce final product (C_2H_6). The insertion of CO into $*CH_2$ produced CH_3COO^-. The $*CO—CO$ dimer produced the $*CH_2CHO$ intermediate via series of protonation and electron transfer steps, serving as selectivity determining step to generate the C_2H_4 and C_2H_5OH.[65,66]

Some experimental works were carried out on the surface of bulk metals for CO_2RR, following those results, theoretical trends have appeared,[67–73] and metal electrodes are classified into four categories: 1) formic acid producing, e.g., Tl, Sn, Cd, In, Hg, Bi, Pb etc.; 2) production of carbon monoxide (Ag, Au, Pd, Ga, and Zn); 3) hydrogen producing metals are Ni, Fe, Pt, and Ti; 4) Cu is categorically placed for the production of different hydrocarbons.[74–76] In addition to these categorized metallic active sites, hydrogen bonding also plays a vital role and competing HER reaction can reduce the efficiency/selectivity of the final product. Consequently, Faradic efficiency (FE) is considered as a fundamental concern during the evaluation of CO_2RR activity. Recent studies have also explained that structural changes or manipulations in native active sites cause variation in products and selectivity, as well as FE. For example, Cu and Zn have similar 3 d electronic configurations but with different catalytic performance, i.e., $2e^-$ reduction of CO_2 to CO is shown by Zn electrode while Cu gives multiple hydrocarbons.[77,78] In other cases, Zn doping in Cu electrode (Cu/Zn) leads to the selective product, i.e., alcohol is produced.[79,80] For instant, the Cu_4Zn catalysts are reported for the production of ethanol with 29.1% FE.[79] Similarly, the physical mixing of CuO and ZnO (1:0.5 wt%) produced methanol with 25.2% FE.[81] However, doping of Sn in Cu could not give better results, which may be attributed to the relatively strong bonding of intermediates ($*CO$) with Cu surface.[82,83] Therefore, the retention time of intermediates on the surface of electrocatalysts is also considered as an important descriptor to control the selectivity of product during CO_2RR, and it is recommended that designed catalysts with prolonged interaction with intermediates may lead to the multicarbon (C2) products.[84–89] For example, Song and coworkers recently demonstrated the adsorption state switching of CO_2^- intermediates and realized an improvement in the selectivity of CO_2RR to formate by doping S to Cu-based catalysts.[89] It is observed that the reductive state of Cu as the active site could be stabilized via S doping, the in situ Raman spectroscopy results confirmed the CO_2RR mechanism involves the variation in adsorption state of CO_2^- intermediates

from coexisting O^*CO^- and OC^*O^{*-} to the dominating OC^*O^{*-}. Density functional theory (DFT) calculations confirmed that intermediate binding energy on S-doped Cu(111) surface is lower than that on the undoped sample. The performance of this electrocatalyst reaches 76.5% of the highest Faradaic efficiency and a maximum partial current density of 21.06 mA cm^{-2}.

Recently, textural properties of catalysts are also considered to alter the reaction kinetics/mechanism toward the selectivity of products and porous materials are getting specific attention due to their properties such as improvement in surface-to-volume ratio and active sites, tunability of pore structure for mass transport of reactants/products, and controlled local pH.[86,90] For example, He and coauthors used self-assembly of two polymers to prepare hierarchically mesoporous–macroporous (320 and 20 nm) Cu/Zn alloys and results showed that Cu_5Zn_8 exhibits the better performance for CO_2 reduction to ethanol (46.6% at −0.8 V) with good stability for 11 h.[71] The decrease in the pore size from 300 to 30 nm enhanced the FE from 8%–38% with ethylene as a key product. Further, the nanostructure of electrocatalysts also has a significant effect on the CO_2RR performance, for example, Au and SnO_2 with similar morphologies showed similar effects during CO_2RR.[88,91] Yang et al. proposed the morphology-dependent reaction kinetics for CO_2 conversion into C2 products.[84] They used a Cu-based mesoporous catalyst with precisely controlled size (morphology) and showed that morphology has an effective role in accelerating the C—C coupling and prolonging retention times by controlling the pH and flow field.[84] Being highly tunable surface area and porosity with series of nanostructures, MOFs are very attractive for CO_2 electrocatalysis and widely studied. For example, 2D Bi-based MOF with accessible porosity showed better performance for CO_2RR with 92.2% FE at −0.9 V versus reversible hydrogen electrode (RHE) and durability of 30 h. The mass-specific HCOOH partial current density is up to 41.0 mA mg$_{Bi}^{-1}$, exceeding four times higher than that of commercial Bi_2O_3 and Bi sheets at −1.1 V (vs RHE).[92]

Therefore, MOF-based catalysts are summarized for improved performance of CO_2RR based on following parameters to monitor the efficiency of an electrocatalyst: 1) low fabrication cost of materials; 2) large FE for a specific product; 3) durability of catalysts for long-time operation; and 4) large current density and low over-potential.

3. Pristine MOFs for CO$_2$RR

MOF-based electrocatalysts, which combine the beneficial properties of homogeneous and heterogeneous materials,[93] have been studied as a new class of typical catalysts to understand the reduction of electrochemical carbon dioxide. In 2012, the first MOF-based electrocatalyst was prepared and applied for CO_2RR,[42,43] and CR-MOF (copper rubeanate MOF) carried out for CO_2 reduction into formic acid with 100% FE.[42] In the same year, Senthil Kumar et al.[43] used Cu–BTC (1,3,5-benzenetricarboxylic acid [BTC]) thin film deposited on glassy carbon electrode in N,N-dimethylformamide (DMF) for CO_2RR and oxalic acid was observed with 51% FE as a major product. These two pioneer studies showed that two factors are important 1) density of active sites (metal center) and 2) electronic environment (ligand) for efficiency and product selectivity, respectively.

Recent approaches, such as increasing the thin layers of MOF in porous 3D structures can be considered as more effective ways to develop in situ electrocatalysts to reduce CO_2. These porous structures have actively created electrocatalytic centers on large sites and along the edges of the material. The controlled adjustment of the MOF structure is useful for the formation of dendrites with higher catalytic activity to convert CO_2. In the latter case, the combination of Cu(II) and MOF porphyrin wheels (Cu_2(CuTCPP)) in nanosheets, which showed good performance and selectivity for CO_2 conversion into formate and acetate (**Figure 2**a,b).[94] The calculated FE for the formate production was 68.4% at the −1.55 V, whereas the C—C coupling at −1.40 and −1.62 V resulted in the formation of acetate with 38.8–85.2% FE. However, the spectroscopic results revealed that Cu_2(CuTCPP) was converted into Cu_4O_3, Cu_2O, and CuO, which considerably catalyzed CO_2 to acetate and formate.
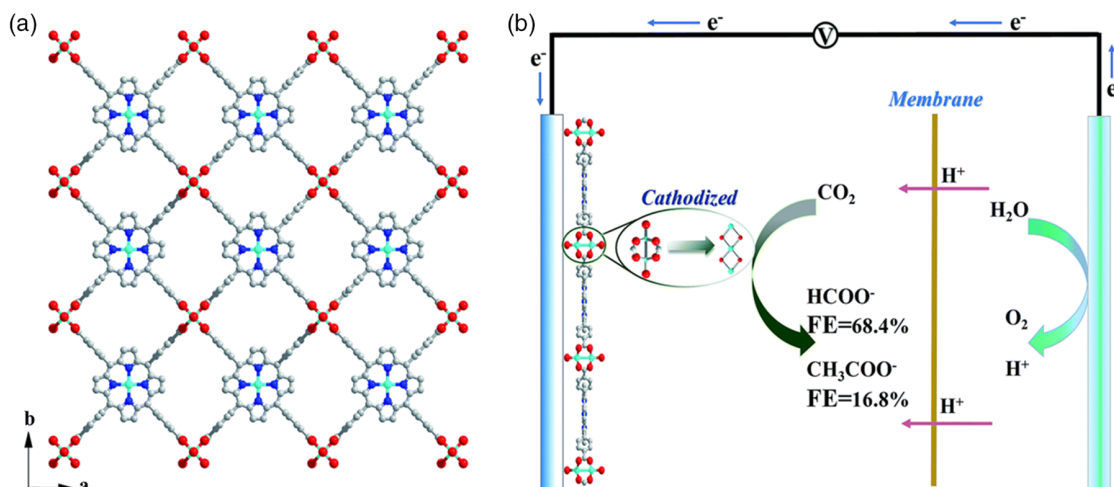
Figure 2. a) Representation of Cu_2(CuTCPP) crystalline nanosheets; b) Cu_2(CuTCPP) nanosheets as the electrocatalyst for CO_2 electrochemical reduction system. Reproduced with permission.[94] Copyright 2019, Royal Society of Chemistry.

In addition to Cu, other inorganic active centers such as Co, Ni, and Fe are also used to synthesize MOFs with potential CO_2RR performance. For example, the Fe–porphyrin incorporated in the thin MOF-525 membrane had a high performance toward CO_2RR, resulting in ≈100% FE, which benefited the conversion of CO_2 to CO.[95]

With the reduction of carbon dioxide by MOFs, there has been a constant growth in the area of MOF-based catalysts, however, a number of challenging features, including the effective strategy of new MOFs with high efficacy, many redox active sites, selectivity and long-term stability, which still required to be constantly discovered.[96] Preceding studies have confirmed that two factors can be boosted 1) redox potential ($E°$) for electron transmission and 2) a number of chemical reactions (conversion of CO_2 to product) in homogeneous catalysts, through ligand design and sensible selection of metal centers.[97] Therefore, tuning of the metal centers and ligands in MOFs are also proved approaches for the enhancement of catalytic activity.

3.1. Role of Metal (Inorganic Moiety)

A typical CO_2RR process is assumed that a simple cathodic voltage is mandatory and most probably, the metal center is an active site to reduce carbon dioxide. The majority of electrocatalysts used so far, actually act as precatalytic converters, in electrochemical CO_2 reduction. Active metal sites are usually either oxidized or reduced during the catalytic process, so the actual active sites differ from those detected before the catalytic process.[98] For instance, among various metals, copper oxide–derived copper is widely studied due to its inherent selectivity towards CO_2RR. Similarly, in MOF, Senthil Kumar et al.[43] testified Cu–BTC thin films on glassy carbon electrodes by cyclic voltammetry in 0.1 M KCl and distinct Cu(II)/Cu(1) and Cu(I)/Cu(0) reversible redox response was detected. Chen and coworkers[98] described the phase transitions of Cu–electrode using in situ X-ray absorption spectroscopy (XAS), and also explored the dynamic oxidation state and the local structure. The formation of metallic Cu(0) is an important step to produce hydrocarbons/alcohols instead of Cu(I) and the competing oxidation reaction of Cu(0) governed the chemical state of CO_2RR active sites. Furthermore, the Raman spectroscopy (in situ) verified the reoxidation reaction which is dominating in the chemical state of copper (**Figure 3**a). Furthermore, Sargent and coworkers[99] studied the overtime of Cu reduction and examined the ratio of Cu species at varying potentials using in situ XAS (Figure 3b), and therefore suggested the significant relationship between the surface state of Cu and the product profile, and found that the presence of Cu^+-stabilized ethylene intermediates. To further explore active sites in other metal-based MOFs, Yaghi and coworkers studied cobalt oxidation states in Co–MOF thin films using in situ spectroelectrochemical measurements during the CO_2RR.[100] The study showed that most centers are redox available and Co(II) is reduced to Co(I) during the CO_2RR, which disclosed that Co reduction is the first step toward reaction mechanism. If Co is reduced to Co(I), then CO will be formed because of CO_2 adsorption on the central metal atom. However, MOF-derived catalysts with metallic active sites did not show this type of transition during the catalytic process. Recently, Hu and coworkers[101] reported an excellent Faradaic efficiency toward CO with extremely low overpotential exhibited by Fe-based single-atom catalyst (SAC). Further, in situ XAS analysis exposed the active species as isolated Fe^{3+} ions coordinated with pyrrolic-N atoms, and capable of maintaining their +3 state during electrocatalysis. In addition, the role of metal center was also determined experimentally over Co-, Ni-, and Zn-impregnated MOF-74 and Zn-center carried out the electrochemical CO_2 reduction 78.3% at −0.91 V versus RHE and selective H_2 production by Co- and Ni–MOF-74 with no carbon product.[102] Further, inorganic modifications have also been shown to affect the selectivity and activity of CO_2RR on the Zn–MOF catalyst. Wang et al. fabricated a number of Zn-based nanomaterials (ZIF-8) via introducing different sources of zinc as a reactant and examined the different effects of zinc to reduce carbon dioxide into CO.[103] Results showed that ZIF-8 synthesized using $ZnSO_4$ produces better catalytic performance to reduce CO_2, with a high FE to CO (FE_{CO}) 65% and total current density
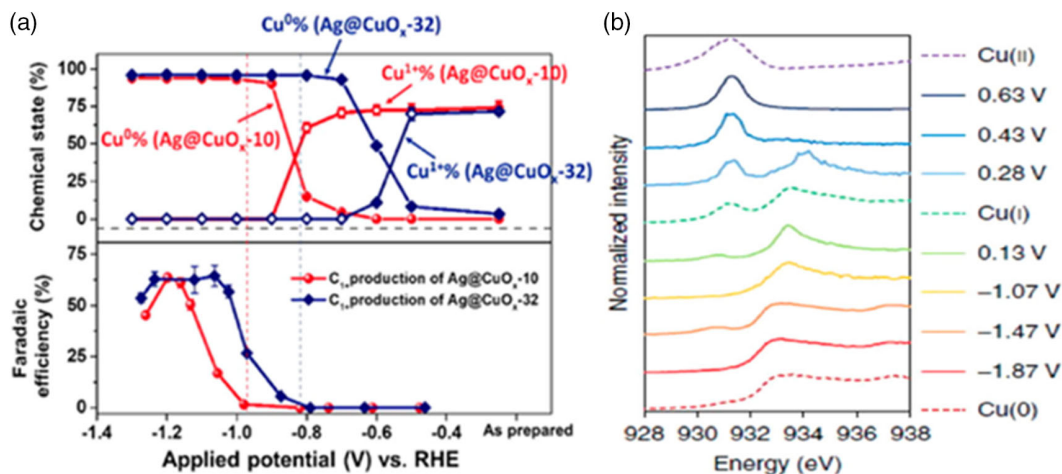
Figure 3. a) Identification of chemical states of copper attained through in situ XAS as a function of applied potential. Reproduced with permission.[98] Copyright 2019, American Chemical Society. b) In situ Cu L3-edges, XAS spectrum of electro-redeposited (ERD) copper at varying applied potentials (solid lines). Reproduced with permission.[99] Copyright 2018, Springer Nature.

ADVANCED
SCIENCE NEWS
www.advancedsciencenews.com

small
structures
www.small-structures.com

(j) ≈ 3 mA cm^{-2}, creating a link between CO_2 activity and Zn precursor, and claiming that the key active species are distinct Zn nodes in ZIF-8. High and selective ZIF-8 activity with SO_4^{2-} can be attributed to smaller interactions between SO_4^{2-} and Zn nodes, which assist the anionic exchange of charge balance when the oxidation state of Zn node is being altered. In contrast, some studies reported that due to the completely filled 3 d orbital of Zn(II) in Zn-based complexes or MOFs, the metal centers are not active sites for the CO_2RR process.[104–107] For instance, Jiang et al.[106] recognized using in situ XAS and DFT that imidazole coordinated with Zn(II) center in zeolitic imidazole framework (ZIF) act as catalytic sites for CO_2RR.

Hence, the identification of actual active centers in MOFs is still debatable and requires more deep studies to solve this puzzle. The in situ or operando analysis has played a vital part in pursuing dynamic progression during electrocatalysis, recognizing the actual active sites and helps in understanding the mechanism. However, great efforts are still highly desired for developing next-generation electrocatalysts with the guide of powerful in situ techniques.

3.2. Role of Linker (Organic Moiety)

Ligands have strength to alter the catalytic performance of MOFs, for instance, a ligand with electron donating capability can enhance the activity of MOF via encouraging the movement of electrons from the active sites toward the antibonding orbitals of CO_2, which results in generating *COOH via proton coupling.[107] Keeping this point of view, various studies have been carried out to test the effect of surrounding ligands in MOFs for CO_2RR. In this section, we have discussed the ligand effect on catalytic performance categorically, i.e., micro- and macroligands.

The influence of ligands on the CO_2 reduction product was observed in the pioneering work of MOF-based catalysts. Noticeably, the Cu center is active for CO_2RR but two Cu–MOFs reduced CO_2 to various products, due to the presence of different ligands attached with the same metal (Cu) center.[42,43] When the ligand having O donor atoms was used by Senthil Kumar et al.[43] the CO_2 conversion product was oxalates, whereas Hinogami et al.[42] reported N- and S-containing donor atoms and the formic acid as the reaction product. This difference in ligands could modify the electronic configuration of the metallic active center leading to different conversion products. This factor was also further studied for CO_2RR by synthesizing four Cu-based MOFs, i.e., 1) Cu–BTC (HKUST-1); 2) Cu-Adeace; 3) Cu–dithiooxamidate (DTA) mesoporous metal–organic aerogel (MOA), and 4) CuZn–DTA, MOA supported on gas diffusion electrode.[108] The cumulative maximum FE (15.9%) for the CO_2RR was measured with Cu–BTC-based electrodes with a current density of 10 mA cm^{-2}. The MOFs with unsaturated (USA) metal sites have been shown to contribute for CO_2 reduction into alcohol. In addition, the Cu–BTC catalyst showed stable electrical output for 17 h. In this decade, ZIF has proven to be a flexible catalyst and is particularly known for high adsorption properties for CO_2, which is an attractive feature of carbon dioxide catalysis as this suggests that the diffusion of carbon dioxide is enhanced leading to more interaction with active sites. ZIF-8, a typical MOF prepared by Jiang et al.[106] and

confirmed with XAS measurement and DFT calculations that coordination of imidazole ligand with Zn(II) in ZIFs are actually the active catalytic sites for CO_2RR. Further they examine a group of ZIFs with the same sodalite topologies but various organic ligands such as ZIF-8, ZIF-108, ZIF-7, and SIM-1 for CO_2RR in aqueous electrolyte, interestingly, ZIF-8 had a higher FE$_{CO}$ 81.0% at -1.1 V versus RHE among all catalysts, however, 12.8 mA cm^{-2} of current density at -1.3 V versus RHE was achieved over ZIF-108. The Fe-based porphyrin catalysts belong to the highly efficient class of homogeneous catalysts, first established by Savéant and coworkers,[109] and have been widely used in CO_2RR.[110–112] In view of homogeneous use of Fe–porphyrin, a porphyrin-based component considered to be transmitted within the structure of MOF for two scientific aims: 1) the potential use of MOFs for electrocatalysis with developed electron-transfer abilities are essential for CO_2RR; 2) modifying the catalytic structure by the insertion of the active molecule with characteristics including surface control, tunable porosity, and access to active sites, as well as chemical stability.[113] Furthermore, the immobilization of MOFs on conductive support can also enhance the electronic conductivity, which is the utmost necessary part of electrocatalysis. For example, Hod et al.[95] incorporated Fe–porphyrin into the MOF-525 and used as a catalyst for CO_2RR, the incorporated structure was confirmed by the X-ray diffraction (XRD) (**Figure 4**a,b). The method produced a mixture of CO and H_2 (FE$_{CO}$ = 50%) and this catalytic activity is accredited to the electrochemical surface area of Fe–porphyrins, these results showed that Fe–porphyrins incorporated on the surface of MOF are accessible for CO_2RR (Figure 4c,d).

Furthermore, Co atoms, coordinated in the porphyrin ring, are also observed as catalytic active sites for CO_2RR. For example, Yaghi and coworkers synthesized a porphyrin-based MOF with Co as metallic center and named as $Al_2(OH)_2$TCPP-Co, whereas H_4TCPP = 4,4′,4′′,4′′′-(porphyrin-5,10,15,20-tetrayl)-tetrabenzoic acid and tested its performance for CO_2RR.[100] The catalytic performance with enhanced current density and FE$_{(CO)}$ (76% at -0.7 V vs RHE) confirmed that Co is the active site, whereas the aluminum is directly linked with oxygen atoms in the carboxylate moiety. In addition, authors claimed that Co(II) metal centers are not actually active sites but Co(I) are responsible for CO_2 reduction into CO.[100] These primary experiments revealed that the CO_2RR performance of MOF-based electrocatalysts can be tuned by changing the ligands.

3.3. Role of Metal-Linker Bonding Strength

Further, the ability of MOFs for long-standing resistance against chemical environments, "chemical stability" is also important for electrocatalytic applications, which is dependent on the strength of metal-linker bond in the MOF's network. The thermal stability and mechanical stability of MOFs usually correlate with the ability of MOFs to preserve their structural integrity upon exposure to heat, vacuum, or pressure treatment.[21] As the MOFs are largely used in electrolytes during electrocatalysis with varying pH, fixing the MOFs' stability with wide range of pH is significant. For example, highly stable Bi–MOF was reported as an efficient electrocatalyst for CO_2RR to produce formic acid with 92.2% FE at -0.9 V versus RHE and high stability of 30 h.
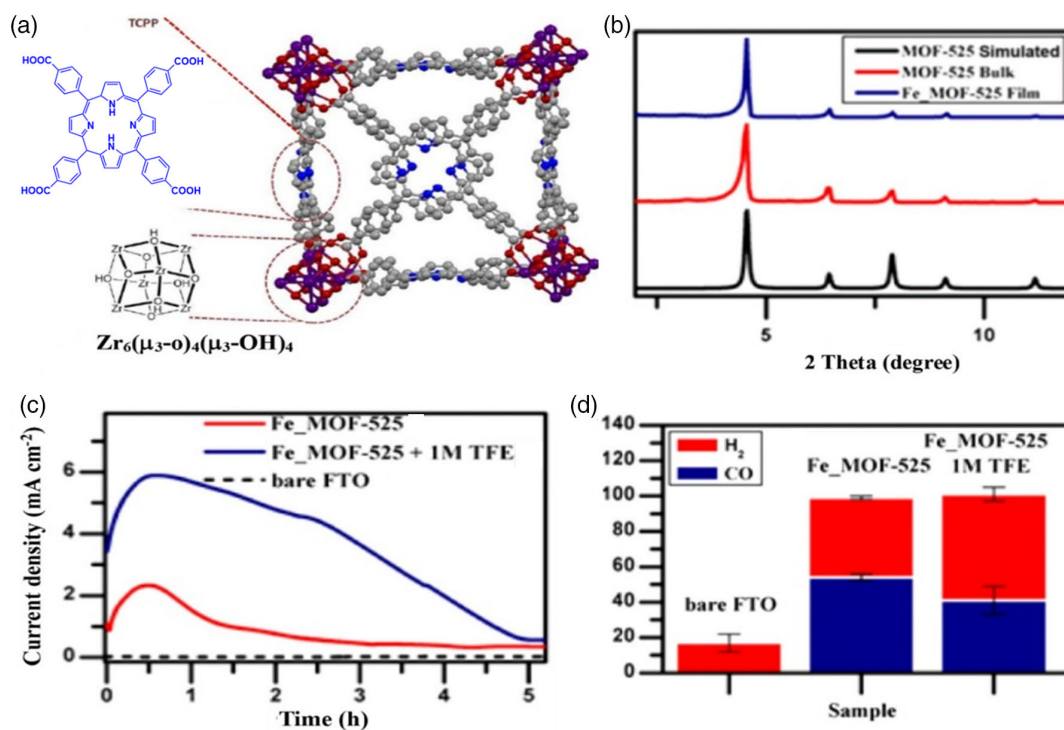
Figure 4. a) The chemical structure of metal node and the crystal structure of MOF-525; b) The PXRD results of MOF-525 and Fe–MOF-525 film; c) current density versus time at varying conditions; d) Faradaic efficiency over about 4 h of electrolysis. Reproduced with permission.[95] Copyright 2015, American Chemical Society.

The highest partial current density (14.0 mA cm^{-2}) for HCOOH was observed at low overpotential (0.61 V) in 1 M KOH. The in situ and ex situ X-ray absorption fine structure spectroscopy further revealed a structural feature associated with Bi–MOF to preserve Bi (3+) during and after long-term CO$_2$RR, indicating the electrochemical stability of Bi–MOF.[92] In another study, Bi–BTC-D MOF was synthesized using conventional hydrothermal method for CO$_2$RR. The Bi–BTCD was found to be effective and stable catalysts for formate production with 90–95.5% FE over a wide range of potential windows with an average FE of 93%. After the continuous operation of 12 h, the FE was observed 90%, which may be attributed to the high electrochemical stability of MOF structure.[114] A cobalt–porphyrin MOF was used for CO$_2$RR with better initial performance (76% at −0.7 V), however, the reported stability was only 7 h.[100] Similarly, Zr-based MOF-525 with Fe–porphyrin units was used for CO$_2$RR, the activity of this Fe–MOF decreased during the 4 h of reaction, pointing that stability is still a key challenge for this type of catalysts.[95] Despite the considerable efforts have been devoted to the synthesis of new MOFs with high stability using different methods. There is still need to expand further research for enhancing the stability of MOFs as well as the systematic elucidation of catalytic degradation. For this purpose, more postanalysis characterization is required to check the structural features such as composition, electronic structure, and morphology.

4. Functionalization of MOFs for CO$_2$RR

In MOF chemistry, functionalization permits structural modifications in materials to incorporate the new functions without

rescinding or altering the structure.[115,116] These functionalities can be incorporated in situ during the synthesis of MOFs and/or some postsynthetic procedures are used to enhance the functions.[117] The postsynthetic strategies are involved incorporation or exchange of targeted metal ions and organic linker-based functional groups or metal nanoparticles (NPs) in the pores of MOFs.[115,118–120] In addition, MOFs are notorious for their low electric conductivity, therefore, to enhance the conductivity of MOFs, several strategies such as donor–acceptor interaction, redox matching, mixed valences and some others, have been applied. In addition to the improvement in intrinsic conductivity, the MOFs in contact with electron collecting substrates for example glassy carbon (GC), metallic (Au, Cu, Ni, and Ag) foils/foams, fluorine-doped tin oxide (FTO) and/or indium tin oxide (ITO) glass, are also widely used.

4.1. Linker Functionalization

Metal centers are usually considered as active sites for CO$_2$RR in MOFs, the modification or addition of coordinated ligands can tune the electronic structures of metal centers and enhance the catalytic performance. For example, porphyrin-based molecular electrocatalysts have been extensively utilized in CO$_2$RR.[110–112] Thus a porphyrin like a ligand can be considered within the consensus group (MOF) for scientifically two main causes: 1) manipulating the potential of MOFs for electron transmissions; 2) the introduction of an active molecule into the catalyst structure which acts as a front electrode with surface control properties such as balanced pores and active sites availability, as well as permanent

**ADVANCED
SCIENCE NEWS**

www.advancedsciencenews.com

**small
structures**

www.small-structures.com

porosity and chemical stability.[113] In addition, electroactive porphyrins as ligands are also utilized for the formation of MOF. Dong et al.[121] presented a Fe–TCPP porphyrin to prepare PCN-222(Fe) as CO_2RR electrocatalyst. The PCN–222(Fe)/C (1:2 of mass ratio of MOF and carbon) revealed better catalytic performance in aqueous electrolyte with 91% FE following the current density of $1.2 \, mA \, cm^{-2}$ with only 494 mV overpotential, attaining $0.336 \, site^{-1}s^{-1}$ of TOF. The Cu–MOF-based porphyrinic nanosheets were used by Wu et al.[94] for CO_2RR and results were interesting due to the production of formate and acetate. The major product was formate at -1.55 V with 68.4% FE while the acetate was prepared at 1.40–1.65 V with 38.8–85.2% FE.

The increasing charge density on the active sites is an effective approach for boosting the CO_2RR performance. In this aspect, an approach has been proposed via post-treatment step to induce more electron density on the ligand sites of MOFs. During the doping of new ligand, a robust electron-donating ability generated on the MOFs which induces supplementary charge density on the neighboring original ligand sites results in boosted CO_2RR activity. Although, functionalization or ligand doping of MOF-based materials have exhibited enhanced performance for photocatalytic reduction of CO_2,[122] however, the research work on designing the charge density of active sites by ligand modification is still at an initial stage.

Further than the tuning of the electronic structure of catalysts, the incorporated ligands may also act as a coactive site for CO_2RR. The activated linear CO_2 molecule by adsorbing electron is considered as rate-determining step,[123] and the introduction of ^-OH in MOF structure is helpful for linear molecule activation. This step may be easily activated because ^-OH can coordinate with an electropositive metallic center of MOF and the ^-OH captured on the surface of MOF activates the CO_2 in the form of HCO_3^- chelated with a metal center. The coordinated ^-OH is responsible for the transformation of single crystal to single

crystal–CO_2 (NNU-15 to NNU-15-CO_2), as shown in **Figure 5**a,b, and produces HCO_3^- as an intermediate product during CO_2RR. The DFT calculations further confirmed that O- and C-adsorbed showed inclined geometries toward HCO_3^- formation because of ^-OH as presented in the anticipated mechanism (Figure 5c).[124]

Further to these structural effects, the organic ligands in MOFs have also been functionalized for enhancing the CO_2RR performance. Generally, the poor conductivity of MOFs is considered a major obstacle for catalytic applications, so, Dou et al.[107] enhanced the charge transfer ability of MOFs using ligand-doping method, thus enhancing the performance of catalyst to CO_2RR. During this study, 1,10-phenanthroline molecule with the robust ability of donating electrons is used to introduce in the ZIF-8 framework for CO_2RR electrocatalysts. The ligand-doped ZIF-8 showed a remarkable enhancement in CO_2RR performance with 90% production of CO. This outstanding performance was attributed to the electron-donating ability of doped ligand (phenanthroline), which facilitates the transfer of charge and assists the formation of *COOH intermediate, finally the resultant catalyst acts much better than pristine ZIF-8. Similarly, Xia and coworkers[125] also reported the dual Cu–adenine MOF with acetic acid doping (s-Cu-ade MOF), adenine and acetic acid ligands were directly coordinated with Cu metallic nodes. The CO_2RR on the prepared catalysts showed better performance with methane and ethane as major products with 73% FE at -1.6 V versus RHE.[125] These studies provide an evidence that linker functionalization can alter the CO_2RR performance by acting as active site or changing the electronic structure of central metal.

4.2. Metal Cluster Functionalization

In electrocatalysis, the "active sites" are termed as the surface where three-phase interaction is taking place, thus active sites
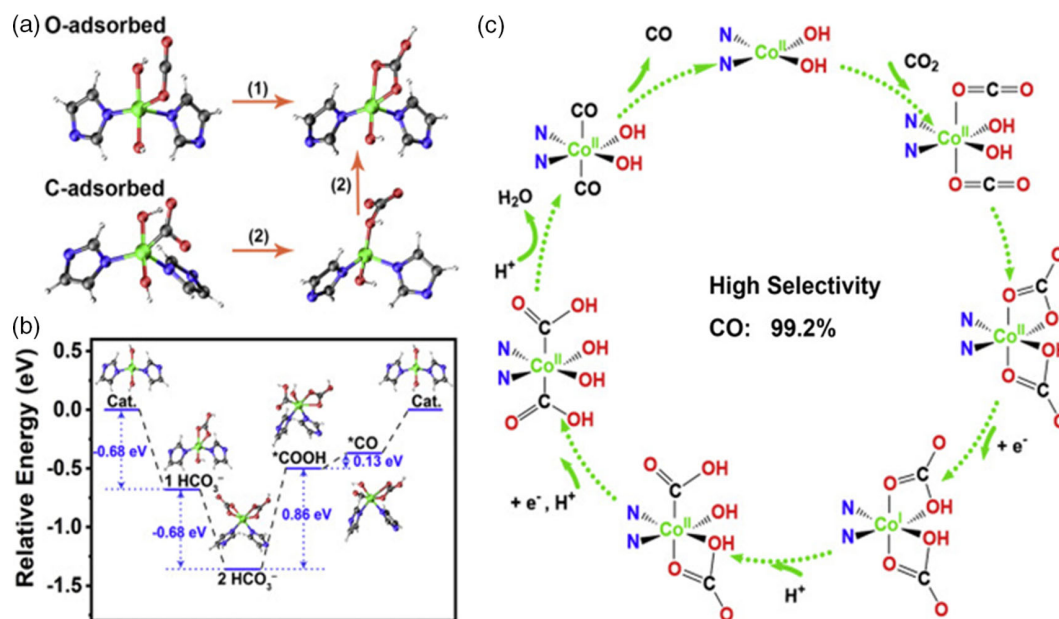
Figure 5. The proposed mechanism of CO_2RR, calculated by DFT calculations, a) CO_2 adsorption. b) free energies during CO_2RR in NNU-15. c) anticipated mechanism of CO_2RR on the surface of NNU-15. Reproduced with permission.[124] Copyright 2019, Elsevier.

**ADVANCED
SCIENCE NEWS**

www.advancedsciencenews.com

**small
structures**

www.small-structures.com

are playing an important part during electrocatalysis of CO_2RR.[126] By improving the performance of these active sites, the overall activity of catalysts can be increased and vice versa. As the catalytic process occurs at the surface of the catalyst, therefore, the surficial exposed active sites are considered more reliable. There are several methods reported to explore/enhance the active sites of MOFs, we have summarized these strategies by considering in two main categories, i.e., enhancing the number of active sites and intrinsic activity. In MOFs, the coordinated unsaturated sites (CUSs) are considered as more active sites for catalytic reaction, however, the coordination number (CN) of metals fully saturated with ligands limits the catalytic performance of MOFs.[18,127] Accordingly, building geometry with sufficient CUSs is instantly required for the enhancement of electrocatalytic performance of MOFs.[4,38] Further, constructing the ultrathin MOFs having larger surface exposure along with producing dangling bonds by eliminating the ligand's portion via ligand engineering on the MOFs, could be a favorable approach for boosting the catalytic active sites on MOFs. To improve MOF's catalytic activity, it is therefore imperative to create geometry with many CUSs. During the catalytic process, the reduced CN or CUSs are accessible for reactants and act as active sites. Though these active sites are available in less

density, it is still an emerging method to increase the catalytic activity of MOFs. As compared with single-metal-site, multimetal-site catalysts are more encouraging for CO_2RR. For example, Li and coworkers[128] reported a diatomic paired Cu_1^0–Cu_1^{x+} catalysts and the presence of Cu—Cu bond was confirmed by EXAFS analysis. Speculative findings proposed that the Cu_1^0 site motivates the CO_2 adsorption and the adjacent Cu_1^{x+} favors H_2O. These atomic pairs work collectively for CO_2 reduction, with improved FE than single Cu sites (**Figure 6**a,b). In addition, heteropaired multimetallic-based electrocatalysts also displayed enhanced catalytic performance similar to homopaired multimetallic-based electrocatalysts. Furthermore, Zhao and coworkers[129] described the effect of synergism in the isolated Ni–Fe diatomic pairs on NC supports, which reduced the reaction barrier for converting CO_2 to CO. Zhu et al.[130] also investigated the electronic effect between two neighboring metal atoms, the Zn atom of diatomic Zn–Co displayed the low energy in both *COOH adsorption and *CO desorption than Co or Zn dimer (Co/Co or Zn/Zn atoms). Therefore, the Co atoms could act as the active sites for *COOH adsorption and *CO formation, in the meantime, the neighboring Zn atoms adsorbed *CO and finally desorbed CO.[130]
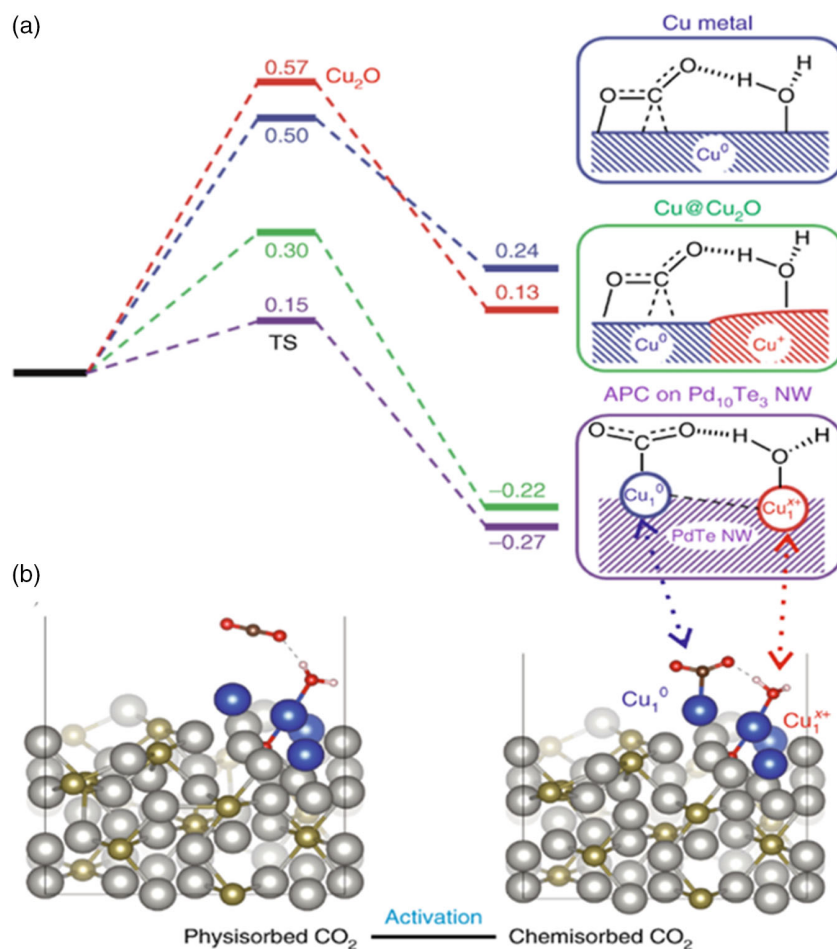

Figure 6. Free energy profiles for CO_2 activation mode. Reproduced with permission.[128] Copyright 2019, Springer Nature.

The incorporation of various metal centers into MOFs with synergism can also confirm a greater selectivity to certain CO_2RR products. Recently, Feng et al.[131] presented an efficient electrocatalyst for CO_2 reduction using 2D MOF containing copper-phthalocyanine and zinc-bis(dihydroxy) complex as ligand and nodes (**Figure 7**a,b). Operando XAS following the theoretical calculations confirmed that ZnO_4 are the main active sites for CO_2RR and CuN_4 works as a support to enhance the mass transport (transfer of electrons and protons), thus synergistic effect between two species controls the ratio of products and produces syngas (Figure 7c,d).[131]

The metal atom has a prominent role in the catalytic performance and introduction of secondary metal synergistically enhanced the catalytic performance. Today, the physical effect between dual metallic sites is highly desirable but rarely reported, which possibly offers great opportunities for further research.

4.3. MOF Composites

As the pristine MOFs are notorious for their low electrical conductivity, various MOF-composites with conductive materials (carbon black, graphene oxides) are widely used for CO_2RR.

MOFs can also be used as a support for several species (guest–host interaction) that can be inserted or connected to a frame, such as metal complex/NPs or even biomolecules such as enzymes. In these cases, MOF serves as a means of providing great stability and porosity to deliver scaffolding with limited spaces, resulting in size-selective catalysis.

4.3.1. MOF Composites with Polyoxometalates

The structural tenability of MOFs provides more possibilities to enhance the characteristics properties. The combination of various MOFs with crystalline porous materials has more construction diversity. Therefore, recent researches offer high potentials for such materials for a wide range of applications. For example, MOF@MOF assembled from MOFs with different apertures can serve as molecular sieves for selective adsorption and separation, in which core MOFs with large pores perform as a cargo transport highway and shell MOFs with small pores act as a filter and also enhanced the catalytic performance.[132] Thus, the intrinsic diversity of MOFs is considered, the combination of MOFs and MOFs displays an excessive improvement panorama no matter in synthesis, design of structure, or application. The large pores of
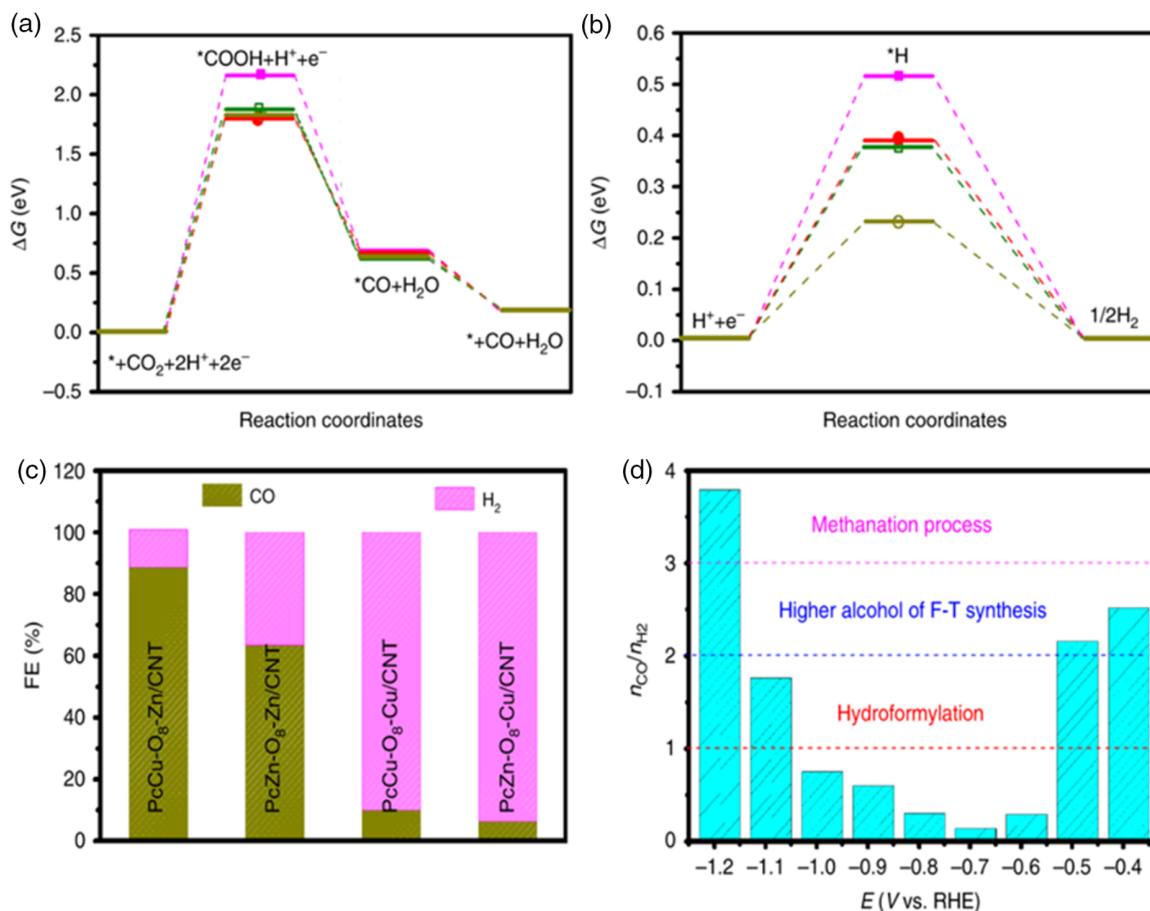
Figure 7. a,b) Representation of energy profiles for CO_2RR and HER on M–N_4 sites in PcM-O8-M1 at $U = 0.0$ V, respectively. Inset in a): atomistic structure of PcM–O_8–M1. c) Faradaic efficiency of CO and H_2 for PcCu–O_8–Zn/CNT, PcCu–O_8–Cu/CNT, PcZn–O_8–Zn/CNT, and PcZn–O_8–Cu/CNT at −0.7 V versus RHE. d) Molar H_2/CO ratio at different applied potentials of PcCu–O_8–Zn/CNT. Reproduced under the terms of the Creative Commons CC BY license.[131] Copyright 2020, Springer Nature.

ADVANCED
SCIENCE NEWS
www.advancedsciencenews.com

small
structures
www.small-structures.com

UiO-66-NH$_2$ (0.6 nm) were used to overlap with the pores of ZIF-8 (0.4 nm) to produce an incommensurate combination (MOF@MOF) produced smaller pores at the interface by improving the molecular sieve performance.[133] Using crystalline porous materials such as covalent organic framework (COF), the following properties are precisely controlled on the basis of principle designs in reticular chemistry: 1) active molecular building block can be prearranged for connecting structures; 2) the post-treatment route would be used for functionalization without altering the topological framework; and 3) availability of resources such as pores, influencing the mass transfer mechanism can be adjusted electronically. These aforementioned features of the catalyst-based reticular coordination offer the possibility of realizing a multifactorial nature, which can exceed the sum of the individual molecular parts.[112]

Postsynthetic modifications are generally considered superior and easily applicable as compared with the preassembly or in situ synthetic strategies. The postsynthetic modifications, especially composite materials are famous for the wide range of reactions involving electron-donating entities. Polyoxometalates (POMs) are a well-known class of nanomaterials, containing metal-oxygen clusters and electron-rich aggregates also called electro sponges. The transportation of electrons can be facilitated by incorporating POMs into MOFs channels and finally the performance of the active site can be improved. For example, Lan and coworkers[134] reported POM@PCN-222(Co) composite by combining the electron rich structure of POM and high surface area of MOF (**Figure 8**). As expected, the electron transfer property of composite material was considerably improved and a particular composite named H-POM@PCN-222(Co) showed better CO$_2$RR performance with 96.2% FE$_{CO}$ at -0.8 V versus RHE and stability of 10 h. Further, DFT calculations revealed that Co single sites in PCN-222(Co) were improved by directional electron transfer in the composite and reduced the energy barrier for the rate-determining step.

4.3.2. MOFs on Conductive Supports

MOFs are limited in electrochemical application due to their inherited low conductivity. Incorporating MOFs on conductive support can also yield materials with improved CO$_2$RR activity. For example, an aluminum porphyrin MOF-55 was synthesized containing co-porphyrin as an active site for CO$_2$ reduction to CO. The atomic layer deposition (ALD) method was adopted to form a conductive aluminum oxide thin film, which also
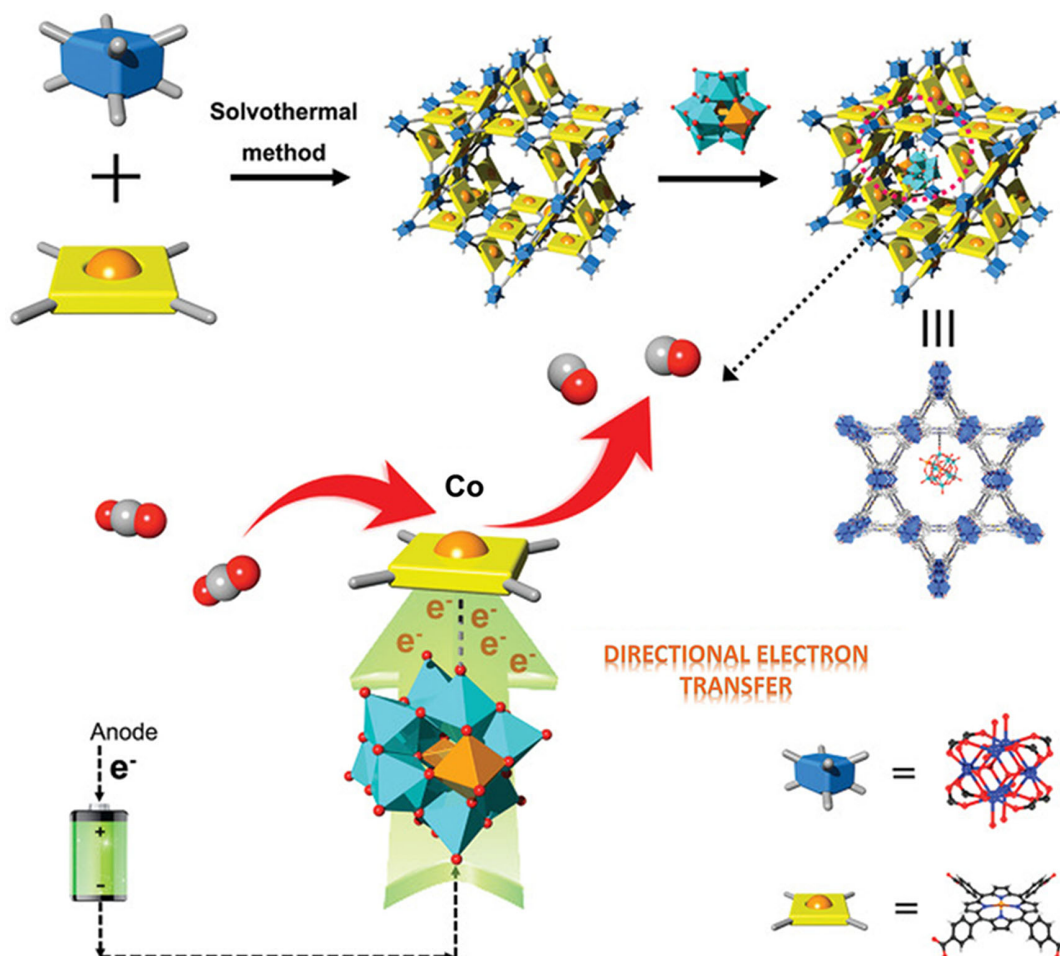
Figure 8. Synthetic and detailed structure of composite including electron transfer from POM to MOF structure. Reproduced with permission.[134] Copyright 2021, Wiley-VCH.

served as metal precursor, following successive MOF formation via reacting coated alumina with a linker.[100] The precursor's thickness can be simply controlled by the number of ALD cycles, which regulate the thickness of the catalyst layer. The activity of resultant MOF catalyst was primarily enriched by maximizing the thickness of film to 2.8 mA cm^{-2}, thus a higher power showed the exchange between electrons and mass transportation. The optimized thickness of catalyst (5 nm) presented the CO production of FE up to 76% for 7 h test. Further, Wu et al.[94] used FTO glasses as conductive support and $Cu_2F(CuTCPP)$ nanosheets were cathodized, the catalyst showed better performance for CO_2RR, resulting formate as product at −1.55 V versus Ag/AgCl with 68.4 % of FE. The layered structure of Re-SURMOF was also deposited on the FTO surface via layer-by-layer growth using high-throughput automated spray system (**Figure 9**a,b). The high FE_{CO} (93–98%) was attributed to the well-oriented layered sheets of MOF which can facilitate charge transport (Figure 9c,d). However, the degradation of $Re(CO)_3Cl$ complex is considered as the major cause of expected low stability of catalysts (Figure 9e). Therefore, it is urgent to improve the stability of catalysts for further practical applications.[120]
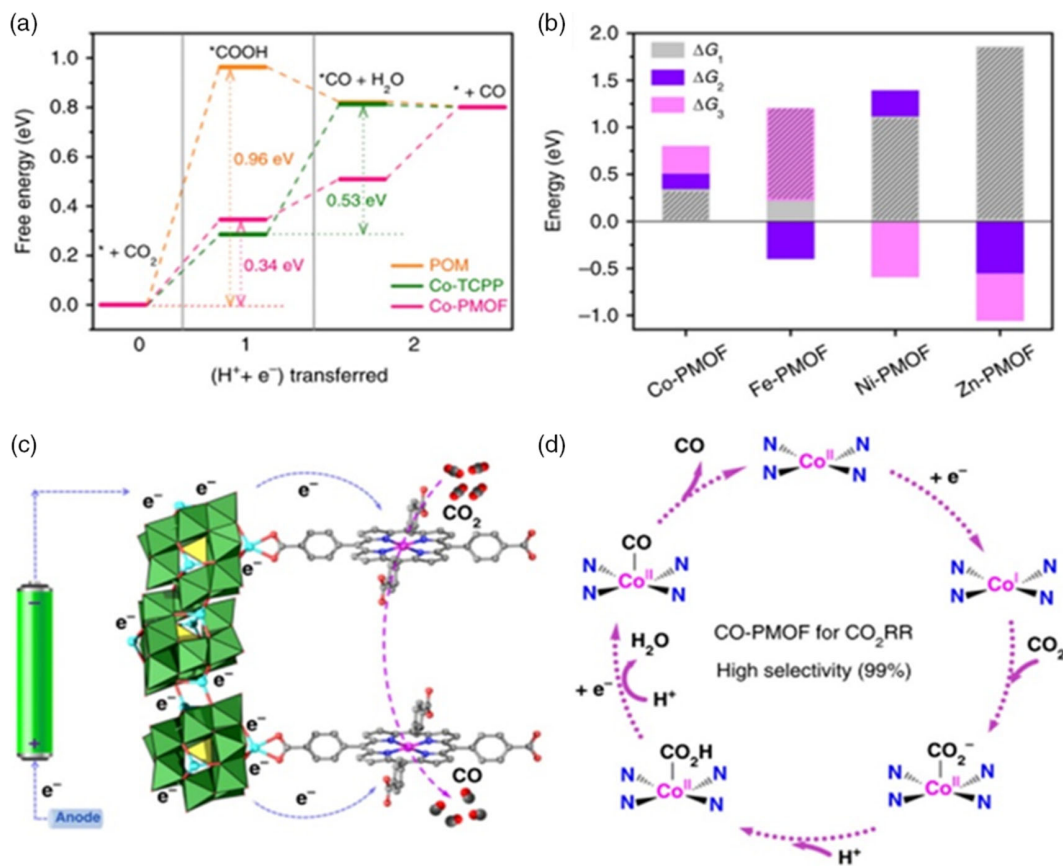
4.3.3. MOF-Supported Active Catalysts

It was observed that the highly porous MOFs offered much needed surface area for the high distribution of active sites, which allowed the increased transport of CO_2 and charge transfer, leading to greater reduction activity. Recently, Buonsanti and coworkers[135] revealed that colloidal crystals can be combined with the MOF (Al-PMOF) to create a hybrid platform (Ag@Al-PMOF) for the active conversion of CO_2 into CO. The authors claimed that this hybrid has more capability to suppress the HER but helping the CO_2RR at the same time as compared with Ag nanocrystals alone. Furthermore, the synergistic effect between the silver nanocrystals and Al-PMOF resulted in high electronic properties by partial removal of native MOF ligands. Lan and coworkers also reported that the synergistic effect of POMs to Co-porphyrin also enhanced the catalytic performance with 99% FE of CO production in 0.5 M $KHCO_3$ electrolyte.[136] The adsorbed free energies were found to be less for *CO and *COOH (intermediates) by DFT calculations, which further verified that Co-PMOF is a better choice for CO_2RR (**Figure 10**a,b). Following by the previous concept, this study again confirmed that Co atoms in the Co-porphyrin are the major active sites while POMs having electron-rich aggregates are helping to enhance the electronic transport. (Figure 10c,d).

In another study, Wang and coworkers[137] presented a MOF-supported catalyst with two different active sites, the pyridine and Co-porphyrin (termed as CoPP) were supported on ultrathin MOF nanosheets. These catalysts with dual active sites showed better performance as compared with pyridine-free CoPP-based catalysts and in situ spectroscopic and DFT studies further revealed that pyridine and CoPP supportively stimulate carbon
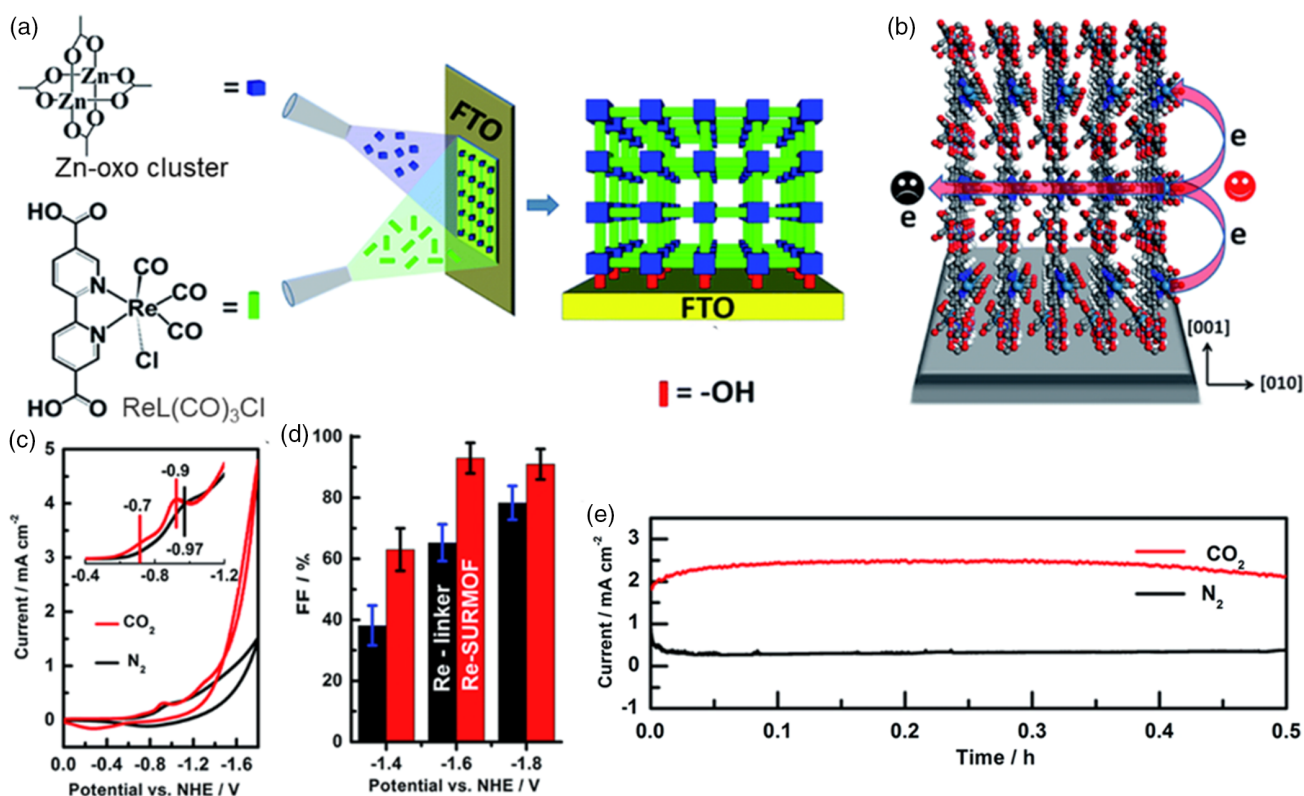
Figure 9. a) Synthetic methodology of Re-SURMOF assembled by Zn-oxo cluster and ReL(CO)$_3$Cl (L = 2,2′-bipyridine-5,5′-dicarboxylic acid) linker on the FTO, b) representation of preferred charge transfer mechanism, c) Cyclic voltammetry (CV) performance, d) FE, and e) current density at −1.6 V versus RHE for first half hour. Reproduced with permission.[120] Copyright 2016, Royal Society of Chemistry.

ADVANCED
SCIENCE NEWS
www.advancedsciencenews.com

small
structures
www.small-structures.com

Figure 10. a) The free-energy calculations of different catalysts for the reduction of CO_2 to CO, * symbolizes active sites on the surface, b) the free-energies for the formation of *COOH (ΔG_1), *CO (ΔG_2), and CO desorption (ΔG_3) in CO_2RR, c,d) The anticipated CO_2RR mechanism for Co-PMOF catalysts. Reproduced under the terms of the Creative Commons CC BY license.[136] Copyright 2018, Springer Nature.

dioxide to produce key $pyH^+-^-O_2C$–CoPP intermediates, backing better CO_2RR activity. Similarly, Hod et al.[95] used Fe-porphyrin merged into MOF-525 as a structural and functional element for CO_2 reduction. This approach led to a high electrochemically surface area of Fe-porphyrin (1015 sites cm^{-2}), resulting in the production of syngas ($FE_{CO} = 50\%$). Despite the CO_2RR with low efficiency, results showed that molecular catalysts incorporated in the MOF structures are accessible for CO_2RR. Consequently, it can be anticipated that the addition of molecular catalysts into MOF may be more beneficial to design advanced CO_2RR catalysts.
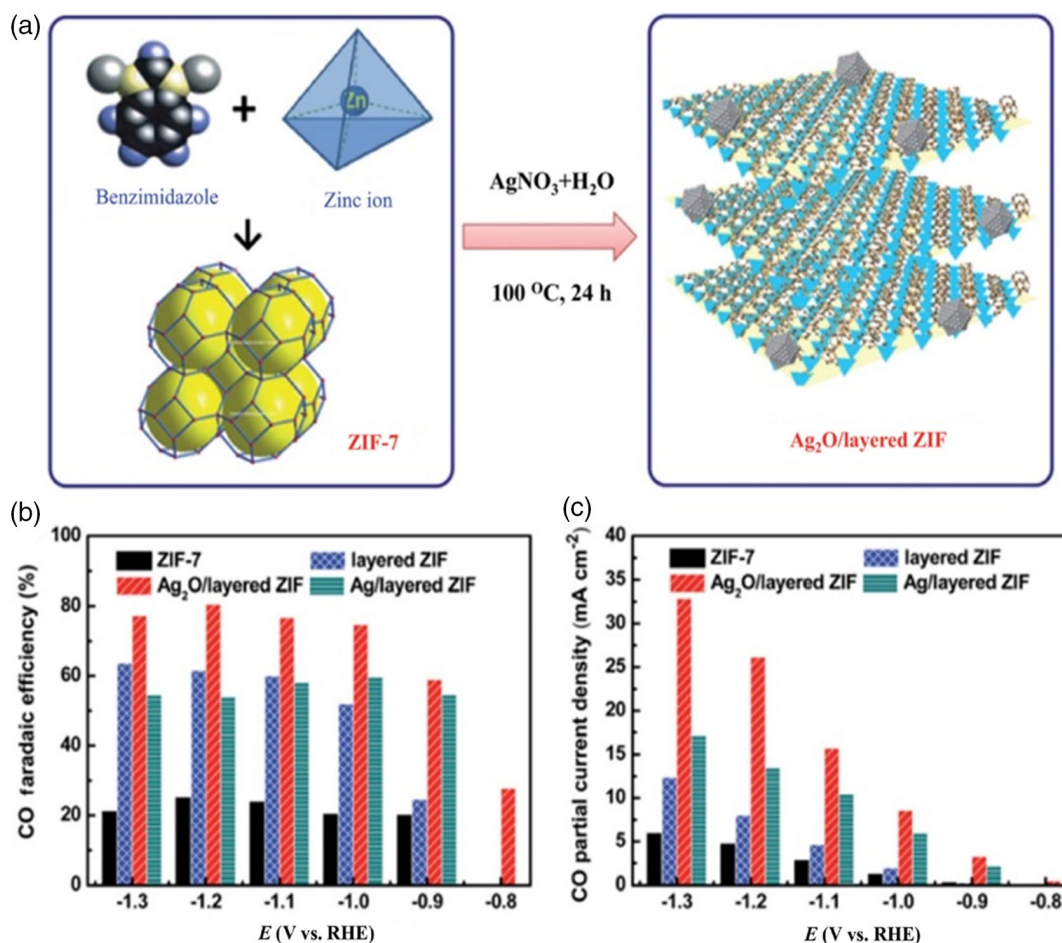
4.3.4. MOF-Supported Metal NPs

So, important metal NPs have been investigated as electrocatalysts to reduce CO_2. But, the agglomeration of these small particles into large moieties always remains a big problem during the catalytic process. Several approaches have been implemented to overcome this problem and enhanced the availability of more catalytic active sites, including the modification of the size and shape of metal NPs.[39,138] In addition to molecular catalysts, MOFs as porous structures having higher special surface area, provide an improved ground for the production of functional materials. Which not only serve as supporting materials for molecular immobilizers of metals but also as a model that

encourages the even distribution of small NPs formation to reduce CO_2. For example, Jiang et al.[139] synthesized Ag_2O/ZIF composite via combining $AgNO_3$ and aqueous ZIF-7, followed by refluxing at 100 °C (**Figure 11**a). The as-prepared catalysts (Ag_2O/ZIF-7) showed better CO_2RR performance ($FE = 80\%$) than that of Ag/C and ZIF-7. The increase in performance was accredited to the synergistic effect between Ag_2O NPs and ZIF-7 multilayers and facilitated mass transfer via a specific surface area. It turned out that the small Ag_2O NPs were homogeneously distributed throughout the ZIF layer. Further, it was observed that the Ag_2O/ZIF-7 has a more positive starting potential of −0.6 V versus RHE for CO_2 reduction from Ag_2O/ZIF-8 in 0.25 M K_2SO_4. As compared with ZIF-8 or Ag/C alone, Ag_2O/ZIF-8 showed a greater co-Faradic yield of 80.6% at −1.2 V versus RHE. This outstanding activity is attributed to the synergism between the greater surface area of ZIF and the small size of NPs (Figure 11b,c).

Further, Hupp and coworkers reported the catalysts for CO_2RR by incorporating the Cu NPs on the surface of stable MOF(NU-1000).[140] The as-prepared catalyst showed the catalytic performance to a two-phase product: a liquid ($HCOO^-$) and a gas phase (CO and H_2). However, the formate ($FE = 31\%$) was determined as the major product at −0.82 V versus RHE.

These studies illustrate that the incorporation of metal NPs on/in the MOF's surface is a prestigious methodology for

**ADVANCED
SCIENCE NEWS**
www.advancedsciencenews.com

**small
structures**
www.small-structures.com

Figure 11. a) The synthetic scheme for Ag_2O/ZIF-7, b) FE (%), c) *j* values for different catalysts at varying potentials for CO production. Reproduced with permission.[139] Copyright 2017, Royal Society of Chemistry.

improved electrocatalytic performance. The studies also showed that the high surface area and porosity of MOFs not only facilitate the mass transportation and inhibits the NPs agglomeration but also facilitate the activation of CO_2 molecule via the synergistic effect between the surface area and NPs.

5. MOF-Derived Electrocatalysts for CO_2RR

MOFs have been rapidly developed in the past 10 years, their powerful pore chemistry, high surface area, and well-tuned organic–inorganic hybrid structures are attractive in material chemistry for various applications.[3,4,8,38,141–149] In terms of assembly, pristine MOFs are a type of crystalline nanomaterials containing flexible metal ions or clusters and organic ligands, with the basic benefit of higher surface area and porosity. Though, the inadequate conductivity and lack of structural stability of MOFs hindered the development and use of electrocatalytic CO_2 reduction. Although several MOF-based CO_2-catalysis have been reported, some work with MOF directly as electrocatalysts in the CO_2RR claimed that MOF electrocatalysts displayed long-term durability during the test, but many did not perform

postreaction analysis to justify these claims.[150] In this aspect, MOF consumption as a precursor to produce more stable catalysts can be a useful way to efficient CO_2RR. The recent developments in electrocatalysis coupling the MOF-derived nanomaterials are incessantly growing for the application of energy-related problems.[31,32,151–154] Consequently, these materials are also being developed for CO_2RR, preceding the drawbacks of pristine MOFs, these are being synthesized from MOFs either via high-temperature pyrolysis or electrochemical conversion. Categorized by MOFs' inherited porosity and surface area with addition of enhanced stability and conductivity, MOF-derived materials are being more attractive for catalytic applications including CO_2RR.[33–35,155–157] From the past decade, many researchers have reported efficient CO_2RR catalysts synthesized via calcination/pyrolysis of MOFs at various temperatures. The studies showed that the performance of the catalysts derived from MOF could be altered through controlling three factors; 1) annealing temperature; 2) time duration of pyrolysis; and 3) atmosphere of pyrolysis (air/inert).[157–159] Moreover, the MOFs with guest species may lead to more functionalities such as heteroatom doping, metal NPs incorporation.[160–162] These materials derived from MOF, comprising metal NPs, single-

metal atom coordinated N-doped graphitic carbon materials and/or metal-free catalysts, represented clear benefits for the reduction of CO_2 with abundant properties, e.g., respectable electronic conductivity, larger surface area, evenly dispersed NPs or single-atom active sites. In addition, MOFs are also being used as a basis of highly dispersed metal sources, following by the addition of external heteroatom (N source) to stabilize the SACs with high-performance CO_2RR.[163,164] In the following sections, we have categorically summarized the MOF-derived catalysts for electro-reduction of CO_2.

5.1. Electrochemical Conversion of MOFs

The rigid porous structure that makes MOFs as fascinating materials in a range of applications also hinders their electrocatalytic stability and activity. Factors like the 3D geometry impeding the long-range charge movement, the poor overlap of O atoms and metal d orbitals, and the redox-inactive nature of many carboxylate-based organic linkers determine the poor conductivity of MOFs. To enhance the CO_2RR performance, Kim et al.[160] decomposed MOF using electrochemical reduction method to produce an efficient catalyst for CO_2RR, the obtained catalysts produce methane with FE of >50% at −1.3 V versus RHE. Retaining the advantages of MOF-74, low-dimensional structure prevents the agglomeration of reduced Cu cluster and the derived Cu NPs also showed 2.3-fold higher current density than commercial Cu NPs and high performance was attributed to the MOF–precursor for the production of isolated Cu NPs with higher surface area. Similarly, Kung et al.[140] reported the Cu NPs incorporated into NU-1000 thin films, first, Cu single sites were introduced into MOF-based thin film and then electrore-duction method was applied to convert Cu(II) into Cu(0). The as-prepared Cu NPs are not only accessible active sites but also showed better performance for the formate production with 28% FE at −0.82 V versus RHE. It is here worth mentioning that the crystallinity and nanostructures (morphology) are not affected by electrochemical reduction, however, the pore size of MOF generally affects the size of metal NPs. By tuning the pore size of MOFs, the NPs size can be tuned which has a direct effect on the catalytic performance.

Recently, Xu et al.[165] utilized Bi–MOFs for in situ electrochemical transformation process to produce atomically thin bismuthene (Bi-ene) with 1.28–1.45 nm thickness. The high-active sites exposure improves the intrinsic activity of Bi-ene for CO_2RR having ≈100% FE in a wide range of the potential window. In addition, 72.0 mA cm^{-2} of high partial current density and strong stability for electrochemical reduction of CO_2 to formate was also achieved. Further, first-principle DFT measurements were used to investigate the CO_2RR mechanism over Bi-ene and the generation of *HCOOH from *OCHO was considered to be the RDS. Though, in situ attenuated total reflection infrared spectroscopy (ATR-IR) analysis specified that adsorption of HCO_3^- ions contribute during CO_2RR route (**Figure 12**b-d), thus a new CO_2RR mechanism with contributing HCO_3^- for formate production is put forward, which could further support in understanding the process of CO_2RR (Figure 12e, f).

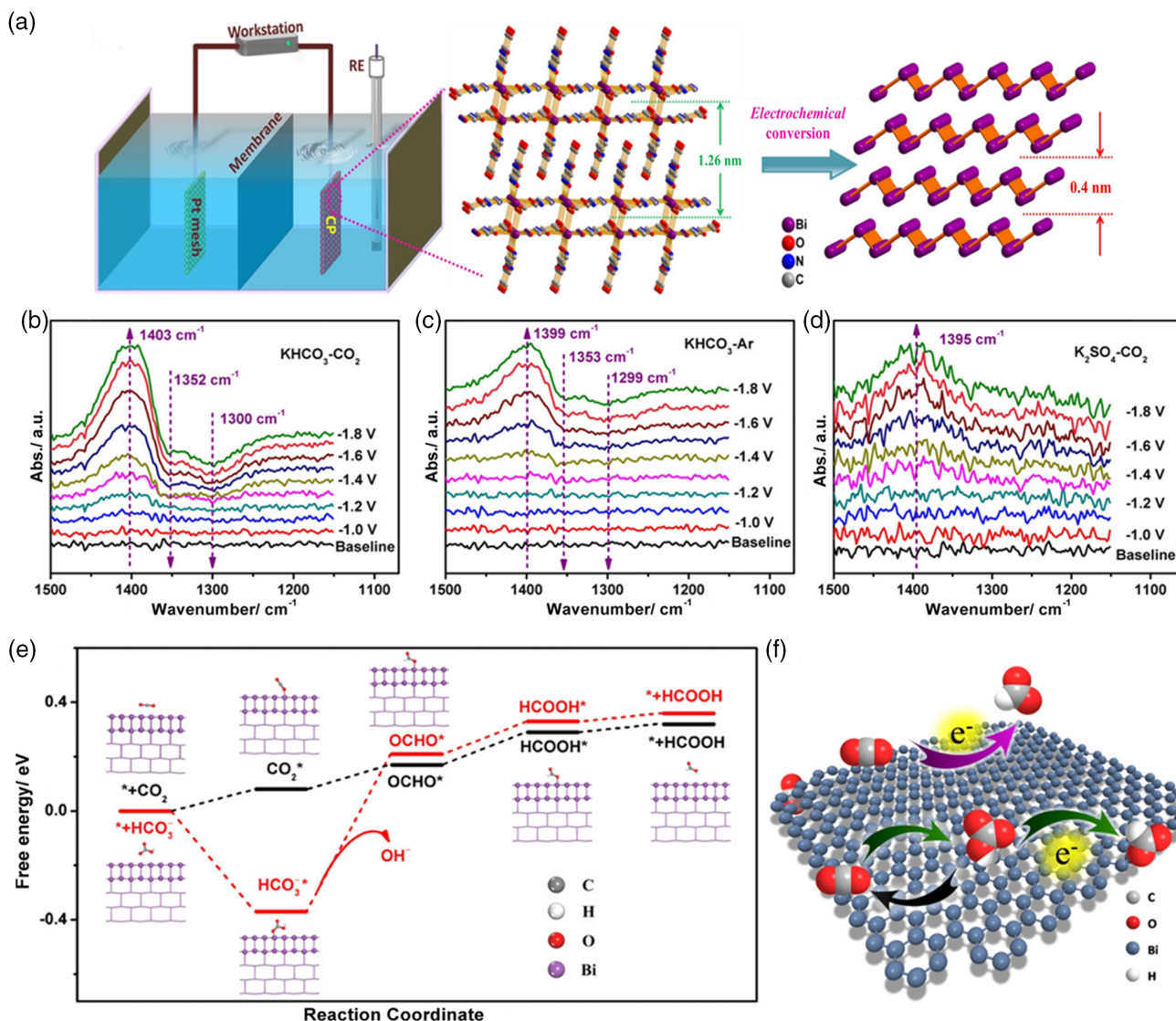Lamagni et al.[166] synthesized a bismuth-based MOF bi(1,3,5-tris(4-carboxyphenyl)benzene), namely Bi(btb). The Bi(btb) material assists as a precatalyst and endures some rearrangements in the structure of the MOF at low potentials and converted into Bi-based NPs distributed in a porous carbon material, the Bi NPs work efficiently as active sites for high selectivity during CO_2RR. The consequences exposed the high selectivity of as-synthesized MOF over a wide potential range during CO_2RR toward formate generation with 95% of FE and 261 A g^{-1} of current density. The improved performance was ascribed to the highly distributed Bi NPs with well exposure of active sites. The electrochemical conversion of MOFs into highly active catalysts proposed an innovative methodology for synthesizing metal-based catalysts with enhanced selectivity, activity, and electronic conductivity for CO_2RR application. However, this nascent approach requires further attentions to explore the salient features.

5.2. Thermal Conversion of MOFs

The controlled thermal decomposition environment of MOFs typically leads to the highly active and stable catalysts with metal constituents into smaller NPs. For example, Zhao et al.[167] prepared 0D Cu/C (oxide-derived Cu/carbon) electrocatalysts via pyrolysis of Cu–BTC MOF (HKUST-1). In addition to metal NPs, the MOF-mediated pyrolysis can also serve as a process for the production of metal oxides, metal carbides, and/or metal coordinated N-doped carbons with highly disclosed active sites for effective catalysis of CO_2RR. Instead of metal catalysts, the carbon-rich organic ligands, coordinated metals having low boiling points such as Zn, is an auspicious precursor to the fabrication of carbon-based electrocatalysts.[168] Furthermore, MOF-derived SACs are also studied for CO_2RR, various approaches are being applied to improve the catalytic activity of these catalysts. For example, adding iron into the structure of ZIF, not only lowered the overpotential of reaction but also affect the selectivity of product.[169] Further addition of conductive carbon support such as multiwalled carbon nanotubes (MWCNTs), is also critical for attaining higher efficacy, the MWCNTs facilitate the electron transport resulting in the enhancement of catalytic performance during electroreduction of CO_2.[169] In the following paragraphs, the MOF-derived catalysts are categorically summarized followed by the various strategies applied to enhance the CO_2RR performance.

5.2.1. MOF-Derived Metal-NPs on Carbon Support

Metal NPs usually exhibit unique catalytic performance; various metallic NPs are widely used for CO_2RR, such as Pd NPs supported on Vulcan XC72R carbon black,[170] Bi NPs decorated on multiwall carbon nanotubes[171] and entrenched in N-doped carbons,[172] Cu/carbon (0D Cu/C) catalysts[167] and some others.[2,173] Due to inherited properties of MOFs, MOF-derived metal NPs thoroughly distributed in carbon matrix are considered more efficient for CO_2RR. For instance, Zhao et al.[167] prepared Cu/carbon (Cu/C) from Cu–BTC MOF (HKUST-1), which showed a very selective reduction in CO_2 into alcohols at −0.7 V versus RHE with an overall 71.2% of FE (**Figure 13**a-c). Further, the effect of carbonization temperature was also elaborated and Cu/C-1000 gave high methanol and ethanol yields with the highest production rates of 12.4 mg L^{-1} h^{-1} at −0.3 V and

ADVANCED
SCIENCE NEWS
www.advancedsciencenews.com

small
structures
www.small-structures.com

Figure 12. a) Presentation of Bi-ene synthesis and proposed CO₂RR mechanism, b-d) ATR-IR (in situ) results at different potentials for b) CO₂- and c) Ar-saturated 0.5 M KHCO₃, d) CO₂-saturated 0.2 M K₂SO₄. e) Free-energy diagrams for HCOOH over Bi-ene. f) The anticipated mechanism of CO₂RR. Reproduced with permission.[165] Copyright 2020, Wiley-VCH.

13.4 mg L^{-1} h^{-1} at -0.7 V. In situ infrared (IR) spectroscopy and theoretical measurements showed that intermediate (*CO) was absorbed on the surface of Cu/C electrocatalyst, and then porous carbon encourages C—C coupling, which is a critical pathway for C2 species formation.

The performance and selectivity of the MOF-derived catalysts toward a specific product attributed to the synergism between the significantly distributed metal sites and the porous carbon matrix. However, the selectivity toward one product is, one of the main problems of CO₂RR, particularly when using Cu-based catalysts. Nam et al.[127] described a MOF-regulated Cu cluster strategy that shifted CO₂ reduction to multicarbon products. The controlled temperature was used to distort the symmetrical paddle-wheel Cu dimer secondary building blocks of HKUST-1 by separating the adjacent tricarboxylate moieties. The results suggested that the Cu moieties with low-CNs are highly active

for the CO₂RR with 45% FE toward ethylene. In addition, N doping in carbon plays a certain effect in the electrocatalytic CO₂RR performance of metal/carbon catalysts. The presence of pyrrolic-N doped carbon supports the adsorption of carbon dioxide and also assists the C—C coupling reaction on the metal surface, resulting in selective C2 products. For example, Cheng et al.[174] reported the Cu NPs supported on N-doped carbon (Cu–NC) derived from Cu–BTC modified with benzimidazole (N source) by simple carbonization. The electrocatalytic performance showed that the high atomic percentage of pyrrolic-N (calcined at 400 °C) assists the production of ethylene and ethanol with a high FE of 11.2% and 18.4% at -1.01 V versus RHE, correspondingly.[174]

MOF-derived porous carbon materials exhibited practical viability because of their high electronic conductivity, greater surface area, and robust chemical stability. Importantly, this

ADVANCED
SCIENCE NEWS
www.advancedsciencenews.com

small
structures
www.small-structures.com
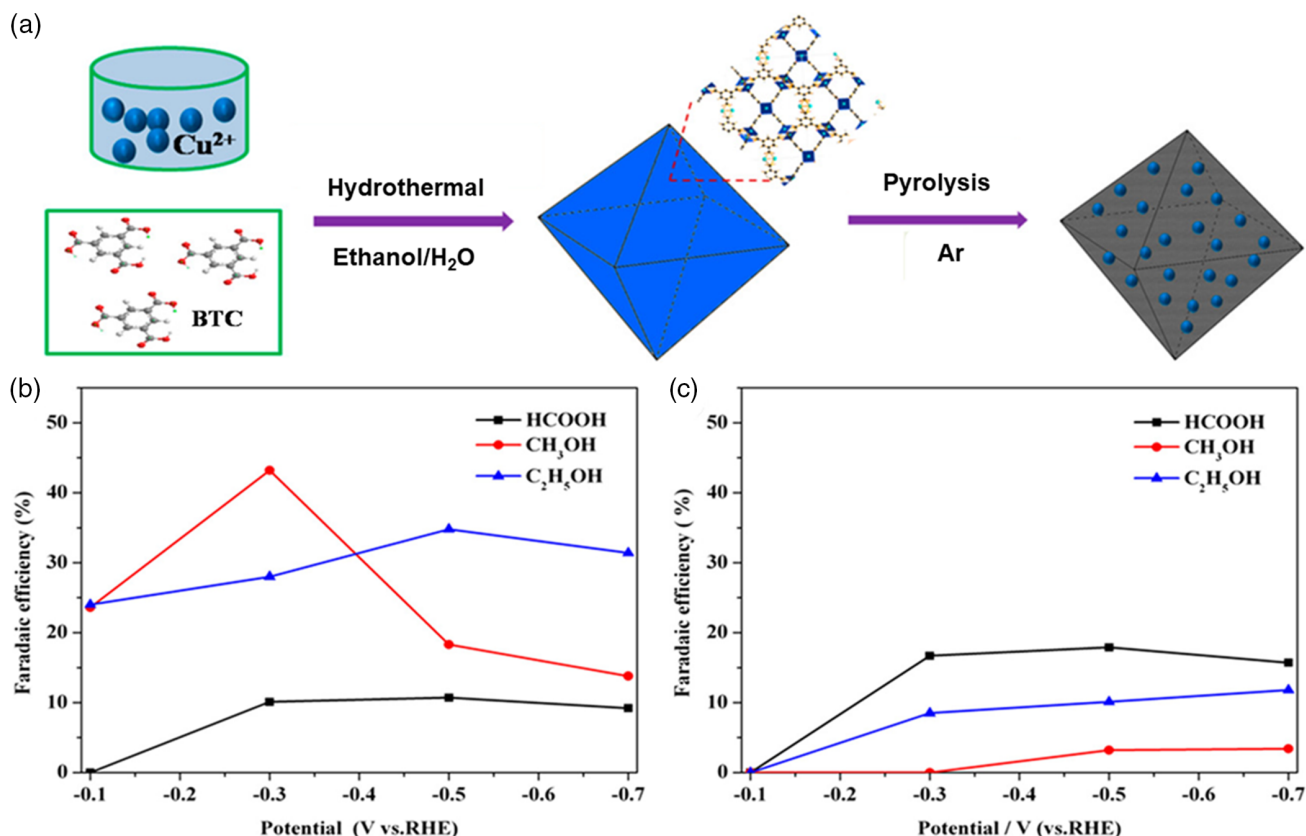
Figure 13. a) Synthesis of MOF-derived Cu/C catalysts, b) FE in 0.1 M KHCO$_3$ for b) 0D Cu/C and c) Cu/C-1000, inset of c showed suggested pathway for the CO$_2$ conversion into alcohols by Cu/C-1000. Reproduced with permission.[167] Copyright 2017, American Chemical Society.

N-doped porous carbon (NPC) derived from MOFs is widely used, as the ideal support of catalysts that not only limit the metal NPs agglomeration but also assure good contact between NPC and catalysts.[27,172] For example, Zhang et al.[172] reported bismuth NPs incorporated in MOF-derived NPC (Bi@NPC) as a capable catalyst for converting CO$_2$ into valuable products. The unique microstructure and NPC support of Bi@NPC catalyst develop greater adsorption of CO$_2$ and faster CO$_2$RR kinetics, generating formate as a major product with 92% FE and stability of 20 h.[172] Conversely, among all types of N doping, pyrrolic-N is subjected to active for CO$_2$RR, whereas graphitic- and oxidized-N are active for HER. Consequently, optimization of the N structure is essential for establishing the constructive effect of synergism between metal NPs and supportive N-doped carbon materials.

5.2.2. MOF-Derived Metal Oxides on Carbon Support

The cracking of MOFs has become an encouraging strategy that allows to adapt metal oxide configurations via different methods that help extensively for producing industrial necessities. Thanks to MOF assembly, which consists of the coordinated central metal atom with organic ligands, and the controlled pyrolysis under different conditions tend to produce unique morphologies tailored to the inherited porosity of MOFs. MOF-based metal oxides (MOs) also have these inherited advantages as compared

with the MOs synthesized by conventional methods. For example, Deng et al.[175] used bismuth-based MOFs to prepare Bi$_2$O$_3$@C electrocatalyst for enhanced performance during CO$_2$RR pathway (**Figure 14**a-c). The Bi–BTC (MOF) nanorods pyrolyzed at 800 °C in an Ar atmosphere, further an oxidation treatment proceeded at 200 °C for the synthesis of Bi$_2$O$_3$@C. The Bi$_2$O$_3$@C-800 exhibited −0.28 V versus RHE of onset potential, 93% of FE stability, and 200 mA cm^{-2} of high partial current density at −1.1 V versus RHE in a flow cell configuration for the fast production of formate (Figure 14d,e). These findings demonstrated the Bi$_2$O$_3$@C hybrid synergistically stimulates the selective and fast reduction of CO$_2$, and the supporting carbon framework enriched the performance and boosted the current density, whereas oxide species are favorable for refining the selectivity and reaction kinetics. He and coworkers synthesized ZIF-67-derived ultrasmall Co$_3$O$_4$ NPs encapsulated in the carbon nanotubes named Co/CNT.[176] The electrochemical CO$_2$ was observed with 90% FE at only −0.7 V versus RHE. The efficient FE was also retained for 40 h of stability test and this performance was attributed to the hybrid nanostructures formed in situ during the pyrolysis process.

MOs derived from MOFs offer additional distinctive features in the production of materials, having multiple types of metals in the same framework. Miscellaneous MOs (common type AB$_2$O$_4$) have recently gained great interest due to their complex chemical composition, developed electrochemical and magnetic properties due to the synergy effect of different types of metals and the
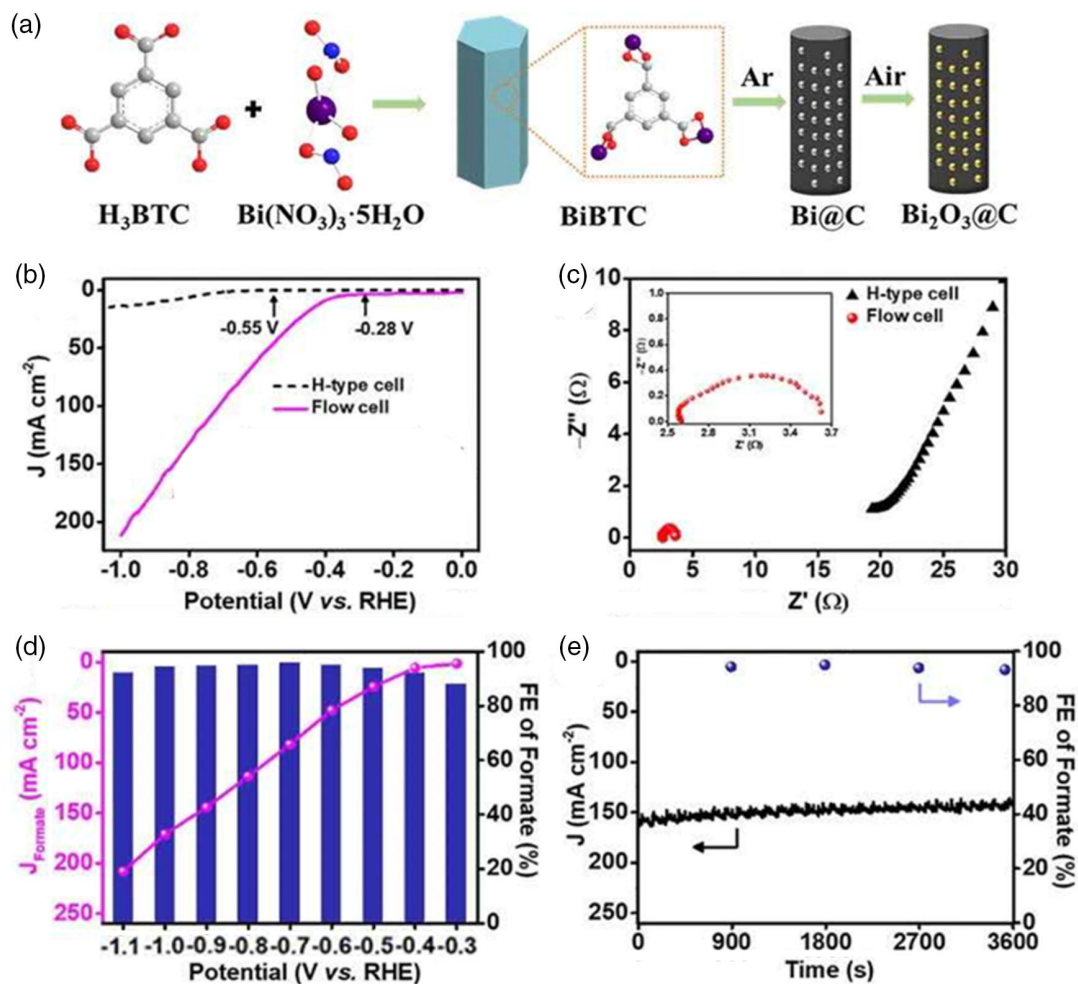
Figure 14. a) Schematic illustrations of a synthetic method of Bi₂O₃@C-800 and CO₂RR performance. b) Linear sweep voltammetry (LSV) curves at a scan rate of 10 mV s⁻¹ (inset is the schematic flow cell), c) Nyquist plots (inset is the enlarged flow cell result), d) FE and partial current density of formate, e) stability at 0.9 V versus RHE in the flow cell. Reproduced with permission.[175] Copyright 2020, Wiley-VCH.

presence of variable valances of several contributing metals, but the controlled composition of these materials remains a major challenge. Recently, MOF-based bimetallic oxide catalysts are optimized CO_2RR performance.[177] These bimetallic oxides (In–Cu) were produced by the cracking of Cu–In-bimetallic MOF. By regulating the ratios of In and Cu, the CO_2RR performance was increased to 92.1% FE toward the production of CO having a high current density of 11.2 mA cm⁻¹.

5.2.3. MOF-Derived Metal-Free Electrocatalysts

Metal-free carbon materials have recently attracted intensive attention due to their low cost, high surface area, and tunable conductivity,[178,179] which are among the most promising alternatives to the expensive noble metals for CO_2RR.[180] Up to now, various kinds of heteroatom-doped carbon nanostructures, such as N-doped carbon, chlorine-doped carbon,[181] fluorine-doped carbon,[182] Se-doped carbon,[183] N-, B- codoped porous carbon,[184–186] nitrogen and phosphorus codoped carbon,[187] and graphene[188] have been explored for CO_2RR.[189] In addition, the capacity to suppress the competing H₂ evolution reaction

makes the N-doped carbon materials much more appealing for selective CO_2 conversion.[190,191] However, the low productivity and selectivity remain the major challenges yet to be tackled.

MOFs are being considered as tremendous sacrificial agents for the synthesis of porous materials using metal with a low boiling point in MOF such as Zn or Cd. By the pyrolysis of these MOF precursors metal-free carbon catalysts can be produced at high temperatures. For example, Wang et al.[192] synthesized N-doped carbon, via the pyrolysis of a famous MOF named ZIF-8. The resultant NC-based CO_2RR electrocatalyst exhibited high FE_{CO} (78%) and the temperature of pyrolysis determined the amount of N in the carbon, where the pyridinic-N and quaternary-N have a significant role in the selectivity and activity of catalyst. The catalysts prepared from Zn-based MOFs especially ZIF-8 are usually no less than other nitrogen containing carbonaceous materials and are active without any additional metal. Therefore, one should not forget that it compares their performance with materials developed from other routes.[193] Zheng et al.[157] studied the effect of pyrolysis temperature and the mechanism in the ZIF-8-derived N-doped carbon (NC) and results showed that an increase in pyrolysis temperature caused

better CO_2RR activity, and the highest catalytic activity and selectivity was observed with 95.4% FE_{CO} at 0.5 V versus RHE and also sustained its 90% performance after 20 h of operation. DFT calculations showed that the increase in activity can be attributed to the formation of pyridinic-N, which offered more effective active sites. Thus, the ability to reduce carbon dioxide (CO_2) by N-doped carbon (NC) depends to a large extent on N doping and its nature, as well as on the porosity of catalysts.

Recently, Kuang et al.[161] developed a postdevelopment strategy to facilitate electrochemical CO_2RR by regulating N-doping configurations and N contents by treating with DMF as solvent. The catalysts have a clear mesoporous structure with abundant defects, compared with graphene or nanotubes, which promotes the production of pyridinic-N doping at the edge sites. The resulting mesoporous N-doped carbon (MNC-D) was used as an effective electrocatalyst to reduce the CO_2 into CO with high efficiency (92%) at −0.58 V versus RHE. Electrochemical analyses also showed that the active positions in N-doped carbon catalysts were pyridinic-N and defects produced by DMF therapy, which improved the activation and adsorption of CO_2 molecules.[161]

Furthermore, Ye et al.[194] demonstrated the effect of various types of N doping on CO_2RR, highly porous (pore size =10 nm) metal-free N-doped carbon was synthesized from Zn-MOF-74 as a precursor. This catalyst showed better performance toward CO_2RR with 98.4% FE_{CO} at −0.55 V, this high performance was attributed to the pyridinic-/graphitic-N (68.31%) and highly porous structure which facilitates the easier transportation of reactants and products to and from active sites.[194]

To reduce the limit of electron transmission associated with MOF-intervened strategy, Guo et al. prepared a conductive material via cocalcination of ZIF-8 grown on MWCNTs.[169] This catalyst has enhanced the selective CO_2RR performance with ≈100% FE and 7.7 mA cm^{-2} of current density at an overpotential of 740 mV, comparatively 50% higher FE from ZIF-8 derived catalysts in the same conditions. These results showed that MOF-derived metal-free carbon-based catalysts also have a great potential for CO_2RR, however, it requires some efforts to explore the synthetic strategies as well as active sites for the rational design of new materials.

5.2.4. MOF-Derived Metal-Coordinated N-Doped Carbons (M–N–C)

Thermal treatment of nitrogenous compounds mixed with individual metal salt with one or more carbon precursors is a common strategy for integrating catalytically active M–N$_x$ sites into heterogeneous catalysis. In these materials, nitrogen is processed into a carbon structure and produces various doping of N sites such as pyrrolic-, pyridinic-, and graphitic-N. Metal atoms coordinate with these N functions and produce similar active sites to metal–N macrocycles in conductive catalysts. M–N–C-based catalysts have been widely established as a cost-effective Pt alternate to cathode catalyst in fuel cell operation due to their better performance for the oxygen reduction reaction.[24,30,32–35,39,195] Recently, these M–N–C-based catalysts have been considered as CO_2RR catalysts because the synthetic approach is a more cost effective alternative to producing a heterogeneous catalyst that contains M–N$_x$ functions. But working with this category of

materials, it is significant to note that there are several possible active sites. The first question to be answered is whether this performance can actually be ascribed to metal-based sites coordinated with N, other N functions, or certain carbon-based supports. That's why Huan et al.[196] explored a number of iron-based catalysts with isolated Fe–N$_4$ sites and Fe NPs. Catalysts with the lower Fe–N$_4$ contents have a higher potential, whereas controlled electrolysis showed that CO selectivity is associated with concentrations of Fe–N$_4$ active sites. In contrast, materials consisting of Fe particles or Fe–C primarily showed HER performance, endorsing that CO_2RR performance is associated with iron, which is incorporated into the carbon assembly through N configuration, and that other Fe-forms possibly contribute to the competitive process, i.e., HER. The significance of Fe–N$_x$ catalysts was further proved by Genovese et al.[197] and showed that iron coordinated with O- and N-doped (Fe/O–C or/and Fe/N–C) has an impact on the selective CO_2 electrolysis. Fe/O–C was mainly responsible for H_2 production, whereas CO_2RR was the prime practice by replacing Fe oxyhydroxide in the NC matrix. It was further interesting because the reduction products in Fe/N–C were HCOOH and CH_3COOH, the latter of which was the product of choice. The authors also found that HER was associated with metallic Fe NPs formation, whereas acetic acid production was associated with the formation of nitrogen of coordinated iron species. In this study, N atoms showed twofold influence on the performance as; 1) N atoms stabilize intermediates of CO_2RR; 2) N also stabilized the Fe(II) type, which prevents the formation of Fe(0). It is worth noting in catalysts studied by Genovese et al.,[197] that Fe/N–C Fe(II) coordinated with N and O atoms, may be considered as the intense reason for selective production of carboxylic acids. However, M–N$_4$ are designed as active sites in M-coordinated N-doped carbon (M–N–C) materials for CO_2RR in various theoretical studies.[198,199] For example, Bagger et al.[199] mentioned the main advantage of these catalysts (M–N–C) over metals in the presence of M–N$_x$ isolated active sites, which limit the competitive process of HER, emphasizing the structural advantage of catalytic materials with Fe–N$_x$ active sites.[199] This inhibition of HER is based on two effects: first, individual locations in the porphyrin-like structure need axial-free space for H_2 at the top of the bond in relation to the cavity on the surface of the metal catalyst. Conferring their calculations, on the porphyrin structure the upper *H-link is generally weaker than the hollow bond, resulting in a higher barrier of energy for HER. Second, HER should follow the Heyrovsky mechanism instead of the preferred Tafel mechanism for each M–N–C single site. These factors prevent HER, which gives a minimum advantage of 0.3 eV to CO_2RR (*COOH vs *H) in M–N–C materials over metal surfaces, making them more discerning catalysts for CO_2RR.

Further, reducing CO_2 to CO, the theoretical study shows that CO can be further reduced to CH_4 or MeOH depending on the metal center. For example, it was predicted that Fe centers would convert CO to CH_4, confirmed by Varela et al.[200] however, CH_4 selectivity on Fe–N–C was less than 1%. It was interesting that Rh-functionalized porphyrin-like graphene would effectively produce methanol from CO at significantly lower overpotential (0.22 V) than that perceived on stretched metallic surfaces. However, this calculation has not been verified experimentally in this study. Further, Ju et al.[201] investigated the significance

**ADVANCED
SCIENCE NEWS**
www.advancedsciencenews.com

**small
structures**
www.small-structures.com

of the central metal atom's nature for CO$_2$RR activity and selectivity and reported an experimental work supported by the theoretical calculations of CO$_2$RR using M–N–C catalysts with five various central metal atoms (**Figure 15**a-d) such as Ni, Co, Cu, Mn, and Fe.[201] Similar to Varela et al.,[200] this study also revealed the CO selectivity for Fe and Mn catalysts at −0.55 V versus RHE, HER was the dominant process, if the potential was more negative (Figure 15a). However, the selectivity in the comparison was markedly different, as Fe–N–C reduced CO$_2$ with FE 65%, whereas that in Mn–N–C was only 40% (Figure 15b). The production of CH$_4$ in the trace amount indicated that CO$_2$ can be directly converted to hydrocarbons via Fe–/Mn–N–C centers (Figure 15c). In contrast, CO selectivity persisted at its low by using Cu–/Co–N–C catalysts throughout the entire range of tested potentials (−0.4 to −0.85 V vs RHE) and H$_2$ was clearly the major product. The highest current density and FE were observed by Ni–N–C as compared with the other metal centers tested, resulting in 85% FE at −0.78 V versus RHE, suggesting Ni-based materials as worthy applicants in a wide range of M–N–C materials for selective CO production from CO$_2$ (Figure 15b,d).

Simulations showed that the original potential of CO$_2$RR relates with *COOH free energy, but the possible increase in overpotential, there are other possible aspects to be considered. In the case of average overpotential, the intermediate overpotential rate determining is moved from *COOH to *CO. The growth of *CO chemisorption is now increasing with the production of CO. The increment in overpotential reduced the Fe–N–C performance for CO production, indicating a speed limit due

to the non-Faradaic water adsorption process and similarly, Co–N–C has also proven to be the most effective catalyst for this production of H$_2$ with the highest FE.

In contrast, nickel-based active sites have fragile binding energy to *H, which leads to the thermodynamically unfavorable at −0.8 V (RHE) leading to observed low H$_2$ production and greater selectivity of CO. In addition, CH$_4$ coexistence in CO correlates with earlier findings by Varela et al.[200] high-performance reduction of CO related with a strong binding energy of *CO. Among the metal centers studied, higher CH$_4$ production is observed in Fe–N–C, where CO is expected to bind more strongly to promote the reduction process. In contrast, in Ni- and Cu-based catalysts, *CO stripped strongly favors to prevent its conversion. Traces of CH$_4$ have also been observed as CO$_2$RR products in gels containing nitrogen and sulfur, suggesting that production of CH$_4$ increased due to the existence of Fe centers and also in the presence of other heteroatoms.[202,203] However, it cannot be generalized to all Fe–N–C-based catalysts, Ye et al.[204] produced isolated active sites of iron and nitrogen, situated in carbon framework, by cracking iron salt of citric acid and ZIF-8 (AFC/ZIF-8) composite. Moreover, the well-exposed areas of Fe and N sites showed the enhanced performance to CO production with a maximum FE of 93% and partial current density (j_{CO} = 9.5 mA cm^{-2}). Similarly, carbon material from ZIF-8 containing Fe–N$_x$ active sites can convert CO$_2$ to CO with significant FE in the wide potential range (−0.33 to −0.83 V vs RHE). The second pyrolysis in NH$_3$ further improved CO$_2$RR activity with higher CO efficacy and current density. Physical–chemical
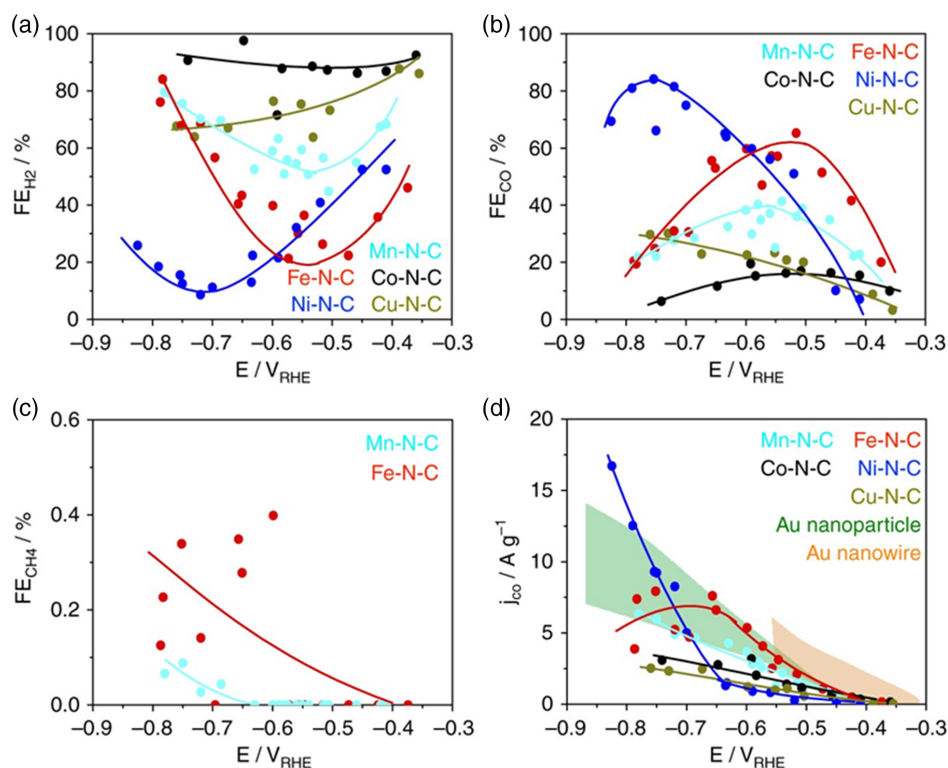
Figure 15. CO$_2$ reduction performance (60 min) of metal–N-doped carbon materials in 0.1 M KHCO$_3$. a) FE$_{(CO)}$, b) partial current density, c, d) simulated free energy diagrams for CO and H$_2$ production during CO$_2$RR and HER, respectively. Reproduced under the terms of the Creative Commons CC BY license.[201] Copyright 2020, Springer Nature.

**ADVANCED
SCIENCE NEWS**

www.advancedsciencenews.com

**small
structures**

www.small-structures.com

properties indicate that the NH_3 treatment assists the sublimation of other Zn species and the engraving of carbides, thereby increasing the exposure of Fe–N_x active sites, resulting in higher FE_{CO} and a much better current density, than other previously Fe–N–C reported electrocatalysts.[205]

The main three steps of CO_2RR (adsorption, intermediate formation, and desorption of products) are directly linked to the electronic structure of metal atoms. Regulation of the local atmosphere of metallic active sites is considered as an emerging tactic for developing the performance during electrochemical CO_2RR.[206,207] The effect of porous support on the performance of electrochemical CO_2 reduction has been further explored. Recently, Hu et al.[208] synthesized N-doped carbon porous support from the Fe-ZIF-8 achieved two representative catalysts using SiO_2 coating to create porosity (**Figure 16**a–d). Figure 16a,b shows that the Fe–CNP (using SiO_2) had a higher 1156.6 $m^2\,g^{-1}$ of surface area with 0.49 $cm^3\,g^{-1}$ of pore volume, whereas the specific range (360.1 $m^2\,g$) for Fe–CNPs-w/o is relatively lower. Fe,N-co-doped porous carbon nanoparticles (Fe–CNPs) having a highly porous structure performed better in converting carbon dioxide with FE_{CO} of 98.8% (Figure 16c). Thus, it can be concluded that CO_2RR performance depends on the porosity and selectivity of CO_2RR in SAC.

In proceeding sections, we will draw attention to optimization strategies, including CN, coordination of atoms, engineering of axial chemical environment, and construction of defective sites in the supporting material.

5.2.5. MOF-Derived Single-Atom Electrocatalysts

SACs or single-atomic catalytic sites with determined atomic proficiency and low coordination of metal centers have led to exceptional performances in various electrochemical reactions.[39,209–212] Uniform active centers and geometric structures are illustrated by spatial and electronic interactions with substrates, favorable for increased catalytic selectivity.[213,214] Therefore, SACs show great potential to achieve high proficiency and selectivity during CO_2RR pathways.[215–217] Single metallic species performed as active sites for reducing CO_2 into valuable products, of course CO_2RR performance is largely dependent on metal's locations, support, and preparation conditions (temperature, time, and preparation methodology).[218,219] The MOF-based synthesis is considered as an important strategy to isolate SACs,[39] for example, Co-,[206] Ni-,[96,164] Fe-,[101] and Cu-[159] based SACs. The first study to utilize SACs for electrochemical CO_2 reduction was reported by Li and coworkers[96] in which ZIF-derived N-doped carbon decorated with single Ni atoms (Ni SAs/N-C) was synthesized. This Ni SAs/N–C displayed tremendous performance to CO_2RR, attaining a high turnover frequency (TOF) of 5273 h^{-1} and a greater FE_{CO} of 71.9% at 0.89 V. The ordered SACs synthesis with a well-defined coordination environment for metal center is essential for optimization of activity and selectivity. This coordination environment has been shown to be strongly influenced by synthetic parameters such as selection of metal atoms, N and carbon supports as well as the
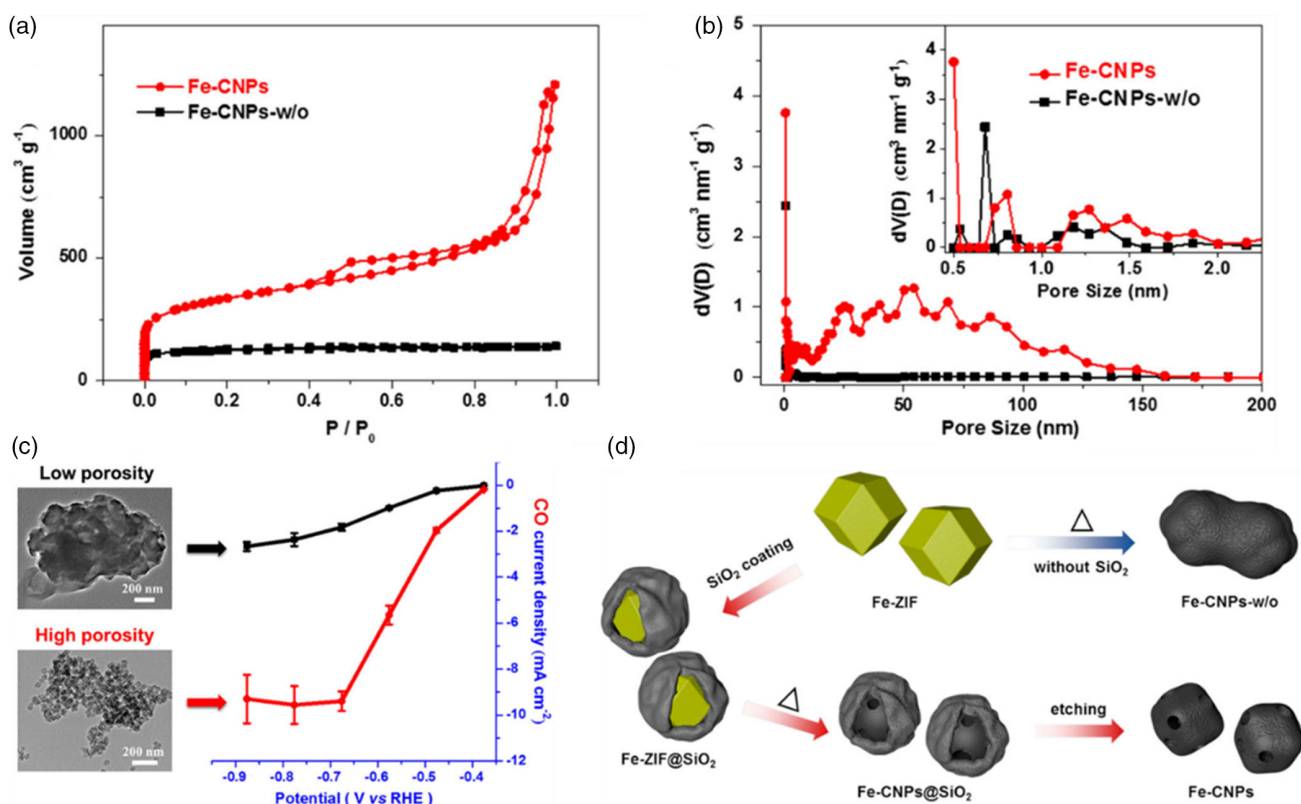
**Figure 16.** a,b) N_2 adsorption/desorption isotherms and pore-size distribution curves for both catalysts. c) CO_2RR performance as a function of porosity with transmission electron microscopy (TEM) images, d) schematic presentation of synthetic approach. Reproduced with permission.[208] Copyright 2019, American Chemical Society.

pyrolysis temperature. For instance, the researchers have adjusted the number of metal species in SACs through controlled volatile C–N fragments via varying pyrolysis temperatures. Further, Xie and coworkers also reported that Ni–N$_4$ active sites can be produced through topochemical transformation approach.[220] Special Ni–N$_4$ moieties worked as active species with improved CO$_2$RR performance and selectivity with high FE (90%) for CO at −0.5 to −0.9 V of potential range, offers 99% of Faradaic efficiency at 0.81 V with the highest current density of 28.6 mA cm^{-2}. In addition, Yang et al.[221] reported high-density, Ni-based SACs sites on the N-doped graphene for effective CO$_2$RR. Analysis of the XAS, in operando, recognized that Ni(I) (with electronic configuration d^9) were actual active sites for CO$_2$RR. This SAC showed high efficiency with an outstanding TOF of 14 800 h^{-1} and of 350 A/g$_{catalyst}$ of specific current at 0.61 V having 97% FE, after 100 h of continuous reaction testing, this catalyst also retained 98% performance.

The carbon supports of SACs also showed several features such as porosity, surface area, and electronic conductivity, which are essential for electrocatalytic performance and intrinsic performance of metal center in SACs tends to fluctuate noticeably even

with the same metal center. To evaluate and compare the exact role of metal in M–N–C, general synthesis of M–N–C SACs with a wide selection of metal species but similar microenvironment and supports are highly desired. Jiang et al.[222] prepared a series of isostructural porphyrinic multivariate-MOFs (MTV-MOFs) from M-TCPP (M = Fe, Co, Ni, and Cu; TCPP = tetrakis (4-carboxyphenyl)porphyrin)). Four types of SACs with different metal atoms (Fe, Co, Ni, and Cu) were prepared with the same microenvironment due to isomorphism of MTV-MOFs and spatial isolation of metal centers in M-TCPP and functioned as model SACs to relate the intrinsic activity of different single-atom metal species (**Figure 17**a). The Ni–N–C shows the highest FE$_{CO}$ (96.8 %) with a TOF up to 11 315 h^{-1} at −0.8 V in pure CO$_2$ (Figure 17b,c). Further, the Ni$_1$–N–C catalyst was able to catalyze the reduction of diluted CO$_2$, although a challenging task, and it offered better performance even at 30% and 15% CO$_2$ concentrations paving superior performance of Ni–N–C for CO$_2$RR in applied conditions.

In addition to the Ni species that have been individualized as active sites for CO$_2$RR, unique cobalt SACs are also being testified for enhancing CO$_2$RR activity. For instance, Lee and his fellow
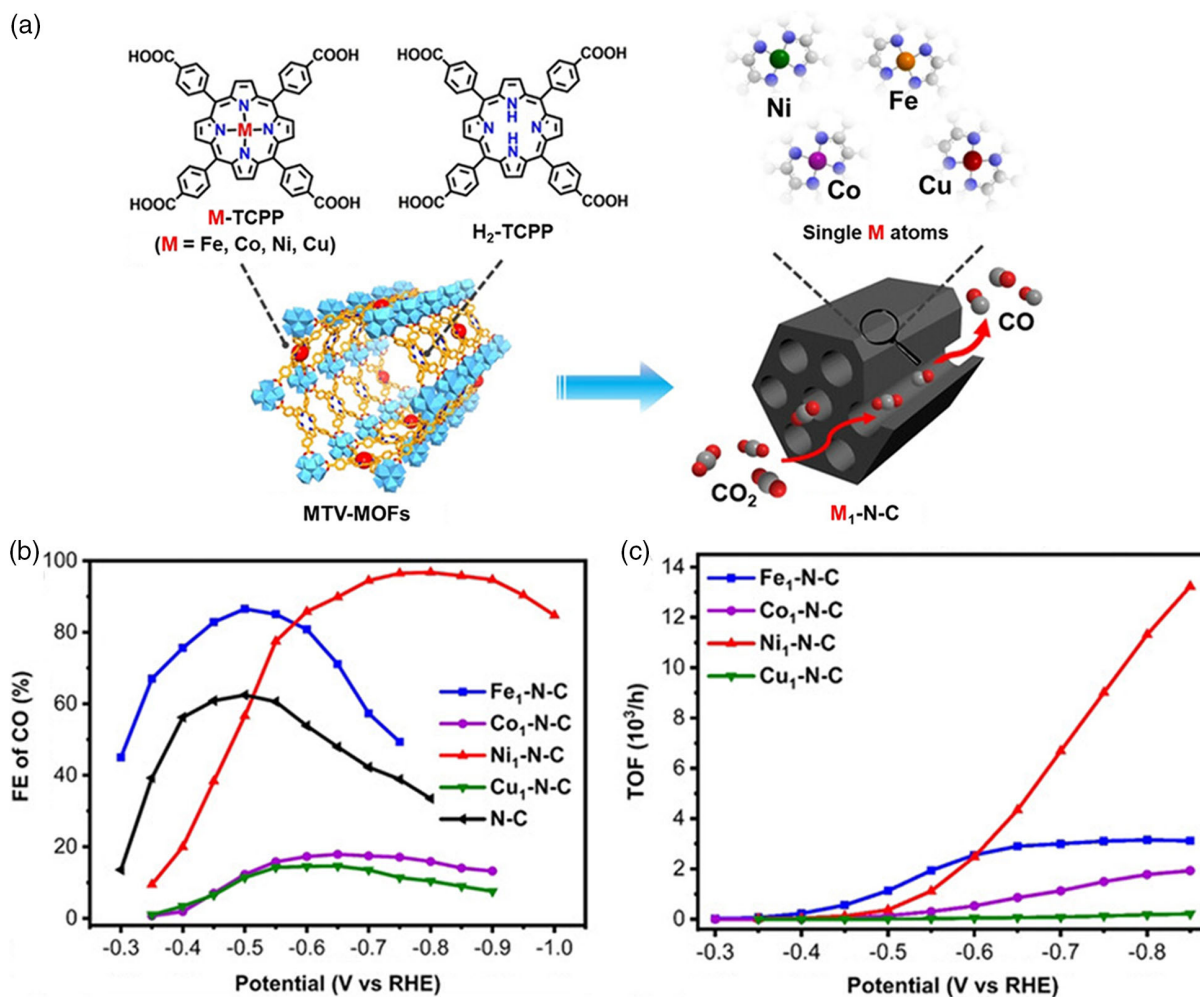
Figure 17. a) General fabrication of SACs with different metal centers from MTV-MOFs, b) FE$_{CO}$, c) TOF for SACs with different metal centers at low pressure CO$_2$RR. Reproduced with permission.[222] Copyright 2020, Wiley-VCH.

**ADVANCED
SCIENCE NEWS**

www.advancedsciencenews.com

**small
structures**

www.small-structures.com

researchers set up a series of Co monoatomic electrocatalysts with varying numbers of N coordination by regulating the CN under varying carbonization atmospheres.[206] In assessing the performance in electrochemical CO_2 reduction, it was found that Co single atomic centers coordinated with two N atoms showed better performance with 94% FE_{CO} and 18.1 mA cm^{-2} current density at 0.52 V overpotential, as compared with other N-CNs. This project demonstrates the key role of regulating coordination in active spaces in the activation of catalyst performance. In addition, Li and coworkers reported Co-SACs affixed in hollow porous carbon spheres derived from N-polymers to CO_2RR.[223] These Co-SACs improved the activity to 15.5 times in comparison with cobalt phthalocyanine (CoPC) and exhibited good performance with high FE_{CO} (90%) at potential from −0.57 to −0.88 V. The experimental results and DFT measurements have shown that the proposed Co–N_5 sites contributed mainly for activating CO, the rapid formation of important *COOH and CO desorption. In addition, Cu-SACs affixed on N-doped porous carbon (CuSAs/TCNF) were synthesized using electrospinned nanofibers of Cu/ZIF-8 and polymer as a Cu, N, and C source.[159] The CO_2RR performance of as prepared CuSAs/TCNF showed better selectivity toward methanol production (FE = 44%) having 93 mA cm^{-2} of current density (**Figure 18**a–c).

Recently, Li's group also reported an MOF-derived Bi SAC, and claimed that Bi–N_4 centers are real active sites to activate CO_2 and producing COOH* intermediates with a lower free energy barrier. The catalyst has a strong internal activity to reduce CO_2 into CO, with high Faradic efficiency (FE_{CO} up to 97%) and 5535 h^{-1} of TOF with a low potential of 0.39 V versus RHE.[158]

The most accepted fact is that CO_2RR mainly involves several steps including CO_2-adsorption, intermediates creation, production of final products, and desorption of reaction products.[224] It is urgent to understand the reaction mechanisms for further development of catalytic materials and the best way for this

understanding is in situ spectroscopic observations. For this purpose, some in situ techniques for characterization along with theoretical/computational studies, have been generally utilized to investigate the variation in valence states of metal ions, together with in situ intermediates formed during the electrochemical CO_2RR pathway.[225–228]

Pan et al.[223] conveyed that the electronic configuration of metal single atomic active sites can change during the reaction, and the electrocatalytic performances are closely correlated to the electronic structure. For example, in CO_2RR, by in situ XAS, the peaks associated with Co K-edge XANES were shifted to higher energy during the reduction process at −0.66 to −0.79 V than that of ex situ, suggesting the increment in the valence of Co during CO_2RR process. During the further higher potential (−0.88), the FE_{CO} is decreased and corresponding Co K-edge spectra showed a noticeable shift, indicating that fixed electronic structure has significance in CO_2RR catalysis.

Usually, the presence of a single metal atom is considered as an active site for CO_2RR, however, the surrounding environment of these active sites also has some impact on the overall performance of the catalysts. For example, Zhang et al.[229] justified this effect and showed that iron coordinated with five N atoms (FeN_5 SACs) has better performance for CO_2RR (FE_{CO} = 97%) as compared with that of FeN_4 active sites. In addition, the DFT calculations further illuminated that the edged M–N_{2+2}–C_8, which connect two adjacent layers of graphite in the shape of an armchair, are more active for CO_2RR than the massively recommended M–N_4–C_{10} moieties that are compactly encapsulated into the graphitic layers.[230] A similar type of active sites is also recently reported by Pan et al. via exploring the activity and active sites of Ni–N–C for the CO_2RR.[231] Atomically dispersed Ni atom, which was coordinated with N-doped C, was produced by thermal activation of chemically Ni-doped ZIF-8. Electrochemical results displayed an increase in internal activity
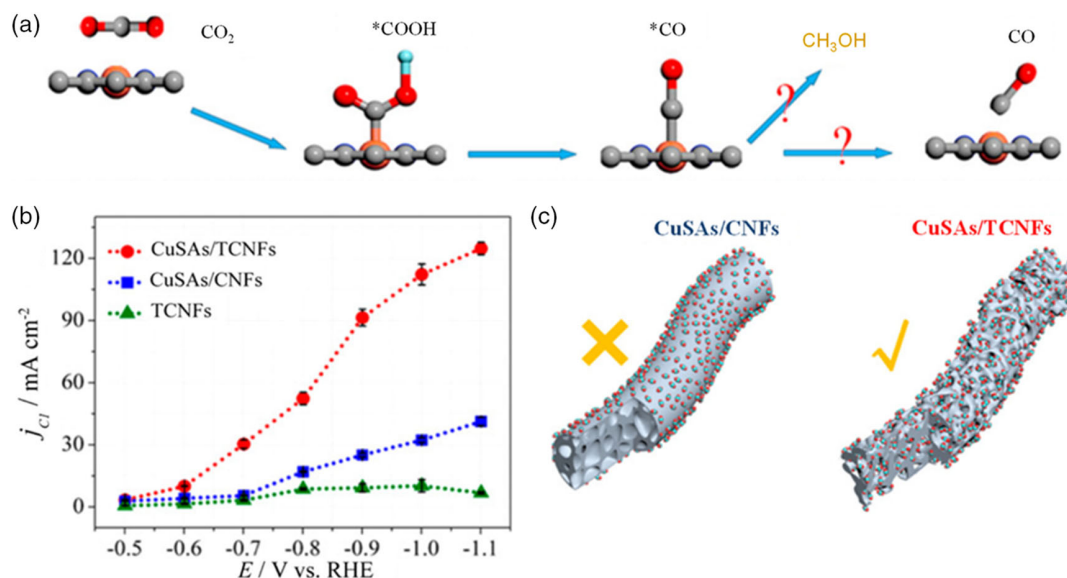

Figure 18. a) Proposed reaction pathways of CO_2RR on the optimized catalyst, b) comparison of the current density of optimized catalyst (CuSAs/TCNFs) with other prepared catalysts for C1 product, c) CO_2 diffusion on the surface of catalysts. Reproduced with permission.[159] Copyright 2019, American Chemical Society.

and selectivity of Ni–N centers to reduce CO_2 to CO, providing the maximum FE (96%) at -0.57 V. DFT calculations predicted that edged Ni–N_{2+2} centers facilitate the C—O bond breakage forming the *COOH intermediate, whereas the bulk Ni–N_4 are inactive.[231]

6. Microenvironment Modulation of MOF-Derived Single-Atom Electrocatalysts for CO_2RR

Mostly, metal atoms are stabilized on carbon support in isolation, this carbon support also ensures electrical conductivity for charge transport and larges surface area to enhance the mass transfer. Further, heteroatom doping (N, S, P, and O) and defective sites are also introduced in carbon supports to enhance the stability and also modify the electronic structure of the central metal atom. The favorite coordination environment (also microenvironment) of metal atoms not only enhanced the density of active sites but also stabilized the isolation by preventing agglomerations of metal atoms.[116,232,233] This microenvironment, may be deified as "the specific chemophysical environment of the metal atom including the coordination and electronic state of metal as well as the types and number of coordinated atoms" provides outstanding benefits to attain better performance following the selectivity and stability for CO_2RR. For example, M-$N_xC_yV_z$ (M = metal, N = N, S, P, O, heteroatoms, V = vacancy) is considered as the most common structure (**Figure 19**) of SACs with excellent performance for electrocatalysis including CO_2RR. MOFs are widely considered as excellent precursors for the synthesis of this type of active site by high-temperature pyrolysis. The various actives sites can be produced by tuning the pyrolysis temperature as well as the MOF-based precursors.
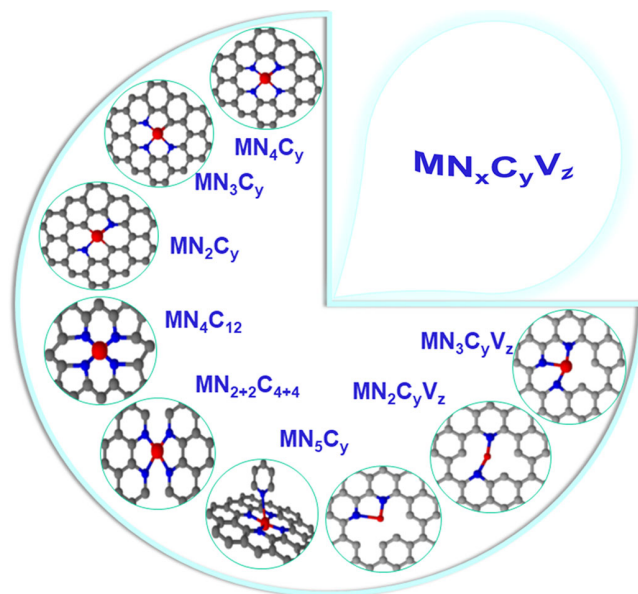
Figure 19. Some typical examples of single-atom active sites with the defined microenvironment.
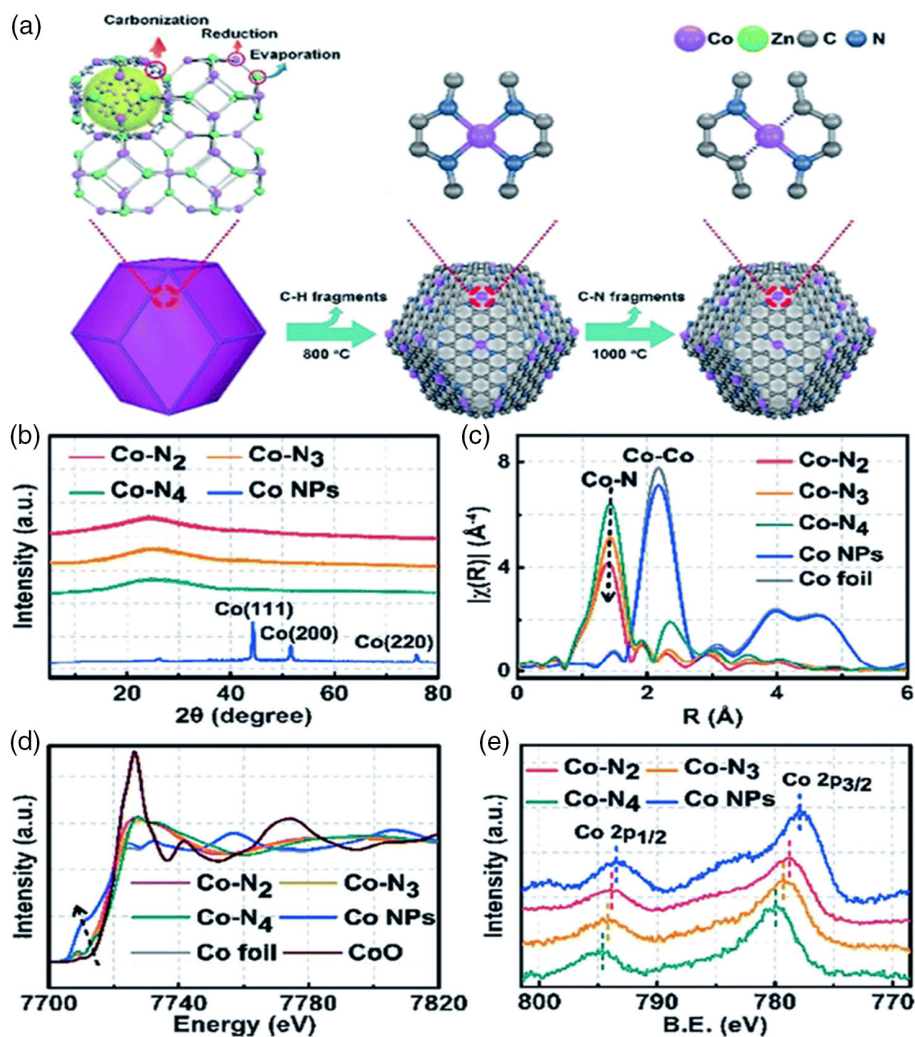
6.1. Tuning Nitrogen Atoms Coordinated with Metal

Transition metal with nitrogen showed high activity and selectivity for CO_2 and thus provide a platform for the improvement of future CO_2RR materials based on the nitrogen-doped transition metal catalysts. Tuning the number of coordinated N atoms with central metal atom by keeping the CN of metal constant, alter the catalytic performance of the catalysts. Several types of active sites are reported including M–N_2–C_2, M–N_3–C, M–N_4, and so on. Agreeing with previous works,[164,164,206] a reduction in the number of N-atoms coordination can effectively optimize the activity of CO_2RR catalysts. **Figure 20**a shows Co-coordinated numbers of N can be adjusted by adjusting the temperature of the pyrolysis.[206] By increasing the temperature, several Co^{II}–imidazolate–Co^{II} linkages were decomposed leading to a change in N—Co bonds, and therefore obtained active sites are assessed as Co—N_x ($x = 2$, 3, 4). The XRD (Figure 20b) result indicates the absence of Co NPs and EXFAS spectrum (Figure 20c) shows that the maximum intensity corresponding to the Co–N decreases as the number of coordination decreases. In addition, XANES (Figure 20d) and XPS (Figure 20e) showed that the oxidation state of Co is between 0 and 2+, and also varied with a change in CN. In the DFT calculations, it was found that the decrease in the CN of local Co centers resulted in the displacement of the Co d-band center and therefore the stronger *CO_2. bonding, the current and mass density of CO are improved significantly.

In addition, regulating the local electronic Ni species environment can possibly activate the catalytic inactive sites, and low-valent Ni species, which can facilitate the adsorption and adsorption process for CO_2, which has improved the conversion of CO_2 into CO.[163,164,234] Yang and coworkers experimentally demonstrated this fact by synthesizing Ni(NC)-based electrocatalysts (**Figure 21**a–e), containing both isolated Ni atoms and Ni NPs, by simple Ni-organic frameworks (MOF)-based strategies, which provide sufficient Ni–N moieties as active sites for CO_2RR.[163] Electrochemical measurements showed a high CO_2RR conversion with 99% FE at -0.75, -0.80 V versus RHE. Significantly high FE_{CO} was achieved at simultaneous current density (j) 40–180 mA cm^{-2} in the flow cell and a remarkable $j = 160$ mA cm^{-2} with a selectivity of 99% FE_{CO}. These findings showed that the surficial N species greatly optimized the electronic configuration of Ni and converts inactive sites into active sites.

These adjusted Ni–N patterns play a significant part in facilitating CO absorption and desorption and concrete the way for the production of effective nitrogen-based metal materials for CO_2RR.[222,235] Recently, our group has reported facile protocols to control the N-CN of central metal atoms in M–N_x-type SACs derived from MOFs[148,164,222]. By optimizing pyrolysis temperature (**Figure 22**a), the optimum Ni_{SA}–N_2–C with a single Ni atom coordinated by two nitrogen and carbon atoms shows exceptional performance and exceeds the object that coordinates Ni center with multiple N atoms such as Ni_{SA}–N_3–C and Ni_{SA}–N_4–C. According to the DFT measurements, the lowermost free energy barrier for the rate-limiting step and very low desorption energy (0.47 eV) of *CO Ni_{SA}–N_2–C are responsible for enhanced catalytic activities of all Ni_{SA}–N_x–C (Figure 22b-d).[164]

ADVANCED
SCIENCE NEWS
www.advancedsciencenews.com

small
structures
www.small-structures.com

Figure 20. a) Synthesis of Co–N_x active sites via temperature controlled pyrolysis, b–e) XRD patterns, EXAFS, XANES, and XPS spectra for as-prepared catalysts. Reproduced with permission.[206] Copyright 2020, Wiley-VCH.

Recently, Jiang and coworkers[235] developed postsynthetic metal substitution (PSMS) strategy to attain low-coordinated Ni single-atom electrocatalysts on ZIF-8-derived N-doped carbon (**Figure 23**a). This strategy illustrates the filling of Ni atoms in the Zn vacancies derived from Zn–N_3–C due to easily breakable Zn–N coordination bonds in acidic media, leaving N-doped carbon (N–C) with abundant Zn vacancies surrounded by 3 N atoms. The Ni–N_3–C, with single Ni atoms coordinated by 3 N atoms on the N-doped carbon presents an ultrahigh CO FE up to 95.6 % with a TOF of 1425 h^{-1} at −0.65 V in the electrocatalytic CO_2RR, much better than that of pure N–C and Ni–N_4–C involving Ni–N_4 sites. Further, Ni–N_3–C showed better performance (CO 90%) as a cathode in Zn–CO_2 battery (Figure 23b,c) and excellent stability.

The density of active sites, i.e., the distance between single metal atoms also affects the selectivity of the product. For instance, Guan et al.[236] discussed the effect of concentration of Cu in Cu–N_x catalysts, the results demonstrated that high Cu concentration (4.9%$_{mol}$), active sites close to each other,

empowers coupling of C–C and produces ethylene. However, CH_4 was obtained by reducing the concentration of Cu species lower than 2.4%$_{mol}$, as a result, the formation of C1 product was favored because of an enlarged distance between Cu–N_x species.[236] The DFT calculations auxiliary explained the aptitude of ethylene generation via two CO intermediates binding on two adjacent Cu–N_2 sites, whereas the adjacent Cu–N_4, single Cu–N_4, and Cu–N_2 sites directed to the CH_4 production. The Cu–N_x active sites were tuned by simple pyrolysis of Cu–MOF in the presence of dicyandiamide (N source) at a different temperature, the synthesis protocol is shown in **Figure 24**a–c.

6.2. Fine Tuning the Coordinating Atoms

In addition to the CN of central metal atoms, the type of coordinated atoms is also highly important in regulating CO_2RR performance.[164,221] Similarly, Fan et al.[224] described the effect of coordinated N atoms with the central metal atom (Ni) and found that pyrrolic-N (Ni@N_3) is more efficient as compared to its
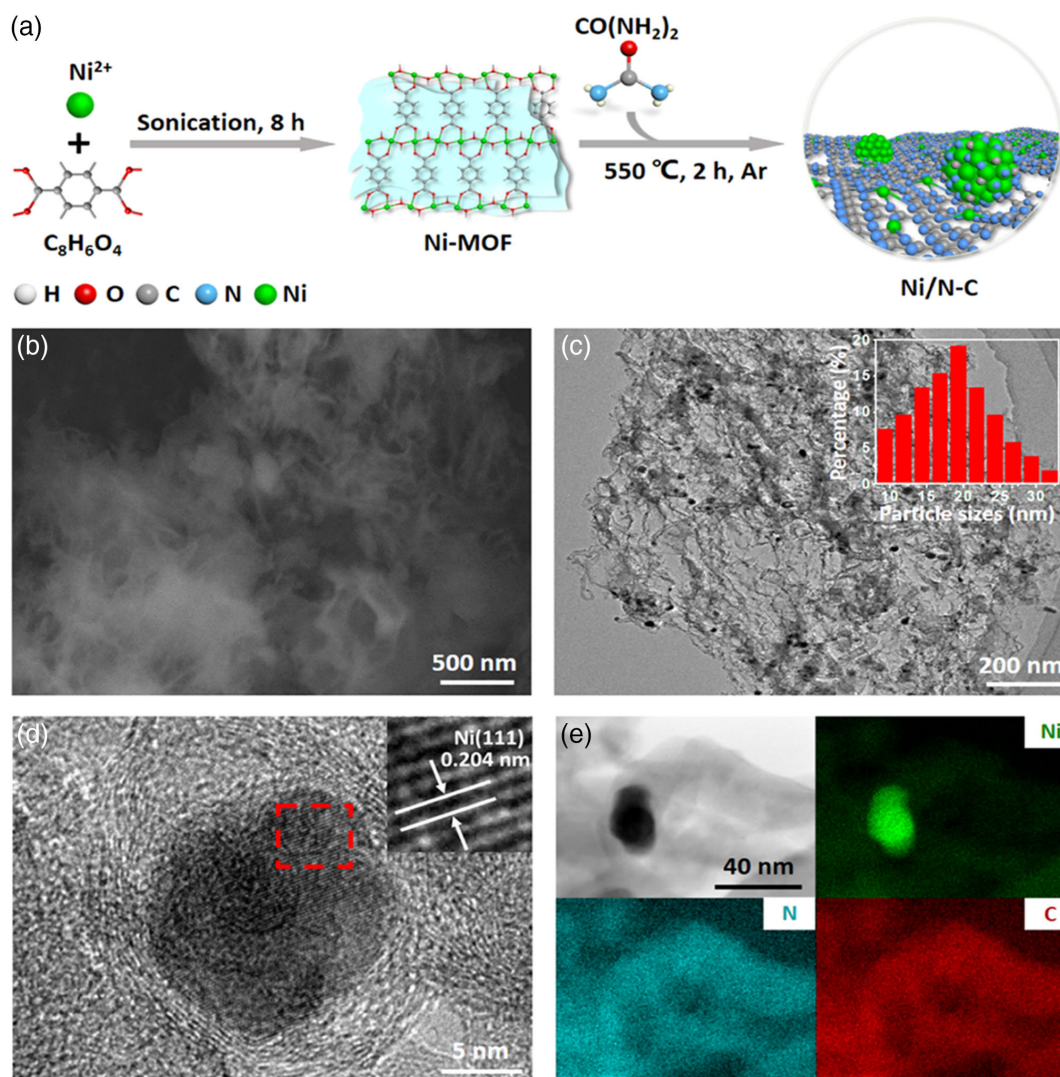
Figure 21. a) Synthetic scheme of Ni(NC) catalysts, b–d) representative scanning electron microscopy (SEM), TEM, and high resolution transmission electron microscopy (HRTEM) images, respectively, e) TEM image of Ni(NC)-1 and elemental mapping images. Reproduced with permission.[163] Copyright 2020, American Chemical Society.

counterpart pyridinic-N(Ni@N₃). The CO₂RR results showed more than 90% FE, $12\,000\,h^{-1}$ TOF, and $10\,600\,mA\,mg^{-1}$ of metal mass activity. The DFT calculations further confirmed the experimental results and showed that theNi@N₃(pyridinic) and Ni(111) active sites are associated with extremely endothermic free energy changes, representing that these sites are easily poisoned by *CO, thus not appropriate for CO₂RR. Though the Ni@N₃ (pyrrolic) exhibited a -0.03 eV of free energy change, indicating the easy CO desorption. Furthermore, the more negative free energy on Ni@N₃(pyrrolic) for *COOH than that of *H eased the thermodynamic conversion of CO₂-to-CO.[224] In addition to this, different heteroatoms directly coordinated with central metal atoms also alter the electronic configurations and definitely affect the catalytic performance. For instance, Yang and coworkers[129] synthesized Ni-based catalysts named single-Ni-atom catalyst with sulfur-doped graphitic nitride

(A-Ni–NSG), in which Ni atoms directly coordinated with dual heteroatoms (N, S) showed fragile electronegativity than that of N-pyrrolic present in Ni(II) Pc, ensuing Ni(I) with d⁹ electronic configuration. Dual-coordinated metal (Ni) atoms with low-valent Ni(I) have been shown as effective for CO₂RR with high current density, TOF and FE_CO of $350\,A/g_{catalyst}$, $14\,800/h$, and 97%, respectively, at only 0.61 V overpotential. Furthermore, an alternative strategy to influence the electronic configuration of metal atoms is the introduction of additional metal atoms to form isolated dual-atom active sites and this has been proven to be a strong approach for changing the catalytic process by breaking down energy barriers within CO₂RR. This strategy was successfully applied by Ren et al. and described Ni/Fe–N–C catalyst with single Fe–Ni active sites.[129] The Ni/Fe–N–C was found considerably superior for the electrocatalytic CO₂ conversion into CO, with a higher current density than that of Fe–N–C and Ni–N–C.
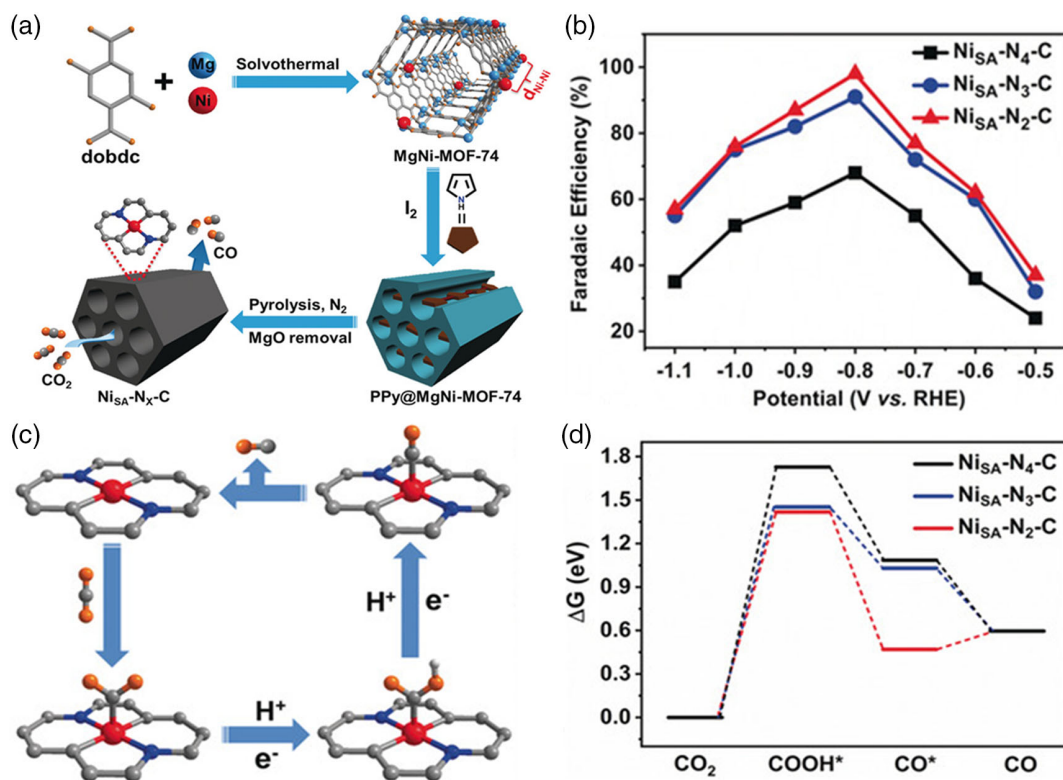
Figure 22. a) Graphic presentation of synthesis of $Ni_{SA}–N_x–C$ materials for CO_2RR. b) FE_{CO} of $Ni–N_x–C$ at different potentials, c) proposed reaction paths for CO_2RR with $Ni_{SA}–N_2–C$ as a model, d) Free-energy diagram of CO_2 reduction to CO over $Ni_{SA}–N_x–C$ catalysts. Reproduced with permission.[164] Copyright 2020, Wiley-VCH.

Following the DFT calculations, the rate-determining steps on the Fe–N–C and Ni–N–C catalysts are the desorption of CO and formation of *COOH. For dual-atomic catalyst (Ni/Fe-N-C), the CO_2 is reduced in CO with the formation of CO bridged type Ni(CO) Fe–N–C, thereby reducing the energy barrier to *COOH formation, resulting in an enhanced catalytic performance at the Ni–Fe dual-atomic active sites for CO_2RR. These studies suggest that tuning the coordinating atoms can alter the catalytic performance. There are more studies required to evaluate the optimal effect of coordinating atoms for practical applications.

6.3. Vacancy-Defect Engineering

The vacancy-defect engineering or introducing defects in metallic sites as well as in the catalytic supports are considered as alternative techniques for enhancing performance by improving CO_2 adsorption.[208,237–241] Several strategies are reported for introducing the defects including the doping of heteroatoms in the carbon support (environmental modulation) or removing the weak coordinated atoms of central metal. For example, very recently, Rong et al.[242] established a controlled methodology for synthesizing Ni-based catalysts with defective vacancy round the Ni–N_3–V active sites by gradually removing the oxygen—Ni weaker bond under high temperature (800 °C) pyrolysis. The vacancy-defect Ni–N_3–V SACs boosted the CO_2RR activity with 90% FE, much better than that of no-vacancy-defect Ni–N_4 SAC. The DFT and experimental outcomes showed that vacancies have

a strong influence on enhancing the performance of Ni–N_3–V active sites, indicating the benefits of introducing defects in improving the electrocatalytic performance. In addition, defects around M–N_x can also have a crucial role in catalytic activity.[237] Defective vacancies in metals, as shown in **Figure 25**a–c, were used as models for calculating the free energies of two competitive reactions (HER and CO_2RR), including NiN_4, NiN_3, NiN_3V, and NiN_2V_2, the free energy for *COOH was found highest on Ni–N_4 active sites indicating the desorption of *CO is the most difficult, whereas Ni–N_3–V indicating the high activity for CO_2RR.[237]

In addition to the defects in metal–N centers, Qin et al.[238] used Fe metal centers to study the effect of defect engineering in support, and in situ fourier transform infrared spectroscopy (FTIR) studies were supported by DFT calculations to identify the actual active sites for CO_2RR. The results indicated that active sites (Fe–N_4) embedded in the defective carbon layers are more effective for CO_2-to-CO conversion (**Figure 26**a). In contrast, Fe-centers (Fe–N_4) affixed to the perfect graphite layer revealed CO poisoning effect due to strong CO adsorption. These consequences encouraged researchers to develop in-depth understanding toward the local environment of metal centers. As porosity in support may also improve mass transfer and CO_2RR kinetics along with more efficient metal centers on the porous edge of supporting materials, it is valuable for designing more porous supports. Cheng et al.[239] fabricated an USA tip-anchored Ni SAC on graphene oxide (referred to as Ni–N–MEGO having
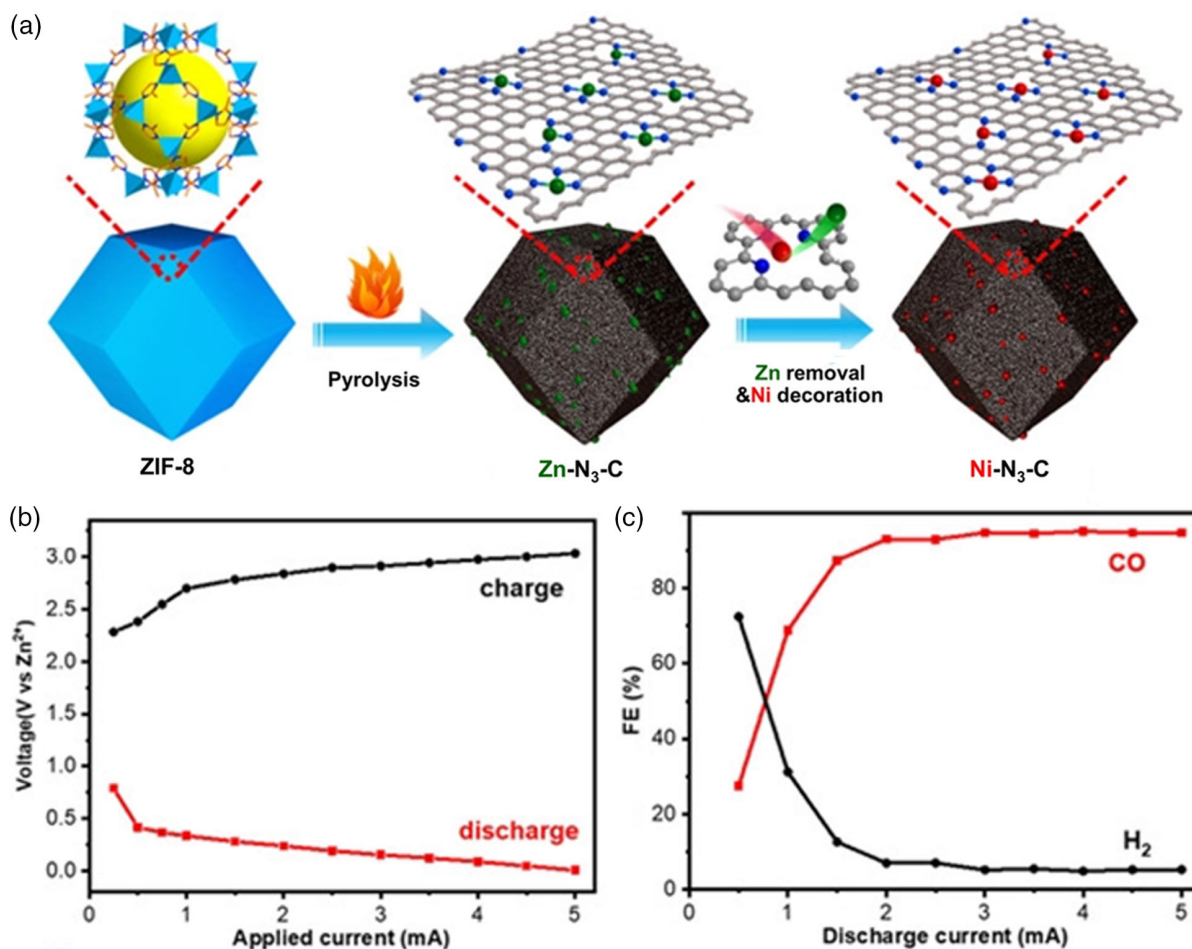
Figure 23. a) Synthesis of Ni–N₃–C SACs, charging, and discharging curves of Zn–CO₂ battery, b) voltage, and c) FE of CO and H₂. Reproduced with permission.[235] Copyright 2021, Wiley-VCH.
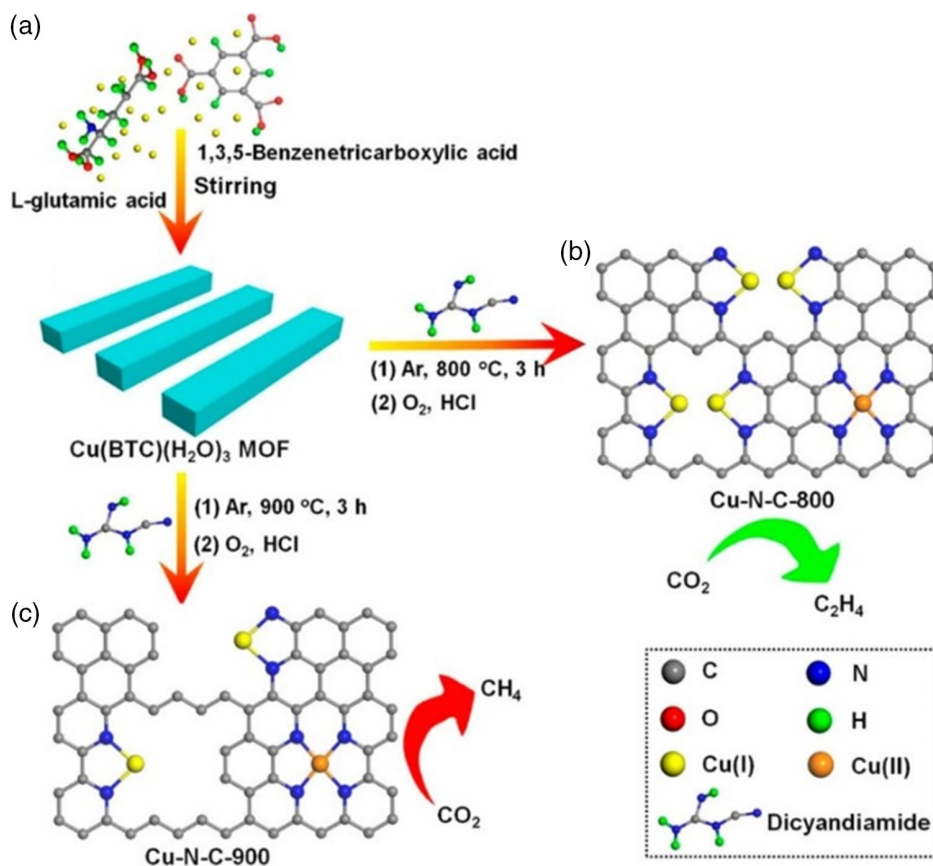
6.9 wt% Ni contents) and evaluated CO_2RR activity. Figure 26b further shows that the individual Ni centers were largely anchored at the edges and served as main active sites. The DFT measurement proposed that nickel atoms having USA N species have high efficiency for reducing CO_2 as compared with located in-plane assemblies (Figure 26c).

7. Conclusion and Future Outlook

MOFs have been developed rapidly as promising materials to replace conventional catalysts. Among others, MOFs are also considered as potential candidates for electrocatalysis of carbon dioxide, which is alarming greenhouse gas for human society. CO_2 can be converted into various useful products but the selectivity and activity of a catalyst toward a specific product are mainly dependent on the nature of active sites present in the catalyst. In MOF, metal centers are usually considered as catalytic active sites and ligands facilitate the conversion process. The catalytic performance of pristine MOFs can be further enhanced by using various strategies, such as tuning/changing the ligand, encapsulation of active metal centers and/or modifying the electronic structure. The porous structure of MOFs facilitates mass transport and a high surface area with dispersed metallic nodes can provide an enhanced number of active sites.[243] Even with amazing improvements in the CO_2RR performance by MOF-based electrocatalysts, there are still some challenges for practical applications. The inherited limited conductivity, chemical stability, and short mass permeability due to microporous structure, hindered the MOFs for commercial applications. The conductivity and stability are severe problems for MOFs, particularly with the very negative potential commonly used in CO_2RR, more negative than the reduction potential of many metals utilized in MOF preparation. The studies also showed that the inherited conductivity of MOFs can also be enhanced by compositing with conductive materials or capturing the MOFs on conductive supports. Nevertheless, simple analysis pageants that many MOFs are indeed unstable during the reduction process of carbon dioxide in aqueous electrolytes at highly negative potentials. Therefore, the metal NPs produced by reducing MOFs worked as electrocatalysts for CO_2RR. Consequently, the stability of MOF-based catalysts is a critical issue to be resolved.

In this aspect, an easy approach is to convert MOFs into stable and electrically conductive materials having featured

**ADVANCED
SCIENCE NEWS**

www.advancedsciencenews.com

**small
structures**

www.small-structures.com

Figure 24. Illustration of synthetic procedure of catalyst, a) MOF precursors. Cu–N–C–temp prepared by the pyrolysis of dicyandiamide/MOF at b) 800 °C, c) 900 °C, favors CO_2RR conversion into C_2H_4 and CH_4, respectively. Reproduced with permission.[236] Copyright 2020, American Chemical Society.

characteristics of MOFs such as porous structure, high surface area, and fully dispersed metallic active sites. Currently, two main strategies are being applied for conversion of MOFs, i.e., electrical conversion and thermal conversion, the latter is a more appealing and widely used technique. MOF-derived catalysts attract rather more attention for electrocatalysis, because of their high mass transportation ability (porous structure), widely dispersed actives sites (high surface area), and conductivity (heteroatom-doped carbons). The MOF-derived electrocatalysts can be termed as, metal oxides, metal NPs on carbon supports, metal-coordinated N-doped carbons such as SACs, metal-free electrocatalysts, and nanocomposites on the basis of structure and functional properties.

Despite the appealing developments in the MOF-based/-derived materials for electrocatalytic CO2RR, there are still existing challenges for using MOFs for CO_2RR including but not limited to: 1) For pristine MOFs, the electrical conductivity and stability of MOFs should be carefully evaluated and proper strategies should be established that could warrant these factors. The results indicate that pristine-MOFs are reduced/oxidized during electrocatalytic reduction of carbon dioxide. An intuitive and accurate model that can describe the actual structure–activity relationship is urgently required for the design and development of pristine MOF for electrochemical reduction of CO_2. To resume these issues, researchers should do efforts in the future regarding the use of MOFs for CO_2RR. a) more conductive MOFs should be prepared to facilitate the rapid charge transfer. b) the mass transportation problem can be resolved by developing hierarchical porous or ultrathin foliated structures. c) the stability problem should be resolved by preparing/improving the thermal, mechanical or chemical stability of MOFs, because the structural and chemical stabilities are major contributors for electrocatalytic performance. 2) There are extensive opportunities to explore MOF composites for CO_2RR, very few literatures are available. The MOF composites with other crystalline porous materials including MOF–MOF and MOF–COF composites for electrocatalytic reduction of CO_2 may have great potential. Further, research should be focused on this specific field, because MOF has wide diversity to in the synthetic protocols for MOF/COF@MOF core–shell structures. 3) Most of studied catalysts are yet to be commercialized, but the high cost of precursors is also an obstacle. Costly ligands (porphyrins) and organic solvents (DMF) are used for the synthesis of MOFs, which made this technology economically unaffordable. Therefore, the researchers should also have to consider the cost factor in future research to discover cost-effective MOFs for commercial use. 4) MOF-derived catalysts showed a strong structure–activity relationship and the coordination atmosphere as well as CN of active sites (usually metal) have a significant impact on the performance of catalysts. Among all, metal-coordinated N-doped
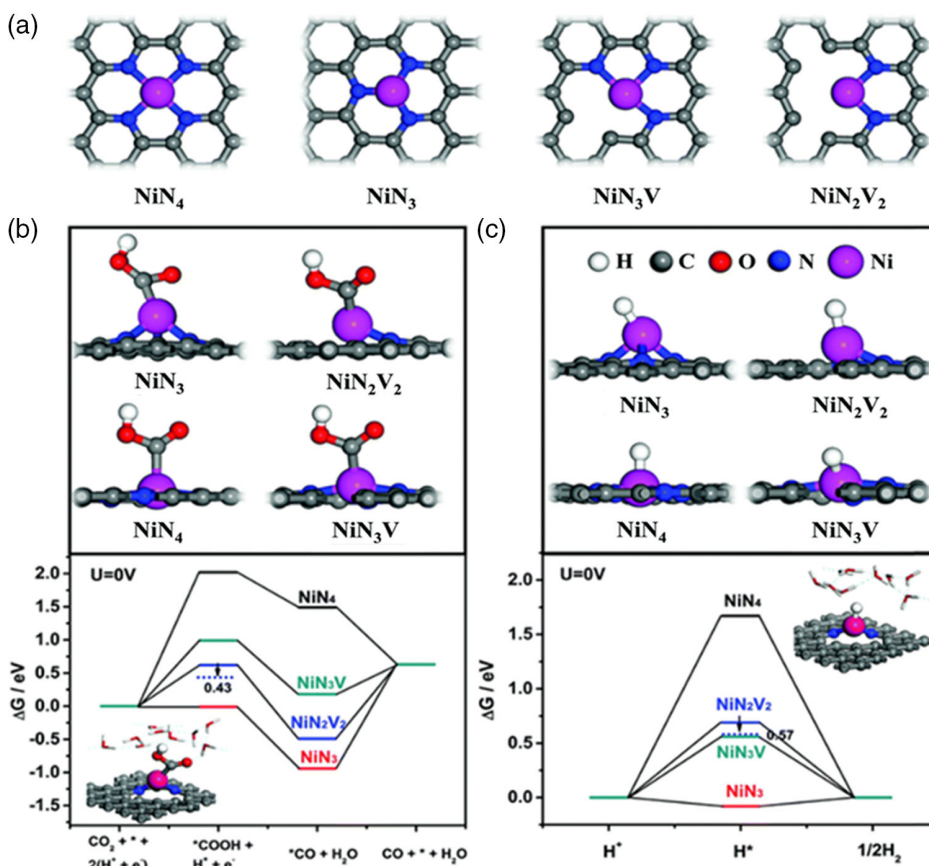
Figure 25. a) Optimized representative structures of active sites, b,c) Free energy diagrams representing the solvation effect on CO_2RR and HER mechanism. Reproduced with permission.[237] Copyright 2018, The Royal Society of Chemistry.
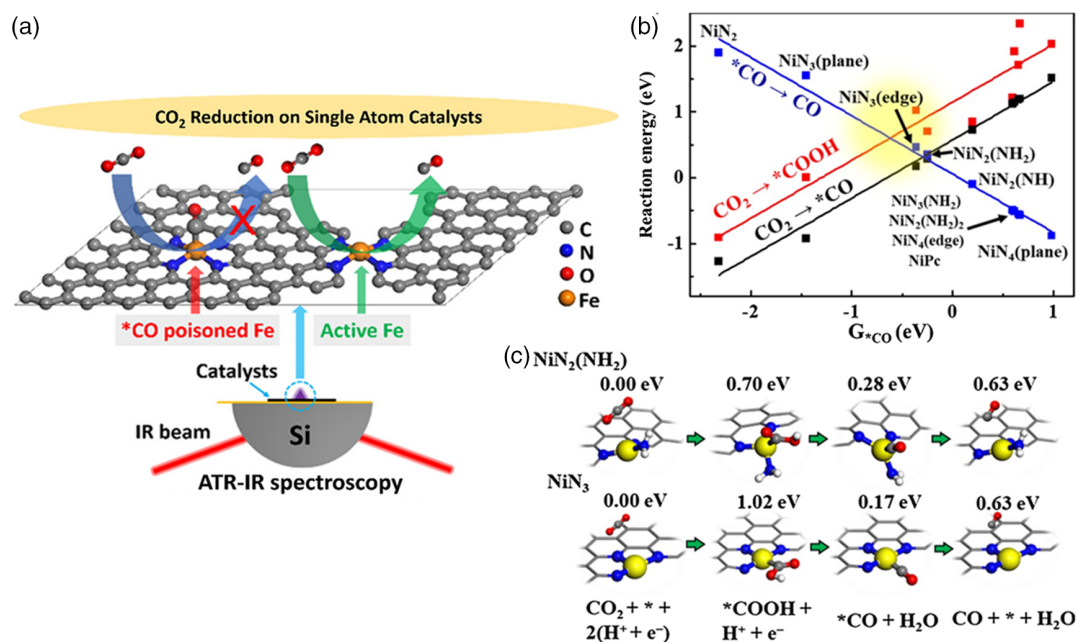
Figure 26. a) Active sites of heterogeneous Fe SAC in electrochemical CO_2RR. Reproduced with permission.[224] Copyright 2020, Wiley-VCH. b) Reaction energy is proportional to energy of adsorption *CO in active sites, c) the reaction path for edge-located NiN_3 and $NiN_2(NH_2)$ active sites with free adequate energy. Reproduced with permission.[239] Copyright 2019, Elsevier.

**ADVANCED
SCIENCE NEWS**

www.advancedsciencenews.com

**small
structures**

www.small-structures.com

carbons with single-atom active sites are considered as better catalysts for CO_2RR. Therefore, advanced spectroscopic techniques such as high-angle annular dark-field scanning transmission electron microscopy (HAADF-STEM), extended X-ray absorption fine structure (EXAFS), electron energy loss spectroscopy (EELS), X-ray absorption near edge structure (XANES), and X-ray photoelectron spectroscopy (XPS), etc. are being used to reveal the actual structure of active sites. Though, DFT calculations have resolved the puzzle by identifying various active sites for different materials. Some in situ studies also revealed the structure changes during the electrocatalytic CO_2RR process under various ranges of applied potential, which showed that in situ active sites are relatively different than that of ex situ. Consequently, it is recommended that more in situ spectroscopic techniques should be applied to monitor the structural changes during the CO_2RR process and this would be helpful for the optimization of catalysts for commercial applications. 5) Moreover, it can be noted that high loadings of metal contents do not essentially guarantee high performance, probably a significant number of metal atoms encased in carbon materials with low availability for reacting species. Catalytic activities of SACs are therefore mainly related to the metal atoms affixed on the available surface. In addition, the high surface energy of individually isolated metal atoms also poses a major challenge for the stability of SACs. For selective control of the reaction pathways, the central descriptors and binding energy of intermediate products must be assumed first and the rational design of a catalyst must be established on the basis of these descriptors. The electrocatalytic capacity primarily depends upon the internal environment (intrinsic active sites) of material. But it can also be altered via structure engineering with doping, alloying, and changing the morphology. 6) Most MOF-derived catalysts used for CO_2RR are limited to ZIF-8, or some simple MOFs. The other MOFs should be used to further explore the potential of MOF-derived electrocatalysts. Using MOFs with different morphologies and porosities may give a suitable control to the activity and selectivity of reaction.

Withstanding these challenges, the achievements thus far looks very promising and clear from this review that MOF-based/derived catalysts approach for CO_2RR is still in its early stage. In short, MOFs are emerging materials for CO_2RR, several major breakthroughs along this direction are shown in **Figure 27** and much more are still to be discovered. The continues efforts are required for developments in this regard, there are great opportunities to achieve controlled synthesis for selective catalysis.

Acknowledgement

Conflict of Interest

The authors declare no conflict of interest.

Keywords

[1] R. Snoeckx, A. Bogaerts, *Chem. Soc. Rev.* **2017**, *46*, 5805.

[2] L. Li, Y. Huang, Y. Li, *J. Energy Chem.* **2020**, *2*, 100024.

[3] D. Li, M. Kassymova, X. Cai, S.-Q. Zang, H.-L. Jiang, *Coord. Chem. Rev.* **2020**, *412*, 213262.

[4] L. Jiao, J. Y. R. Seow, W. S. Skinner, Z. U. Wang, H.-L. Jiang, *Mater. Today* **2019**, *27*, 43.

[5] D. Zhao, C. Kong, H. Du, Y. Yan, Z. U. Wang, H.-L. Jiang, L. Chen, *Sci. China Mater.* **2018**, *62*, 448.

[6] G. Centi, E. A. Quadrelli, S. Perathoner, *Energy Environ. Sci.* **2013**, *6*, 1711.

[7] J.-D. Xiao, H.-L. Jiang, *Acc. Chem. Res.* **2019**, *52*, 356.

[8] X. Ma, L. Wang, Q. Zhang, H.-L. Jiang, *Angew. Chem. Int. Ed.* **2019**, *58*, 12175.

[9] Y.-Z. Chen, R. Zhang, L. Jiao, H.-L. Jiang, *Coord. Chem. Rev.* **2018**, *362*, 1.

[10] J. Xie, Y. Huang, M. Wu, Y. Wang, *ChemElectroChem* **2019**, *6*, 1587.

[11] A. Vasileff, Y. Zheng, S. Z. Qiao, *Adv. Energy Mater.* **2017**, *7*, 1700759.

[12] S. Gao, Y. Lin, X. Jiao, Y. Sun, Q. Luo, W. Zhang, D. Li, J. Yang, Y. Xie, *Nature* **2016**, *529*, 68.

[13] M. Liu, Y. Pang, B. Zhang, P. De Luna, O. Voznyy, J. Xu, X. Zheng, C. T. Dinh, F. Fan, C. Cao, F. P. G. de Arquer, T. S. Safaei, A. Mepham, A. Klinkova, E. Kumacheva, T. Filleter, D. Sinton, S. O. Kelley, E. H. Sargent, *Nature* **2016**, *537*, 382.

[14] X. Zhi, Y. Jiao, Y. Zheng, K. Davey, S.-Z. Qiao, *J. Mater. Chem. A* **2021**, *9*, 6345.

[15] F. Li, H. Yang, W. Li, L. Sun, *Joule* **2018**, *2*, 36.

[16] X. Zheng, P. De Luna, F. P. García de Arquer, B. Zhang, N. Becknell, M. B. Ross, Y. Li, M. N. Banis, Y. Li, M. Liu, O. Voznyy, C. T. Dinh, T. Zhuang, P. Stadler, Y. Cui, X. Du, P. Yang, E. H. Sargent, *Joule* **2017**, *1*, 794.

[17] X. Zhang, Z. Wu, X. Zhang, L. Li, Y. Li, H. Xu, X. Li, X. Yu, Z. Zhang, Y. Liang, H. Wang, *Nat. Commun.* **2017**, *8*, 14675.

Figure 27. Major research outputs in MOF-based/-derived electrocatalysts for CO_2RR.

[18] L. Zhang, Z.-J. Zhao, J. Gong, *Angew. Chem. Int. Ed.* **2017**, *56*, 11326.

[19] C. Costentin, M. Robert, J.-M. Savéant, A. Tatin, *Proc. Natl. Acad. Sci.* **2015**, *112*, 6882.

[20] H. Furukawa, K. E. Cordova, M. O'Keeffe, O. M. Yaghi, *Science* **2013**, *341*, 1230444.

[21] M. Ding, X. Cai, H. -L. Jiang, *Chem. Sci.* **2019**, *10*, 10209.

[22] T. Qiu, S. Gao, Z. Liang, D. G. Wang, H. Tabassum, R. Zhong, R. Zou, *Angew. Chem. Int. Ed.* **2021**, *133*, 17455.

[23] L. Li, Z. Li, W. Yang, Y. Huang, G. Huang, Q. Guan, Y. Dong, J. Lu, S.-H. Yu, H.-L. Jiang, *Chem* **2021**, *7*, 686.

[24] S. S. A. Shah, T. Najam, M. K. Aslam, M. Ashfaq, M. M. Rahman, K. Wang, P. Tsiakaras, S. Q. Song, Y. Wang, *Appl. Catal. B* **2020**, *268*, 118570.

[25] M. A. Nazir, N. A. Khan, C. Cheng, S. S. A. Shah, T. Najam, M. Arshad, A. Sharif, S. Akhtar, A. U. Rehman, *Appl. Clay Sci.* **2020**, *190*, 105564.

[26] T. Najam, M. Wang, M. S. Javed, S. Ibraheem, Z. Song, M. M. Ahmed, A. U. Rehman, X. Cai, S. S. A. Shah, *J. Colloid Interface Sci.* **2020**, *578*, 89.

[27] T. Najam, X. K. Cai, M. K. Aslam, M. K. Tufail, S. S. A. Shah, *Int. J. Hydrogen Energy* **2020**, *45*, 12903.

[28] N. A. Khan, S. Shaheen, T. Najam, S. S. A. Shah, M. S. Javed, M. A. Nazir, E. Hussain, A. Shaheen, S. Hussain, M. Ashfaq, *Toxin Rev.* **2020**, 1.

[29] N. A. Khan, T. Najam, S. S. A. Shah, E. Hussain, H. Ali, S. Hussain, A. Shaheen, K. Ahmad, M. Ashfaq, *Mater. Chem. Phys.* **2020**, *245*, 122737.

[30] T. Najam, S. S. A. Shah, W. Ding, Z. Wei, *J. Phys. Chem. C* **2019**, *123*, 16796.

[31] T. Najam, S. S. A. Shah, W. Ding, Z. Ling, L. Li, Z. D. Wei, *Electrochim. Acta* **2019**, *327*, 134939.

[32] T. Najam, S. S. Ahmad Shah, W. Ding, J. Deng, Z. Wei, *J. Power Sources* **2019**, *438*, 226919.

[33] S. S. A. Shah, T. Najam, C. Cheng, L. Peng, R. Xiang, L. Zhang, J. Deng, W. Ding, Z. Wei, *Chem. Eur. J.* **2018**, *24*, 10630.

[34] S. S. Ahmad Shah, T. Najam, C. Cheng, S. Chen, R. Xiang, L. Peng, L. Lu, W. Ding, Z. Wei, *Electrochim. Acta* **2018**, *272*, 169.

[35] S. S. A. Shah, L. Peng, T. Najam, C. Cheng, G. Wu, Y. Nie, W. Ding, X. Qi, S. Chen, Z. Wei, *Electrochim. Acta* **2017**, *251*, 498.

[36] S. S. A. Shah, T. Najam, D. Cheng, A. Hafeez, Y. Lu, A. Waseem, *Curr. Med. Imaging Rev.* **2018**, *14*, 669.

[37] R. Zhang, L. Jiao, W. Yang, G. Wan, H.-L. Jiang, *J. Mater. Chem. A* **2019**, *7*, 26371.

[38] D. Li, H.-Q. Xu, L. Jiao, H.-L. Jiang, *J. Energy Chem.* **2019**, *1*, 100005.

[39] L. Jiao, H.-L. Jiang, *Chem* **2019**, *5*, 786.

[40] L. Zhuang, L. Ge, H. Liu, Z. Jiang, Y. Jia, Z. Li, D. Yang, R. K. Hocking, M. Li, L. Zhang, X. Wang, X. Yao, Z. Zhu, *Angew. Chem. Int. Ed.* **2019**, *58*, 13565.

[41] Y. Pan, Y. Qian, X. Zheng, S.-Q. Chu, Y. Yang, C. Ding, X. Wang, S.-H. Yu, H.-L. Jiang, *Natl. Sci. Rev.* **2020**, *8*.

[42] R. Hinogami, S. Yotsuhashi, M. Deguchi, Y. Zenitani, H. Hashiba, Y. Yamada, *ECS Electrochem. Lett.* **2012**, *1*, H17.

[43] R. Senthil Kumar, S. Senthil Kumar, M. Anbu Kulandainathan, *Electrochem. Commun.* **2012**, *25*, 70.

[44] C.-X. Zhao, B.-Q. Li, J.-N. Liu, Q. Zhang, *Angew. Chem. Int. Ed.* **2020**, *60*, 4448.

[45] X. Wen, Q. Zhang, J. Guan, *Coord. Chem. Rev.* **2020**, *409*, 213214.

[46] Y. Luo, M. Ahmad, A. Schug, M. Tsotsalas, *Adv. Mater.* **2019**, *31*, 1901744.

[47] L. Jiao, Y. Wang, H.-L. Jiang, Q. Xu, *Adv. Mater.* **2018**, *30*, 1703663.

[48] M. Ding, R. W. Flaig, H.-L. Jiang, O. M. Yaghi, *Chem. Soc. Rev.* **2019**, *48*, 2783.

[49] L. Sun, V. Reddu, A. C. Fisher, X. Wang, *Energy Environ. Sci.* **2020**, *13*, 374.

[50] A. Liu, M. Gao, X. Ren, F. Meng, Y. Yang, L. Gao, Q. Yang, T. Ma, *J. Mater. Chem. A* **2020**, *8*, 3541.

[51] P. Gotico, Z. Halime, A. Aukauloo, *Dalton Trans.* **2020**, *49*, 2381.

[52] W. Zhang, Y. Hu, L. Ma, G. Zhu, Y. Wang, X. Xue, R. Chen, S. Yang, Z. Jin, *Adv. Sci.* **2018**, *5*, 1700275.

[53] H. Cui, Y. Guo, L. Guo, L. Wang, Z. Zhou, Z. Peng, *J. Mater. Chem. A* **2018**, *6*, 18782.

[54] J.-M. Savéant, *Chem. Rev.* **2008**, *108*, 2348.

[55] R. Kortlever, J. Shen, K. J. P. Schouten, F. Calle-Vallejo, M. T. M. Koper, *J. Phys. Chem. Lett.* **2015**, *6*, 4073.

[56] H. A. Hansen, J. B. Varley, A. A. Peterson, J. K. Nørskov, *J. Phys. Chem. Lett.* **2013**, *4*, 388.

[57] J. T. Feaster, C. Shi, E. R. Cave, T. Hatsukade, D. N. Abram, K. P. Kuhl, C. Hahn, J. K. Nørskov, T. F. Jaramillo, *ACS Catal.* **2017**, *7*, 4822.

[58] W. Ni, Y. Xue, X. Zang, C. Li, H. Wang, Z. Yang, Y.-M. Yan, *ACS Nano* **2020**, *14*, 2014.

[59] S. Zhang, P. Kang, T. J. Meyer, *J. Am. Chem. Soc.* **2014**, *136*, 1734.

[60] A. S. Varela, W. Ju, A. Bagger, P. Franco, J. Rossmeisl, P. Strasser, *ACS Catal.* **2019**, *9*, 7270.

[61] J. Li, P. Yan, K. Li, J. You, H. Wang, W. Cui, W. Cen, Y. Chu, F. Dong, *J. Mater. Chem. A* **2019**, *7*, 17014.

[62] X. Nie, M. R. Esopi, M. J. Janik, A. Asthagiri, *Angew. Chem. Int. Ed.* **2013**, *52*, 2459.

[63] H. Zhang, X. Chang, J. G. Chen, W. A. Goddard, B. Xu, M.-J. Cheng, Q. Lu, *Nat. Commun.* **2019**, *10*, 3340.

[64] Y. Zheng, A. Vasileff, X. Zhou, Y. Jiao, M. Jaroniec, S.-Z. Qiao, *J. Am. Chem. Soc.* **2019**, *141*, 7646.

[65] L. Fan, C. Xia, F. Yang, J. Wang, H. Wang, Y. Lu, *Science Adv.* **2020**, *6*, 3111.

[66] I. Ledezma-Yanez, E. P. Gallent, M. T. M. Koper, F. Calle-Vallejo, *Catal. Today* **2016**, *262*, 90.

[67] L. Wang, S. Nitopi, A. B. Wong, J. L. Snider, A. C. Nielander, C. G. Morales-Guio, M. Orazov, D. C. Higgins, C. Hahn, T. F. Jaramillo, *Nat. Catal.* **2019**, *2*, 702.

[68] Y. Momose, K. Sato, O. Ohno, *Surf. Interface Anal.* **2002**, *34*, 615.

[69] X. Zhi, Y. Jiao, Y. Zheng, A. Vasileff, S.-Z. Qiao, *Nano Energy* **2020**, *71*, 104601.

[70] M. A. Tekalgne, H. H. Do, A. Hasani, Q. Van Le, H. W. Jang, S. H. Ahn, S. Y. Kim, *Mater. Today Adv.* **2020**, *5*, 100038.

[71] X. Su, Y. Sun, L. Jin, L. Zhang, Y. Yang, P. Kerns, B. Liu, S. Li, J. He, *Appl. Catal. B* **2020**, *269*,118800.

[72] F. Zhang, A. C. Co, *Angew. Chem. Int. Ed.* **2020**, *59*, 1674.

[73] Y. Feng, W. An, Z. Wang, Y. Wang, Y. Men, Y. Du, *ACS Sustain Chem. Eng.* **2020**, *8*, 210.

[74] Y. Hori, H. Wakebe, T. Tsukamoto, O. Koga, *Electrochim. Acta* **1994**, *39*, 1833.

[75] W. Ma, S. Xie, T. Liu, Q. Fan, J. Ye, F. Sun, Z. Jiang, Q. Zhang, J. Cheng, Y. Wang, *Nat. Catal.* **2020**, *3*, 478.

[76] Q. Hu, Z. Han, X. Wang, G. Li, Z. Wang, X. Huang, H. Yang, X. Ren, Q. Zhang, J. Liu, C. He, *Angew. Chem. Int. Ed.* **2020**, *59*, 19054.

[77] D. H. Won, H. Shin, J. Koh, J. Chung, H. S. Lee, H. Kim, S. I. Woo, *Angew. Chem. Int. Ed.* **2016**, *55*, 9297.

[78] H. S. Jeon, I. Sinev, F. Scholten, N. J. Divins, I. Zegkinoglou, L. Pielsticker, B. R. Cuenya, *J. Am. Chem. Soc.* **2018**, *140*, 9383.

[79] D. Ren, B. S.-H. Ang, B. S. Yeo, *ACS Catal.* **2016**, *6*, 8239.

[80] G. Keerthiga, R. Chetty, *J. Electrochem. Soc.* **2017**, *164*, H164.

[81] J. Albo, A. Sáez, J. Solla-Gullón, V. Montiel, A. Irabien, *Appl. Catal., B* **2015**, *176–177*, 709.

[82] S. Sarfraz, A. T. Garcia-Esparza, A. Jedidi, L. Cavallo, K. Takanabe, *ACS Catal.* **2016**, *6*, 2842.

[83] M. Morimoto, Y. Takatsuji, R. Yamasaki, H. Hashimoto, I. Nakata, T. Sakakura, T. Haruyama, *Electrocatalysis* **2018**, *9*, 323.

[84] K. D. Yang, W. R. Ko, J. H. Lee, S. J. Kim, H. Lee, M. H. Lee, K. T. Nam, *Angew. Chem. Int. Ed.* **2017**, *56*, 796.

[85] F. Li, L. Chen, G. P. Knowles, D. R. MacFarlane, J. Zhang, *Angew. Chem. Int. Ed.* **2017**, *56*, 505.

[86] H. Song, M. Im, J. T. Song, J.-A. Lim, B.-S. Kim, Y. Kwon, S. Ryu, J. Oh, *Appl. Catal., B* **2018**, *232*, 391.

[87] A. Dutta, M. Rahaman, N. C. Luedi, M. Mohos, P. Broekmann, *ACS Catal.* **2016**, *6*, 3804.

[88] A. S. Hall, Y. Yoon, A. Wuttig, Y. Surendranath, *J. Am. Chem. Soc.* **2015**, *137*, 14834.

[89] Z. Pan, K. Wang, K. Ye, Y. Wang, H.-Y. Su, B. Hu, J. Xiao, T. Yu, Y. Wang, S. Song, *ACS Catal.* **2020**, *10*, 3871.

[90] J.-J. Lv, M. Jouny, W. Luc, W. Zhu, J.-J. Zhu, F. Jiao, *Adv. Mater.* **2018**, *30*, 1803111.

[91] M. Ma, K. Djanashvili, W. A. Smith, *Angew. Chem. Int. Ed.* **2016**, *55*, 6680.

[92] F. Li, G. H. Gu, C. Choi, P. Kolla, S. Hong, T.-S. Wu, Y.-L. Soo, J. Masa, S. Mukerjee, Y. Jung, J. Qiu, Z. Sun, *Appl. Catal. B* **2020**, *277*, 119241.

[93] X. Zhang, J. Han, J. Guo, Z. Tang, *Small Struct.* **2021**, *2*, 2000141.

[94] J.-X. Wu, S.-Z. Hou, X.-D. Zhang, M. Xu, H.-F. Yang, P.-S. Cao, Z.-Y. Gu, *Chem. Sci.* **2019**, *10*, 2199.

[95] I. Hod, M. D. Sampson, P. Deria, C. P. Kubiak, O. K. Farha, J. T. Hupp, *ACS Catal.* **2015**, *5*, 6302.

[96] C. Zhao, X. Dai, T. Yao, W. Chen, X. Wang, J. Wang, J. Yang, S. Wei, Y. Wu, Y. Li, *J. Am. Chem. Soc.* **2017**, *139*, 8078.

[97] E. E. Benson, C. P. Kubiak, A. J. Sathrum, J. M. Smieja, *Chem. Soc. Rev.* **2009**, *38*, 89.

[98] C.-J. Chang, S.-F. Hung, C.-S. Hsu, H.-C. Chen, S.-C. Lin, Y.-F. Liao, H. M. Chen, *ACS Cent. Sci.* **2019**, *5*, 1998.

[99] P. De Luna, R. Quintero-Bermudez, C.-T. Dinh, M. B. Ross, O. S. Bushuyev, P. Todorović, T. Regier, S. O. Kelley, P. Yang, E. H. Sargent, *Nat. Catal.* **2018**, *1*, 103.

[100] N. Kornienko, Y. Zhao, C. S. Kley, C. Zhu, D. Kim, S. Lin, C. J. Chang, O. M. Yaghi, P. Yang, *J. Am. Chem. Soc.* **2015**, *137*, 14129.

[101] J. Gu, C.-S. Hsu, L. Bai, H. M. Chen, X. Hu, *Science* **2019**, *364*, 1091.

[102] I. Choi, Y. E. Jung, S. J. Yoo, J. Y. Kim, H.-J. Kim, C. Y. Lee, J. H. Jang, *J. Electrochem. Sci. Technol* **2017**, *8*, 61.

[103] Y. Wang, P. Hou, Z. Wang, P. Kang, *ChemPhysChem* **2017**, *18*, 3142.

[104] E. S. Donovan, B. M. Barry, C. A. Larsen, M. N. Wirtz, W. E. Geiger, R. A. Kemp, *Chem. Commun.* **2016**, *52*, 1685.

[105] Y. Wu, J. Jiang, Z. Weng, M. Wang, D. L. J. Broere, Y. Zhong, G. W. Brudvig, Z. Feng, H. Wang, *ACS Cent. Sci.* **2017**, *3*, 847.

[106] X. Jiang, H. Li, J. Xiao, D. Gao, R. Si, F. Yang, Y. Li, G. Wang, X. Bao, *Nano Energy* **2018**, *52*, 345.

[107] S. Dou, J. Song, S. Xi, Y. Du, J. Wang, Z.-F. Huang, Z. J. Xu, X. Wang, *Angew. Chem. Int. Ed.* **2019**, *58*, 4041.

[108] J. Albo, D. Vallejo, G. Beobide, O. Castillo, P. Castano, A. Irabien, *ChemSusChem* **2017**, *10*, 1100.

[109] M. Hammouche, D. Lexa, M. Momenteau, J. M. Saveant, *J. Am. Chem. Soc.* **1991**, *113*, 8455.

[110] Z. Weng, J. Jiang, Y. Wu, Z. Wu, X. Guo, K. L. Materna, W. Liu, V. S. Batista, G. W. Brudvig, H. Wang, *J. Am. Chem. Soc.* **2016**, *138*, 8076.

[111] G. Zhu, Y. Li, H. Zhu, H. Su, S. H. Chan, Q. Sun, *ACS Catal.* **2016**, *6*, 6294.

[112] S. Lin, C. S. Diercks, Y.-B. Zhang, N. Kornienko, E. M. Nichols, Y. Zhao, A. R. Paris, D. Kim, P. Yang, O. M. Yaghi, C. J. Chang, *Science* **2015**, *349*, 1208.

[113] S. R. Ahrenholtz, C. C. Epley, A. J. Morris, *J. Am. Chem. Soc.* **2014**, *136*, 2464.

[114] X. Zhang, Y. Zhang, Q. Li, X. Zhou, Q. Li, J. Yi, Y. Liu, J. Zhang, *J. Mater. Chem. A,* **2020**, *8*, 9776.

[115] S. M. Cohen, *Chem. Rev.* **2012**, *112*, 970.

[116] L. Jiao, J. Wang, H.-L. Jiang, *Acc. Mat. Res.* **2021**, *2*, 327.

[117] Y. Shan, L. Chen, H. Pang, Q. Xu, *Small Struct.* **2020**, *2*, 2000078.

[118] Z. Wang, S. M. Cohen, *Chem. Soc. Rev.* **2009**, *38*, 1315.

[119] T. N. Tu, M. V. Nguyen, H. L. Nguyen, B. Yuliarto, K. E. Cordova, S. Demir, *Coord. Chem. Rev.* **2018**, *364*, 33.

[120] L. Ye, J. Liu, Y. Gao, C. Gong, M. Addicoat, T. Heine, C. Wöll, L. Sun, *J. Mater. Chem. A* **2016**, *4*, 15320.

[121] B.-X. Dong, S.-L. Qian, F.-Y. Bu, Y.-C. Wu, L.-G. Feng, Y.-L. Teng, W.-L. Liu, Z.-W. Li, *ACS Appl. Energy Mater.* **2018**, *1*, 4662.

[122] Y. Fu, D. Sun, Y. Chen, R. Huang, Z. Ding, X. Fu, Z. Li, *Angew. Chem. Int. Ed.* **2012**, *51*, 3364.

[123] Q. Wang, Y. Lei, D. Wang, Y. Li, *Energy Environ Sci.* **2019**, *12*, 1730.

[124] Q. Huang, Q. Li, J. Liu, Y. R. Wang, R. Wang, L. Z. Dong, Y. H. Xia, J. L. Wang, Y.-Q. Lan, *Matter* **2019**, *1*, 1656.

[125] F. Yang, A. Chen, P. L. Deng, Y. Zhou, Z. Shahid, H. Liu, B. Y. Xia, *Chem. Sci.* **2019**, *10*, 7975.

[126] S. Dou, X. Wang, S. Wang, *Small Methods* **2019**, *3*, 1800211.

[127] D.-H. Nam, O. S. Bushuyev, J. Li, P. De Luna, A. Seifitokaldani, C.-T. Dinh, F. P. García de Arquer, Y. Wang, Z. Liang, A. H. Proppe, C. S. Tan, P. Todorović, O. Shekhah, C. M. Gabardo, J. W. Jo, J. Choi, M.-J. Choi, S.-W. Baek, J. Kim, D. Sinton, S. O. Kelley, M. Eddaoudi, E. H. Sargent, *J. Am. Chem. Soc.* **2018**, *140*, 11378.

[128] J. Jiao, R. Lin, S. Liu, W.-C. Cheong, C. Zhang, Z. Chen, Y. Pan, J. Tang, K. Wu, S.-F. Hung, H. M. Chen, L. Zheng, Q. Lu, X. Yang, B. Xu, H. Xiao, J. Li, D. Wang, Q. Peng, C. Chen, Y. Li, *Nat. Chem.* **2019**, *11*, 222.

[129] W. Ren, X. Tan, W. Yang, C. Jia, S. Xu, K. Wang, S. C. Smith, C. Zhao, *Angew. Chem. Int. Ed.* **2019**, *58*, 6972.

[130] W. Zhu, L. Zhang, S. Liu, A. Li, X. Yuan, C. Hu, G. Zhang, W. Deng, K. Zang, J. Luo, Y. Zhu, M. Gu, Z. J. Zhao, J. Gong, *Angew. Chem. Int. Ed.* **2020**, *59*, 12664.

[131] H. Zhong, M. Ghorbani-Asl, K. H. Ly, J. Zhang, J. Ge, M. Wang, Z. Liao, D. Makarov, E. Zschech, E. Brunner, I. M. Weidinger, J. Zhang, A. V. Krasheninnikov, S. Kaskel, R. Dong, X. Feng, *Nat. Commun.* **2020**, *11*, 1409.

[132] H. Xu, X. Luo, J. Wang, Y. Su, X. Zhao, Y. Li, *ACS Appl. Mater. Interfaces* **2019**, *11*, 20291.

[133] Z. Song, F. Qiu, E. W. Zaia, Z. Wang, M. Kunz, J. Guo, M. Brady, B. Mi, J. J. Urban, *Nano Lett.* **2017**, *17*, 6752.

[134] M. L. Sun, Y. R. Wang, W. W. He, R. L. Zhong, Q. Z. Liu, S. Xu, J. M. Xu, X. L. Han, X. Ge, S. L. Li, Y. Q. Lan, A. M. Al-Enizi, A. Nafady, S. Ma, *Small* **2021**, *17*, 2100762.

[135] Y. T. Guntern, J. R. Pankhurst, J. Vávra, M. Mensi, V. Mantella, P. Schouwink, R. Buonsanti, *Angew. Chem. Int. Ed.* **2019**, *58*, 12632.

[136] Y.-R. Wang, Q. Huang, C.-T. He, Y. Chen, J. Liu, F.-C. Shen, Y.-Q. Lan, *Nat. Commun.* **2018**, *9*, 4466.

[137] Y. Guo, W. Shi, H. Yang, Q. He, Z. Zeng, J.-Y. Ye, X. He, R. Huang, C. Wang, W. Lin, *J. Am. Chem. Soc.* **2019**, *141*, 17875.

[138] Y. Wu, S. Cao, J. Hou, Z. Li, B. Zhang, P. Zhai, Y. Zhang, L. Sun, *Adv. Energy Mater.* **2020**, *10*, 2000588.

[139] X. Jiang, H. Wu, S. Chang, R. Si, S. Miao, W. Huang, Y. Li, G. Wang, X. Bao, *J. Mater. Chem. A* **2017**, *5*, 19371.

[140] C.-W. Kung, C. O. Audu, A. W. Peters, H. Noh, O. K. Farha, J. T. Hupp, *ACS Energy Lett.* **2017**, *2*, 2394.

[141] C. Xu, Y. Pan, G. Wan, H. Liu, L. Wang, H. Zhou, S.-H. Yu, H.-L. Jiang, *J. Am. Chem. Soc.* **2019**, *141*, 19110.

[142] M. S. Javed, M. K. Aslam, S. Asim, S. Batool, M. Idrees, S. Hussain, S. S. A. Shah, M. Saleem, W. Mai, C. Hu, *Electrochim. Acta* **2020**, *349*, 136384.

[143] L. Wang, S. R. Li, Y. Z. Chen, H. -L. Jiang, *Small* **2021**, e2004481.

[144] W. Zhang, G. Cai, R. Wu, Z. He, H. B. Yao, H. -L. Jiang, S. H. Yu, *Small* **2021**, e2004140.

[145] M. Ding, H.-L. Jiang, *CCS Chem.* **2020**, *0*, 2740.

[146] X. Cai, Z. Xie, D. Li, M. Kassymova, S.-Q. Zang, H.-L. Jiang, *Coord. Chem. Rev.* **2020**, *417*, 213366.

[147] X.-Y. Lin, Y.-H. Li, M.-Y. Qi, Z.-R. Tang, H.-L. Jiang, Y.-J. Xu, *Nanoscale Horiz.* **2020**, *5*, 714.

[148] Q. Yang, C. C. Yang, C. H. Lin, H. -L. Jiang, *Angew. Chem. Int. Ed.* **2019**, *58*, 3511.

[149] S. S. Wang, L. Jiao, Y. Qian, W. C. Hu, G. Y. Xu, C. Wang, H. -L. Jiang, *Angew. Chem. Int. Ed.* **2019**, *58*, 10713.

[150] F. Schüth, M. D. Ward, J. M. Buriak, *Chem. Mater.* **2018**, *30*, 3599.

[151] M. S. Javed, N. Shaheen, S. Hussain, J. L. Li, S. S. A. Shah, Y. Abbas, M. A. Ahmad, R. Raza, W. J. Mai, *J. Mater. Chem. A* **2019**, *7*, 946.

[152] M. K. Aslam, S. S. A. Shah, M. S. Javed, S. Li, S. Hussain, B. B. Hu, N. A. Khan, C. G. Chen, *J. Electroanal. Chem.* **2019**, *855*, 113615.

[153] M. Yang, L. Jiao, H. Dong, L. Zhou, C. Teng, D. Yan, T.-N. Ye, X. Chen, Y. Liu, H.-L. Jiang, *Sci. Bull.* **2021**, *66*, 257.

[154] S. S. A. Shah, T. Najam, M. S. Javed, M. M. Rahman, P. Tsiakaras, *ACS Appl. Mater. Interfaces* **2021**, *13*, 23191.

[155] Y. Zhu, J. Sokolowski, X. Song, Y. He, Y. Mei, G. Wu, *Adv. Energy Mater.* **2020**, *10*, 1902844.

[156] X.-L. Lu, X. Rong, C. Zhang, T.-B. Lu, *J. Mater. Chem. A* **2020**, *8*, 10695.

[157] Y. Zheng, P. Cheng, J. Xu, J. Han, D. Wang, C. Hao, H. R. Alanagh, C. Long, X. Shi, Z. Tang, *Nanoscale* **2019**, *11*, 4911.

[158] E. Zhang, T. Wang, K. Yu, J. Liu, W. Chen, A. Li, H. Rong, R. Lin, S. Ji, X. S. Zheng, Y. Wang, L. Zheng, C. Chen, D. Wang, J. Zhang, Y. Li, *J. Am. Chem. Soc.* **2019**.

[159] H. Yang, Y. Wu, G. Li, Q. Lin, Q. Hu, Q. Zhang, J. Liu, C. He, *J. Am. Chem. Soc.* **2019**, *141*, 12717.

[160] M. K. Kim, H. J. Kim, H. Lim, Y. Kwon, H. M. Jeong, *Electrochim. Acta* **2019**, *306*, 28.

[161] M. Kuang, A. Guan, Z. Gu, P. Han, L. Qian, G. Zheng, *Nano Res.* **2019**, *12*, 2324.

[162] Z. Kou, W. Zang, W. Pei, L. Zheng, S. Zhou, S. Zhang, L. Zhang, J. Wang, *J. Mater. Chem. A* **2020**, *8*, 3071.

[163] C. F. Wen, F. Mao, Y. Liu, X. Y. Zhang, H. Q. Fu, L. R. Zheng, P. F. Liu, H. G. Yang, *ACS Catal.* **2020**, *10*, 1086.

[164] Y.-N. Gong, L. Jiao, Y. Qian, C.-Y. Pan, L. Zheng, X. Cai, B. Liu, S.-H. Yu, H.-L. Jiang, *Angew. Chem. Int. Ed.* **2020**, *59*, 2705.

[165] C. Cao, D. D. Ma, J. F. Gu, X. Xie, G. Zeng, X. Li, S. G. Han, Q. L. Zhu, X. T. Wu, Q. Xu, *Angew. Chem. Int. Ed.* **2020**, *59*, 15014.

[166] P. Lamagni, M. Miola, J. Catalano, M. S. Hvid, M. A. H. Mamakhel, M. Christensen, M. R. Madsen, H. S. Jeppesen, X.-M. Hu, K. Daasbjerg, T. Skrydstrup, N. Lock, *Adv. Funct. Mater.* **2020**, *30*, 1910408.

[167] K. Zhao, Y. Liu, X. Quan, S. Chen, H. Yu, *ACS Appl. Mater. Interfaces* **2017**, *9*, 5302.

[168] B. Liu, H. Shioyama, T. Akita, Q. Xu, *J. Am. Chem. Soc.* **2008**, *130*, 5390.

[169] Y. Guo, H. Yang, X. Zhou, K. Liu, C. Zhang, Z. Zhou, C. Wang, W. Lin, *J. Mater. Chem. A* **2017**, *5*, 24867.

[170] D. Gao, H. Zhou, J. Wang, S. Miao, F. Yang, G. Wang, J. Wang, X. Bao, *J. Am. Chem. Soc.* **2015**, *137*, 4288.

[171] X. Zhang, J. Fu, Y. Liu, X.-D. Zhou, J. Qiao, *ACS Sustain. Chem. Eng.* **2020**, *8*, 4871.

[172] D. Zhang, Z. Tao, F. Feng, B. He, W. Zhou, J. Sun, J. Xu, Q. Wang, L. Zhao, *Electrochim. Acta* **2020**, *334*, 135563.

[173] K. Fan, Y. Jia, Y. Ji, P. Kuang, B. Zhu, X. Liu, J. Yu, *ACS Catal.* **2019**, *10*, 358.

[174] Y.-S. Cheng, X.-P. Chu, M. Ling, N. Li, K.-L. Wu, F.-H. Wu, H. Li, G. Yuan, X.-W. Wei, *Catal. Sci. Technol.* **2019**, *9*, 5668.

[175] P. Deng, F. Yang, Z. Wang, S. Chen, Y. Zhou, S. Zaman, B. Y. Xia, *Angew. Chem. Int. Ed.* **2020**, *59*, 10807.

[176] H. Yang, X. Yu, J. Shao, J. Liao, G. Li, Q. Hu, X. Chai, Q. Zhang, J. Liu, C. He, *J. Mater. Chem. A* **2020**, *8*, 15675.

[177] W. Guo, X. Sun, C. Chen, D. Yang, L. Lu, Y. Yang, B. Han, *Green Chemistry* **2019**, *21*, 503.

[178] M. Zhang, C. Han, W. Chen, W. Luo, Y. Cao, G. Qian, X. Zhou, X. Duan, S. Wang, X. Duan, *Green Energy Environ.* **2020**, *5*, 444.

[179] F. Li, X. Dai, W. Qi, *Green Energy Environ.* **2020**, *5*, 453.

[180] X. Sun, X. Kang, Q. Zhu, J. Ma, G. Yang, Z. Liu, B. Han, *Chem. Sci.* **2016**, *7*, 2883.

[181] D. Yuan, L. Huang, Y. Ding, L. Zhang, L. Qian, G. Zheng, *Mol. Catal.* **2020**, *492*, 111029.

[182] J. Xie, X. Zhao, M. Wu, Q. Li, Y. Wang, J. Yao, *Angew. Chem. Int. Ed.* **2018**, *57*, 9640.

[183] B. Zhang, J. Zhang, F. Zhang, L. Zheng, G. Mo, B. Han, G. Yang, *Adv. Funct. Mater.* **2020**, *30*, 1906194.

[184] G. Wang, M. Liu, J. Jia, H. Xu, B. Zhao, K. Lai, C. Tu, Z. Wen, *ChemCatChem* **2020**, *12*, 2203.

[185] G. Li, Y. Qin, Y. Wu, L. Pei, Q. Hu, H. Yang, Q. Zhang, J. Liu, C. He, *Chinese J. Catal.* **2020**, *41*, 830.

[186] C. Jia, W. Ren, X. Chen, W. Yang, C. Zhao, *ACS Sustain. Chem. Eng.* **2020**, *8*, 6003.

[187] J. Xie, M. A. Ghausi, J. Wang, X. Wang, W. Wang, R. Yang, M. Wu, Q. Zhang, Y. Wang, *ChemElectroChem* **2020**, *7*, 2145.

[188] T. Ma, Q. Fan, X. Li, J. Qiu, T. Wu, Z. Sun, *J. CO2 Util.* **2019**, *30*, 168.

[189] A. G. A. Mohamed, Y. Huang, J. Xie, R. A. Borse, G. Parameswaram, Y. Wang, *Nano Today* **2020**, *33*, 100891.

[190] S. Zhang, P. Kang, S. Ubnoske, M. K. Brennaman, N. Song, R. L. House, J. T. Glass, T. J. Meyer, *J. Am. Chem. Soc.* **2014**, *136*, 7845.

[191] H. Wang, J. Jia, P. Song, Q. Wang, D. Li, S. Min, C. Qian, L. Wang, Y. F. Li, C. Ma, T. Wu, J. Yuan, M. Antonietti, G. A. Ozin, *Angew. Chem. Int. Ed.* **2017**, *56*, 7847.

[192] R. Wang, X. Sun, S. Ould-Chikh, D. Osadchii, F. Bai, F. Kapteijn, J. Gascon, *ACS Appl. Mater. Interfaces* **2018**, *10*, 14751.

[193] R. Walczak, B. Kurpil, A. Savateev, T. Heil, J. Schmidt, Q. Qin, M. Antonietti, M. Oschatz, *Angew. Chem. Int. Ed.* **2018**, *57*, 10765.

[194] L. Ye, Y. Ying, D. Sun, Z. Zhang, L. Fei, Z. Wen, J. Qiao, H. Huang, *Angew. Chem. Int. Ed.* **2020**, *59*, 3244.

[195] L. Jiao, G. Wan, R. Zhang, H. Zhou, S.-H. Yu, H.-L. Jiang, *Angew. Chem. Int. Ed.* **2018**, *57*, 8525.

[196] T. N. Huan, N. Ranjbar, G. Rousse, M. Sougrati, A. Zitolo, V. Mougel, F. Jaouen, M. Fontecave, *ACS Catal.* **2017**, *7*, 1520.

[197] C. Genovese, M. E. Schuster, E. K. Gibson, D. Gianolio, V. Posligua, R. Grau-Crespo, G. Cibin, P. P. Wells, D. Garai, V. Solokha, S. Krick Calderon, J. J. Velasco-Velez, C. Ampelli, S. Perathoner, G. Held, G. Centi, R. Arrigo, *Nat. Commun.* **2018**, *9*, 935.

[198] V. Tripkovic, M. Vanin, M. Karamad, M. E. Björketun, K. W. Jacobsen, K. S. Thygesen, J. Rossmeisl, *J. Phys. Chem. C* **2013**, *117*, 9187.

[199] A. Bagger, W. Ju, A. S. Varela, P. Strasser, J. Rossmeisl, *Catal. Today* **2017**, *288*, 74.

[200] A. S. Varela, N. Ranjbar Sahraie, J. Steinberg, W. Ju, H. S. Oh, P. Strasser, *Angew. Chem. Int. Ed.* **2015**, *54*, 10758.

[201] W. Ju, A. Bagger, G. P. Hao, A. S. Varela, I. Sinev, V. Bon, B. Roldan Cuenya, S. Kaskel, J. Rossmeisl, P. Strasser, *Nat. Commun.* **2017**, *8*, 944.

[202] B. Dembinska, W. Kiciński, A. Januszewska, A. Dobrzeniecka, P. J. Kulesza, *J. Electrochem. Soc.* **2017**, *164*, H484.

[203] A. S. Varela, W. Ju, P. Strasser, *Adv. Energy Mater.* **2018**, *8*, 1703614.

[204] Y. Ye, F. Cai, H. Li, H. Wu, G. Wang, Y. Li, S. Miao, S. Xie, R. Si, J. Wang, X. Bao, *Nano Energy* **2017**, *38*, 281.

[205] C. Yan, Y. Ye, L. Lin, H. Wu, Q. Jiang, G. Wang, X. Bao, *Catal. Today* **2019**, *330*, 252.

[206] X. Wang, Z. Chen, X. Zhao, T. Yao, W. Chen, R. You, C. Zhao, G. Wu, J. Wang, W. Huang, J. Yang, X. Hong, S. Wei, Y. Wu, Y. Li, *Angew. Chem. Int. Ed.* **2018**, *57*, 1944.

[207] Z. Geng, Y. Cao, W. Chen, X. Kong, Y. Liu, T. Yao, Y. Lin, *Appl. Catal. B* **2019**, *240*, 234.

[208] C. Hu, S. Bai, L. Gao, S. Liang, J. Yang, S.-D. Cheng, S.-B. Mi, J. Qiu, *ACS Catal.* **2019**, *9*, 11579.

[209] H. Yang, Q. Lin, C. Zhang, X. Yu, Z. Cheng, G. Li, Q. Hu, X. Ren, Q. Zhang, J. Liu, C. He, *Nat. Commun.* **2020**, *11*, 593.

[210] H. Yang, R. Shi, L. Shang, T. Zhang, *Small Struct.* **2021**, 2100007.

[211] D. Liu, D. Chen, J. Yang, *Green Energy Environ.* **2019**, *4*, 208.

[212] Y. Li, *Green Energy Environ.* **2020**, *5*, 4.

[213] J. Yang, W. Li, D. Wang, Y. Li, *Small Struct.* **2020**, *2*, 2000051.

[214] Q. Yang, Y. Jia, F. Wei, L. Zhuang, D. Yang, J. Liu, X. Wang, S. Lin, P. Yuan, X. Yao, *Angew. Chem. Int. Ed.* **2020**, *59*, 6122.

[215] M. Jia, Q. Fan, S. Liu, J. Qiu, Z. Sun, *Curr. Opin. Green Sustain. Chem.* **2019**, *16*, 1.

[216] Q. Qu, S. Ji, Y. Chen, D. Wang, Y. Li, *Chem. Sci.* **2021**, *12*, 4201.

[217] N. Zhang, X. Zhang, L. Tao, P. Jiang, C. Ye, R. Lin, Z. Huang, A. Li, D. Pang, H. Yan, Y. Wang, P. Xu, S. An, Q. Zhang, L. Liu, S. Du, X. Han, D. Wang, Y. Li, *Angew. Chem. Int. Ed.* **2021**, *60*, 6170.

[218] Y. Wang, Y. Liu, W. Liu, J. Wu, Q. Li, Q. Feng, Z. Chen, X. Xiong, D. Wang, Y. Lei, *Energy Environ. Sci.* **2020**, *13*, 4609.

[219] S. Yang, J. Zhang, L. Peng, M. Asgari, D. Stoian, I. Kochetygov, W. Luo, E. Oveisi, O. Trukhina, A. H. Clark, D. T. Sun, W. L. Queen, *Chem. Sci.* **2020**, *11*, 10991.

[220] X. Li, W. Bi, M. Chen, Y. Sun, H. Ju, W. Yan, J. Zhu, X. Wu, W. Chu, C. Wu, Y. Xie, *J. Am. Chem. Soc.* **2017**, *139*, 14889.

[221] H. B. Yang, S.-F. Hung, S. Liu, K. Yuan, S. Miao, L. Zhang, X. Huang, H.-Y. Wang, W. Cai, R. Chen, J. Gao, X. Yang, W. Chen, Y. Huang, H. M. Chen, C. M. Li, T. Zhang, B. Liu, *Nat. Energy* **2018**, *3*, 140.

[222] L. Jiao, W. Yang, G. Wan, R. Zhang, X. Zheng, H. Zhou, S. H. Yu, H.-L. Jiang, *Angew. Chem. Int. Ed.* **2020**, *59*, 20589.

[223] Y. Pan, R. Lin, Y. Chen, S. Liu, W. Zhu, X. Cao, W. Chen, K. Wu, W.-C. Cheong, Y. Wang, L. Zheng, J. Luo, Y. Lin, Y. Liu, C. Liu, J. Li, Q. Lu, X. Chen, D. Wang, Q. Peng, C. Chen, Y. Li, *J. Am. Chem. Soc.* **2018**, *140*, 4218.

[224] Q. Fan, P. Hou, C. Choi, T.-S. Wu, S. Hong, F. Li, Y.-L. Soo, P. Kang, Y. Jung, Z. Sun, *Adv. Energy Mater.* **2020**, *10*, 1903068.

[225] Z. Zhang, J. Xiao, X.-J. Chen, S. Yu, L. Yu, R. Si, Y. Wang, S. Wang, X. Meng, Y. Wang, Z.-Q. Tian, D. Deng, *Angew. Chem. Int. Ed.* **2018**, *57*, 16339.

[226] J. Li, P. Pršlja, T. Shinagawa, A. J. Martín Fernández, F. Krumeich, K. Artyushkova, P. Atanassov, A. Zitolo, Y. Zhou, R. García-Muelas, N. López, J. Pérez-Ramírez, F. Jaouen, *ACS Catal.* **2019**, *9*, 10426.

[227] J.-H. Liu, L.-M. Yang, E. Ganz, *J. Mater. Chem. A* **2019**, *7*, 3805.

[228] S. Liu, H. B. Yang, S.-F. Hung, J. Ding, W. Cai, L. Liu, J. Gao, X. Li, X. Ren, Z. Kuang, Y. Huang, T. Zhang, B. Liu, *Angew. Chem. Int. Ed.* **2020**, *59*, 798.

[229] H. Zhang, J. Li, S. Xi, Y. Du, X. Hai, J. Wang, H. Xu, G. Wu, J. Zhang, J. Lu, J. Wang, *Angew. Chem. Int. Ed.* **2019**, *58*, 14871.

[230] F. Pan, H. Zhang, K. Liu, D. Cullen, K. More, M. Wang, Z. Feng, G. Wang, G. Wu, Y. Li, *ACS Catal.* **2018**, *8*, 3116.

[231] F. Pan, H. Zhang, Z. Liu, D. Cullen, K. Liu, K. More, G. Wu, G. Wang, Y. Li, *J. Mater. Chem. A* **2019**, *7*, 26231.

[232] X. Li, L. Liu, X. Ren, J. Gao, Y. Huang, B. Liu, *Sci. Adv.* **2020**, *6*, 6833.

[233] Q. Wang, C. Cai, M. Dai, J. Fu, X. Zhang, H. Li, H. Zhang, K. Chen, Y. Lin, H. Li, J. Hu, M. Miyauchi, M. Liu, *Small Sci.* **2020**, *1*, 2000028.

[234] L. Takele Menisa, P. Cheng, C. Long, X. Qiu, Y. Zheng, J. Han, Y. Zhang, Y. Gao, Z. Tang, *Nanoscale* **2020**, *12*, 16617.

[235] Y. Zhang, L. Jiao, W. Yang, C. Xie, H.-L. Jiang, *Angew. Chem. Int. Ed.* **2021**, *60*, 7607.

[236] A. Guan, Z. Chen, Y. Quan, C. Peng, Z. Wang, T.-K. Sham, C. Yang, Y. Ji, L. Qian, X. Xu, G. Zheng, *ACS Energy Lett.* **2020**, *5*, 1044.

[237] C. Yan, H. Li, Y. Ye, H. Wu, F. Cai, R. Si, J. Xiao, S. Miao, S. Xie, F. Yang, Y. Li, G. Wang, X. Bao, *Energy Environ. Sci.* **2018**, *11*, 1204.

[238] X. Qin, S. Zhu, F. Xiao, L. Zhang, M. Shao, *ACS Energy Lett.* **2019**, *4*, 1778.

[239] Y. Cheng, S. Zhao, H. Li, S. He, J.-P. Veder, B. Johannessen, J. Xiao, S. Lu, J. Pan, M. F. Chisholm, S.-Z. Yang, C. Liu, J. G. Chen, S. P. Jiang, *Appl. Catal. B* **2019**, *243*, 294.

[240] S.-G. Han, D.-D. Ma, S.-H. Zhou, K. Zhang, W.-B. Wei, Y. Du, X.-T. Wu, Q. Xu, R. Zou, Q.-L. Zhu, *Appl. Catal. B* **2021**, *283*, 119591.

[241] Z. Gu, N. Yang, P. Han, M. Kuang, B. Mei, Z. Jiang, J. Zhong, L. Li, G. Zheng, *Small Methods* **2018**, *3*, 1800449.

[242] X. Rong, H.-J. Wang, X.-L. Lu, R. Si, T.-B. Lu, *Angew. Chem. Int. Ed.* **2020**, *59*, 1961.

[243] G. Cai, P. Yan, L. Zhang, H.-C. Zhou, H.-L. Jiang, *Chem. Rev.* **2021**, https://doi.org/10.1021/acs.chemrev.1c00243.

Syed Shoaib Ahmad Shah received his Ph.D. (2015–2018) from Chongqing University (China) under the supervision of Prof. Wei Zidong with outstanding student award (2018). Currently, he is a CAS-President Postdoc Fellow (PIFI) at the Department of Chemistry, USTC, under the supervision of Prof. Dr. Hai-Long Jiang. His scientific interests are focused on synthesis of MOF-based porous materials and derived metal-coordinated N-doped carbons (single-atom active sites) for electrocatalysis (CO_2RR), fuel cells, metal–air/CO_2 batteries, supercapacitors.

Hai-Long Jiang earned his Ph.D. (2008) from Chinese Academy of Sciences. He subsequently worked at the National Institute of Advanced Industrial Science and Technology (Japan), as AIST and JSPS fellow during 2008–2011. After a postdoctoral stint at Texas A&M University (USA), he became a full professor at USTC in 2013. He was elected a fellow of the Royal Society of Chemistry (FRSC) in 2018 and was annually listed as a highly cited researcher (chemistry) by Clarivate Analytics since 2017. His research interest currently lies in biomimetic microenvironment modulation (MEM) of catalytic centers based on crystalline porous materials (particularly MOFs).